THE EFFECTS OF ANGIOPLASTY ON THE PASSIVE MECHANICAL RESPONSE AND MICROSTRUCTURE OF PORCINE ARTERIES

by

Jonathan Dennis Kuhlenhoelter

A thesis submitted to the faculty of
The University of Utah
in partial fulfillment of the requirements for the degree of

Master of Science

Department of Mechanical Engineering

The University of Utah

May 2025

The University of Utah Graduate School

STATEMENT OF THESIS APPROVAL

The thesis of **Jonathan Dennis Kuhlenhoelter**

has been approved by the following supervisory committee members:

Kenneth L. Monson	, Chair	**02/18/2025** Date Approved
Claire Acevedo	, Member	Date Approved
Lucas H. Timmins	, Member	**02/13/2025** Date Approved

and by **Bruce K. Gale** , Chair of

the Department of **Mechanical Engineering**

and by Darryl P. Butt, Dean of The Graduate School.

ABSTRACT

Percutaneous transluminal angioplasty is a common treatment for peripheral artery disease. It has a high initial effectiveness rate that decreases significantly over time. The reasons for this are still being investigated. This study contributes to that investigation by finding how an artery's passive mechanical properties and microstructure change after angioplasty. This was done with two experiments, the first of which performed angioplasty on porcine carotid arteries in an in vitro setting. The carotid arteries' axial and circumferential mechanical properties were evaluated before and after angioplasty. The arteries were then stained with collagen hybridizing peptide to identify collagen damage and imaged so that changes to the microstructure could be seen. The results showed a softening of the arteries in both axial and circumferential directions. Collagen damage and changes to the arteries' microstructure were also seen. The second experiment was exploratory and investigated how in vivo angioplasty changes the microstructure and mechanical properties of different porcine arteries and how the arteries heal after an eight- or twelve-day recovery period. This experiment found similar results to the first. Angioplasty caused noticeable damage to all locations studied. It also affected the mechanical properties of the in vitro carotids, similar to the in vivo experiments. The eight- and twelve-day recovery arteries showed signs of returning to a state like the pretreated arteries but still displayed signs of damage. These results can help

inform future studies and guide decisions regarding angioplasty procedures and outcomes.

TABLE OF CONTENTS

LIST OF TABLES

Tables

ACKNOWLEDGMENTS

I would like to acknowledge Alucent Biomedical. Inc. for helping to fund this research and supplying the tissue used in the in vitro experiments. I also want to thank the Cell Imaging Core at the University of Utah for the use of equipment, training, and technical support. I would also like to acknowledge the Department of Defense, Henry M. Jackson Foundation for the Advancement of Military Medicine, Gregory Boiczyk, and Noah Pearson for allowing us to piggyback on your research and use the Göttingen minipigs in the exploratory in vivo experiments.

I would also like to acknowledge and thank Dr. Ken Monson for his never-ending patience and understanding throughout this process. I also want to thank him for all the professional and technical guidance and education he has given me.

Also, thank you to the other members of the Laboratory of Head Injury and Vessel Biomechanics especially Noah Pearson, Will Anderl, and Farshad Mogharrabi. Thank you for lending your time and expertise whenever I was facing a roadblock during these experiments.

Thank you to my family, especially my mother, mother-in-law, and father-in-law. You have all done so much to help and support me and my family during this process, and I am forever grateful.

Lastly, thank you to my wife Mandy. You have supported and challenged me in equal measure, and while I may not always show it, I am always happy and grateful for it.

I did not think grad school would be as eventful as it has been, but we finally knocked it out. Let's see what is next.

CHAPTER 1

INTRODUCTION

Cardiovascular diseases are a widespread and damaging family of disorders. The American Heart Association (AHA) estimated that cardiovascular disease was responsible for 19.05 million deaths in 2020. These diseases are also financially devastating. From 2018 to 2019, cardiovascular disease cost the United States an estimated $407.3 billion in direct and indirect costs (Tsao et al. 2023, e101). One subset of cardiovascular diseases is arterial disease. Arterial disease affects the ability of arteries to function correctly, and a common cause is stenosis, which is a narrowing of the interior of the artery. Stenosis can be caused by atherosclerosis, clots, and vasculitis. When this happens to arteries outside of the coronary and cerebral vasculature, it is known as peripheral artery disease (PAD). In 2020, the AHA estimated PAD to have caused 70,000 deaths worldwide. While this amount may seem small when compared to all cardiovascular diseases, it does not adequately convey the dangers of PAD. It has a wide prevalence, with an estimated 110.32 million cases globally (e582). The risk of developing PAD is between 19% and 30%, with the higher risk belonging to minority populations (e571). PAD can cause a decrease in quality of life, mobility loss, stroke, loss of limb, other cardiovascular diseases, and death (e575).

The primary treatments for PAD are lifestyle changes and pharmaceutical therapies, but surgical interventions are widely available and used regularly (e573). One common surgical treatment is percutaneous transluminal angioplasty or PTA. Over 200 million PTA procedures were performed in 2018 in the United States (e610). The main challenge with PTA is the effectiveness of the procedure. Assorted studies have investigated the initial and long-term success of PTA performed in different regions of the body. Initial treatment success rates are as high as 82-95%, but long-term patency rates can decrease rapidly. At twelve months, primary patency rates are between 36% and 95%, depending on where in the body PTA occurs. Patency rates continue to decline as more time passes since the initial treatment and retreatment is often necessary (Bonvini et al. 2011, 795-797; Goode, Cleveland, and Gaines 2013, 1150-1151; Kasapis et al. 2008, 51; Laird et al. 2012, 5-6; Mousa et al. 2012, 423-424; Mustapha et al. 2016, 3; Schillinger et al. 2007, 2747-2748; Snyder et al. 2023, 11; Tepe et al. 2014, 497-499; Vossen et al. 2018, 694; Xu et al. 2018, 2349-2350). The reasons for this are still being investigated. This study contributes to that investigation by finding how an artery's passive mechanical properties and microstructure change after undergoing PTA.

Background

Arterial Composition and Architecture

Arteries may appear to be simple tubular structures but are complex tissues with both living cells and non-living components. The non-living components of an artery are extracellular matrix, collagen, elastin, other compounds such as proteoglycans, and tissue-bound water. The cellular component includes endothelial cells, fibroblasts, and

smooth muscle cells (SMCs). The SMCs affect the mechanical properties of the artery by actively dilating or constricting it (Vito and Dixon 2003, 415).

Collagen is a structural protein found throughout the body. Individual collagen α-chains form the tropocollagen molecule, which has a triple helix structure. Those helices gather into small fibrils, which bundle into the larger collagen fibers in living tissues. Collagen contributes to the stiffness of the artery, especially at larger stretches, and helps keep the artery from rupturing (Giudici, Wilkinson, and Khir 2021, 256-257). When microscopically imaged, unloaded collagen looks curly or wavey and will have a pattern of stripes called D-bands. This is due to the triple helical structure of tropocollagen and how it bundles together into fibrils. When collagen is loaded, the waves will straighten out, and then the fibers and molecules will begin to stretch. The collagen will fail if stretched enough, and the damage can be seen in the triple helix that forms its microstructure (Converse et al. 2018, 314; Krasny et al. 2017, 346-347).

Elastin is the last major component to be discussed here. As its name suggests, elastin contributes to the elastic behavior of the artery, especially at lower stretches. This is due to elastin having a stiffness much lower than collagen. Elastin also possesses a helical or coiled microstructure. Elastin forms an amorphous group that becomes part of the larger elastic fibers seen in many tissues (Giudici, Wilkinson, and Khir 2021, 256-2567; Yu, Wang, and Zhang 2018, 745-748).

Before discussing how these components are arranged within an artery, it is important to know how an artery's structure changes depending on its location in the body. Arteries are categorized as elastic or muscular. Elastic arteries are closer to the heart and include the aorta, carotid, and iliac arteries. Arteries farther from the heart, such

as femoral, celiac, and cerebral arteries, are considered muscular. Elastic arteries usually have larger diameters than their muscular counterparts. Elastic arteries will also have more elastic laminae that are more prominent than laminae in muscular arteries. These structures will be explained in more detail shortly. The transition from elastic to muscular arteries is gradual, so some arteries do not fit neatly into either category, but these are rare (Holzapfel, Gasser, and Ogden 2000, 5-6). Since most of this study was performed in porcine carotid arteries, an elastic artery, the descriptions of arterial architecture will focus on elastic arteries.

Arteries are composed of three layers: the intima, media, and adventitia. The innermost layer is the intima. The intima's primary function is to isolate the blood flowing through the artery from the interior components of the artery. It is a very thin layer of endothelial cells attached to the basement membrane on the inside surface of the artery. It has been shown to not affect the mechanical properties of the artery in a meaningful way (Holzapfel, Gasser, and Ogden 2000, 6; Vito and Dixon. 2003, 414-415).

The media is the middle layer of the artery, and it is the largest layer as well. The media is made of concentric layers of SMCs, collagen, elastin, and glycosaminoglycans sandwiched between elastic laminae. The elastic laminae are made primarily of elastin and form tight rings or hoops throughout the artery wall with little variation in the direction of the elastin fibers. Small gaps in each lamina, called fenestrations, also help different compounds transport through the artery wall. The elastin between the laminae has a much more varied orientation than that in the laminae. Near the intima, the elastin is arranged more along the length of the vessel; it then transitions to a circumferential orientation in the middle of the media and then switches back to a longitudinal

arrangement near the adventitia (Giudici, Wilkinson, and Khir 2021, 257-258). The collagen within the media is also mainly oriented circumferentially around the artery. Some studies have shown that small layers of collagen near the borders of the media vary from the circumferential direction, but the size of the variance and the amount of collagen in the layers are small compared to the entire media and artery (Ghazanfari et al. 2012, 55-58; Holzapfel, Gasser, and Ogden 2000, 6; Sáez et al. 2016, 188-191). Due to the size and organization of the media, it has been found to have the most significant effect on the artery's mechanical properties (Giudici, Wilkinson, and Khir 2021, 257).

The outermost layer of the artery is the adventitia. The adventitia couples the artery to the surrounding tissues. Large collagen fibers, ground substance, elastin fibers, and collagen- and elastin-producing cells are found in the adventitia. In larger arteries, the vasa vasorum, a system of small blood vessels that provide blood to the outer layers of the artery, is also present (Holzapfel, Gasser, and Ogden 2000, 5-6; Vito and Dixon, 2003, 415). It has been found that the range of adventitial collagen and elastin orientations is wider than their medial counterparts, but both are mostly circumferentially oriented (Giudici, Wilkinson, and Khir 2021, 257-258).

Arterial Tissue as a Material

The proceeding description should make it clear that arterial tissue is complex. This means that more mundane material descriptions do not capture all the nuances of its behavior. In short, arteries are heterogeneous, anisotropic, incompressible, viscoelastic, composite materials. The heterogeneous nature of arteries is apparent from their composition and organization. Arteries are made of many components that all respond to

stress differently. The orientation of those components also causes the anisotropic nature of the artery. An artery will display different stiffnesses in the axial and circumferential loading directions. Another fact gathered from the structure of the artery is that arterial tissue is a composite material. The collagen fibers, elastin fibers, and SMCs are all embedded into the ground substance, which is a different material. The fibers help to reinforce the ground substance in preferred directions similar to engineering materials such as fiberglass or carbon fiber reinforced composites. Water is present in all biological soft tissues, and this includes arteries. At physiological conditions, water is considered incompressible, and this causes arteries to be considered incompressible as well. This means that the volume of the arterial tissue is assumed to be constant while it is being loaded and unloaded during normal physiological conditions, PTA treatments, and the experimental procedures performed in this study. The qualities of viscoelastic materials are hysteresis, creep, and stress relaxation, all of which arterial tissue displays. Adequately preconditioning the artery allows for a repeatable, consistent material response to be found that accounts for the viscoelastic behavior of the artery. The last feature to note is arteries carry residual stress even when in a load free state. This can affect the accuracy of some material models (Holzapfel, Gasser, and Ogden 2000, 7-10; Humphrey 2003, 10-11; Vito and Dixon 2003, 416-419). As previously discussed, the SMCs are living cells that actively adjust the mechanical response of the artery. To observe passive mechanical properties, the SMCs must be deactivated. One way this is accomplished is by storing the arteries in calcium ion-free phosphate-buffered saline (PBS).

The Angioplasty Procedure and the Artery's Response

In PTA, the surgeon accesses the vasculature through a large artery, such as the femoral artery. They guide a wire to the affected site using angiography, which uses X-ray and contrast fluid to provide video of the vasculature and the wire. An angioplasty balloon is inserted; it is advanced over the guide wire to the affected site and is inflated to a set pressure that depends on the balloon. The balloon may be deflated and reinflated several times at the surgeon's discretion. The balloon and guide wire are then removed. Depending on the patient, this procedure may involve more steps, such as performing angioplasty on multiple locations, employing a catch or filter downstream of the procedure site to prevent any plaques or clots from escaping further into the vasculature, delivering medication to the treatment site, or deploying a stent.

The artery's physiological response to PTA has been well documented and will be summarized here. During the actual PTA procedure, the artery experiences an overstretch in the radial direction, and the entire artery wall is compressed. The layer of endothelial cells that are part of the intima may be disrupted or completely removed by this overstretch and compression. This exposes the media and adventitia to the blood flowing within the artery. The collagen and other components of the media and adventitia are thrombogenic, which can help start the healing process but can also lead to future issues if thrombosis is too active. Within the first hour post-procedure, the artery begins the repair process. Platelets gather at the intima, fibrin accumulates, and neutrophils arrive at the treatment location. During the second hour, chemical precursors of repair, such as P-selectin, mRNA, and other proteins, are found at the treatment site, and the neutrophils have spread to the area surrounding the treatment site. Around six hours posttreatment,

the neutrophils reach their peak activity level. At 24 hours posttreatment, the damage from PTA is more apparent. The damage to large-scale fiber units is evident, and SMCs have started to necrose and be removed by macrophages. Thrombotic occlusion has also been observed as early as this stage of arterial recovery. During the next seven days, the endothelium will have mostly regrown, and the number of neutrophils and platelets will return to normal levels. The SMCs will begin to proliferate, and the intima will also thicken. Intimal thickening and SMC proliferation are thought to contribute to potential future restenosis or artery blockage. Signs of restenosis or blockage can be observed at this time as well. Two months after treatment, the regrown endothelium and SMCs are considered mature, but signs of damage and healing and intimal thickening can persist for six months or even longer (Badimon et al. 1998, 309-312; Cottin et al. 2000, 1391-1394; Okamoto et al. 2001, 2229-2234; Steele et al. 1985, 106-110). While these physiological processes are well documented, the changes to the artery's mechanical properties have not been as thoroughly investigated.

Conclusion and Goals

In conclusion, PAD is a life-affecting condition with a widespread and growing prevalence. A common form of treatment is PTA, but it suffers from a significant rate of ineffectiveness, especially in the long term. This is attributed to the complexity of arterial tissue and open questions regarding how arteries are affected by PTA. This study investigates how PTA changes the passive mechanical properties of porcine carotid arteries and connects those changes to microstructural damage in the artery. It will also

provide exploratory data about the effects of PTA on various locations in the vasculature and how those effects are recovered over time.

CHAPTER 2

IN VITRO CAROTID ARTERY EXPERIMENTS

Purpose of Study

This study seeks to understand how ballon angioplasty changes an artery's passive mechanical response and microstructure. This was done by characterizing the circumferential and axial properties of carotid arteries before and after in vitro angioplasty. Microstructural effects were investigated using histological data to evaluate the amount of damaged collagen and visible changes to the structures of the arteries. The experimental procedure, detailed below, was developed based on the protocols described in previous publications (Converse et al. 2018, 308-10; Converse et al. 2021, 3541-2; Mogharrabi et al. 2019, 2-3).

Sample Acquisition and Preparation

Carotid arteries from six to nine-month-old pigs were used for this study. The arteries were purchased from Animal Technologies Inc. (Tyler, Texas) and shipped overnight on ice. Once the arteries were received, they were stored in refrigerated calcium-free PBS so the smooth muscle cells within the arteries would be deactivated, and only the passive response of the artery would be measured. All testing was conducted within 48 hours of receiving the arteries.

Straight arterial segments around 45 mm long, with minimal tapering, no branching vessels, and no holes, were selected to streamline the preparation, testing, and data analysis. Extraneous tissue was removed from the arteries using a dissection scope, surgical scissors, and other dissection tools. Rings, approximately two to three millimeters in length, were removed from both ends of the artery. The rings were imaged next to a scale, and the images were processed using a MATLAB script (see Appendix) to find the average cross-sectional area for the artery. The rings were then saved to serve as control samples for the histological procedures. Barbed luer fittings were inserted into the ends of each artery, and then the ends of the artery were tied and glued down to the fittings using 3-0 suture and cyanoacrylate glue. After the glue had cured, the artery was placed in a petri dish of PBS to hydrate and support the entire artery. The suture-to-suture length was measured and recorded as the resting length of the artery, which was shorter than the 45 mm selection length due to the preparation procedures. The prepared artery and control rings were stored in vials of refrigerated PBS until they were removed from the refrigerator and allowed to come to room temperature before testing.

Testing Equipment

A custom vertical myograph, shown in Figure 1, was used for the mechanical testing of all arteries. The arteries were mounted to adjustable blocks on the stages of the myograph, allowing any torsion or misalignment in the artery to be removed before testing. The stages are moved simultaneously by a lead screw driven by a stepper motor with an encoder. This allowed the center of the artery to remain stationary while the ends of the artery were moved to achieve the desired axial stretch. Axial forces were measured

using a 1.1 kg load cell (MDB-2.5, Transducer Techniques) attached to the artery's top and the myograph stage. A series of tubes connected to the myograph stages supply PBS to the interior of the artery. This is used to pressurize and hydrate the artery. PBS was also periodically applied to the artery's exterior surfaces to prevent dehydration. A linear actuator connected to a syringe pump was used to control the flow of PBS in the system and pressurize the artery. Figure 2 shows a detailed view of the balloon access port that allowed the artery to be treated with angioplasty while still on the myograph. This allowed for a faster testing procedure and removed potential sources of variability during the experiment. A standing water column of the proper height was used for any test that required constant pressure. The pressure was measured using a pressure transducer (Honeywell, MicroSwitch 26PCDFM6G). The sensors were sampled at 100 Hz, and the data were collected using an SCXI-1520 from National Instruments. The sensor data were later filtered to the SAE J211 standard using a Butterworth, 4-pole, phaseless filter. A Pixelink PL-A641 digital camera recorded three images per second during the testing procedures. The data were then upsampled to match the 100Hz sampling rate of the other sensors. Equipment was controlled using NI LabView software and a custom visual interface.

Mechanical Testing

After coming to room temperature, the artery was mounted into the myograph. The artery was preconditioned to control the effects of viscoelasticity and ensure that the artery’s mechanical response was repeatable and consistent. Preconditioning was accomplished by cycling the fluid pressure between 6.7 and 22 kPa five times while the

artery was held at a particular axial stretch. This was repeated at larger axial stretches until the artery was stretched slightly beyond its in vivo length. The in vivo length was identified as the length of the artery at which the axial force would not change during the pressure cycles. After finding the in vivo length, the circumferential and axial properties were characterized. Circumferential evaluation was performed by holding the artery at a constant length and cycling the pressure between 6.7 and 22 kPa. These evaluations were done at in vivo length, 1.05 times the in vivo length, and 1.075 times the in vivo length. Axial evaluation was performed by maintaining a constant pressure and cycling the length of the artery from a buckled state to 1.1 times the artery's in vivo length. Evaluation was done at 6.7 kPa and 13.3 kPa. For this study, the test sequences closest to the in vivo state (i.e., the in vivo length circumferential test and the 13.3 kPa axial test) were later analyzed.

After the initial characterization, angioplasty was performed on the arteries. The artery was set to its in vivo length and drained of fluid. A 5 mm angioplasty balloon was inserted into the artery through the access port, inflated to 1013.25 kPa (10 atm), and held for one minute. The balloon was then deflated and removed from the artery. The characterization procedure was performed again, as outlined above, with one additional step- the treated arteries were circumferentially evaluated at the pre-angioplasty in vivo length.

Histology

After characterization, the arteries were removed from the myograph and the luer barbs. The arteries were then fixed in paraformaldehyde and prepared for cryosectioning.

A ring was removed from the characterized artery, and then the artery and one of the control rings were cut open along their lengths. The arteries were then frozen in optimal cutting temperature (OCT) compound. The cut-open samples were frozen while pressed flat under metal weights so that the samples did not curl shut. All samples were sliced using a Leica cryostat set to cut 50-µm thick sections. The flattened samples were sliced through the thickness of the arterial wall, meaning each slice was from a different location within the intima, media, and adventitia. The ring samples were sliced to create cross-sections perpendicular to the vessel axis. The slices were rinsed with deionized water and refrigerated until stained.

Staining and Imaging Procedure

Collagen hybridizing peptide (CHP) was used to stain the arteries after slicing. CHP binds to denatured collagen and can indicate damage. Slices from each ring and the media of each arterial wall were selected for staining with CHP. Medial slices were selected because past research has shown that damage from circumferential loading is mainly found in the media where fibers are primarily oriented circumferentially (Converse et al., 311). The samples were stained in 5-µM red CHP (Collagen Hybridizing Peptide, Cy3 Conjugate, 3Helix Inx.) for 12-18 hours according to the manufacturer's instructions. The samples were then put into a well plate with deionized water and placed on a shaker plate for 30-60 minutes. This was repeated with clean deionized water for a total of three rinses. After rinsing, the slices were laid flat on glass microscope slides and covered with mounting media (Flouromount F, Southern Biotech) and a cover slip. Samples were imaged using a Nikon A1plus laser scan confocal

microscope set to 4x magnification. The red CHP signal was excited with the 561 nm laser and emitted at 595 nm, and the blue elastin autofluorescence channel was excited with the 405 nm laser and emitted at 450 nm. The final image is a mosaic formed by the microscope's control software to have the entire sample in a single image.

Data Processing

Mechanical Data

The force, pressure, position, and histological data were used to calculate the axial and circumferential stretch and stress using Equations (1), (2), (3), and (4)

$$\lambda_\theta = \frac{d_i + d_o}{D_i + D_o} \tag{1}$$

$$\lambda_Z = \frac{l}{L} \tag{2}$$

$$T_\theta = p_i\left(\frac{d_i}{d_o - d_i}\right) \tag{3}$$

$$T_z = \frac{\lambda_z}{A}\left(F_Z + \frac{\pi}{4} p_i d_i^2\right) \tag{4}$$

where λ_θ is the circumferential stretch ratio, d_i and d_o are the current inner and outer diameters of the artery, D_i and D_o are the inner and outer diameters of the artery in its load-free configuration, λ_Z is the axial stretch ratio, l is the current axial length, L is the load-free axial length, T_θ and T_Z are the circumferential and axial Cauchy stresses, p_i is the current internal pressure, A is the load-free cross-sectional area, and F_Z is the axial force. The inner diameter, d_i, was found by assuming the artery is incompressible or maintains a constant wall volume throughout the characterization procedures (Converse and Monson 2021, 3). To qualitatively compare them, a plot of the stress-stretch response was made for each artery before and after treatment. An exponential equation of the form

$$y = ae^{b(x-x_{offset})} + y_{offset} \quad (5)$$

was fit to the stress-stretch data. The variables *a* and *b* are constant coefficients, and the offset terms, x_{offset} and y_{offset}, allow for a better fit to the experimental data. They may correspond to a residual stress or strain, but that claim would need further investigation. The resulting curve fit was used to calculate the stress and the stiffness at any stretch value. Stiffness was defined as the slope of the curve at the in vivo stretch ratio. The parameters used for comparison were the in vivo stretch ratio and the stress and stiffness at the pre-angioplasty in vivo stretch ratio. Figure 3 shows graphically how these values are found and what they correspond to on the stress-stretch curves. These were found for both the axial and circumferential characterization data. The measurements were taken from the same samples before and after angioplasty, so a paired t-test was used to determine if the changes were statistically significant. Linear regression was also performed to determine whether trends between the angioplasty-induced overstretch and changes in the comparison measures were statistically significant. This was done by comparing the percent change in each measurement parameter with the percent change in circumferential stretch during the angioplasty procedure. The percent change accounted for any influence a higher or lower pretreatment measurement parameter may have on the posttreatment parameter value. For example, an artery with a larger in vivo stretch ratio will naturally have a larger stretch ratio during and after angioplasty.

Histological Data

The images from the red laser wavelengths (450 nm) were analyzed to determine the amount of CHP binding in the arteries. The images were processed through a

MATLAB script (see Appendix) that first applied a digital mask to the images to remove any bright spots or artifacts unrelated to arterial damage. Next, the script determined the mean brightness of the images designated as control samples and set a threshold value equal to two standard deviations above that mean (Anderl et al., 2023, 284). Any pixel in the image and the corresponding treated images brighter than the threshold was considered a bright pixel. The percentage of bright pixels between the control and treated images was then compared and used to indicate collagen damage (Converse et al. 2018, 310).

The intensity of the pixels was used to find other comparison metrics. First, pixel-intensity histograms were generated for each image and plotted in groups from the same artery. This allowed for a qualitative comparison between the pretreatment and treatment groups. The range of the histograms was reduced to allow for better visibility of the differences between the groups. The mode of the pixel intensity was calculated as it corresponds to the tallest peak of the histogram and serves as a good indicator of the overall brightness of the artery without being sensitive to a few overly bright or dim pixels. The mean pixel intensity was also calculated. Any pixel with zero intensity was excluded from the mean and mode calculations so the results from an image with space around the slice of artery would not be artificially reduced.

The last measurement derived from the images was waviness ratios. Waviness ratios are used to see how the wavy fibers and layered structures in the arterial wall change due to different loading conditions and stresses (Chen et al. 2011, 2558; Roy et al. 2010, 89). Waviness ratios are found by measuring the length of a wavy collagen fiber or elastin layer and comparing it to the length of a non-wavy curve that most accurately fits

the structure's shape. This study calculates the ratio by dividing the wavy length by the non-wavy length so that a perfectly non-wavy structure has a ratio equal to one, and wavier structures will have ratios greater than one. The blue channel (450 nm) of the imaged rings was analyzed using an ImageJ plug-in called NueronJ, produced and validated by Meijering et al. (2004) and used to measure the waviness of arterial structures, like collagen (Rezakhaniha et al. 2012). Five fibers from various locations in each arterial ring image were measured, and then the lengths and a list of order pairs describing the traced fibers were saved. Since the fibers and lamina of the artery are circular, a straight line connecting the endpoints of the fiber would not be an accurate comparison. To account for this, the arc length of a smooth curved line was used instead. First, a circle was fitted to each measured wavy fiber using each fiber's list of ordered pairs. The fit provided the radius and center point of the circle. Two vectors were formed using the endpoints of the wavy fibers and the center point of the circle, and then the angle, in radians, between the two vectors was calculated using the dot product. That angle was then multiplied by the radius from the circle fits to calculate the arc length. The waviness ratio was then calculated by dividing the measured wavy length by the calculated arc length. The ten ratios from the two images from each sample were averaged together, providing a single waviness ratio that can be compared between each artery's pre- and posttreatment sample.

Statistical tests were performed on the different measures to see if any differences were significant. Since each measurement parameter was found before and after treatment, a paired t-test was used. Linear regression was also used to determine if any relationship could be found between the percent change in the circumferential stretch

during angioplasty and the percent change in the measurement parameters shown to have statistically significant differences from the control group. The percent changes were used for reasons similar to the mechanical data.

Results and Discussion

Mechanical Characterization

The carotid arteries used for this study had a mean resting length of 24.94 mm after preparation (range: 21.00-28.00 mm), a mean outer diameter of 4.11 mm (range: 3.77-4.47 mm), and a mean resting cross-sectional area of 7.47 mm2 (range: 6.35-9.29 mm2). Pre-angioplasty axial and circumferential mean in vivo stretch ratios were 1.70 (range: 1.59-1.84) and 1.28 (range: 1.08-1.69), respectively. During angioplasty, they reached a mean circumferential stretch ratio of 1.54 (range: 1.40-1.71).

Circumferential Results

Our results show that angioplasty causes circumferential softening in porcine carotid arteries. This can be observed in the circumferential stress-stretch response curves in Figure 4. Every artery's response was shifted to the right following angioplasty, which shows the artery has softened. A greater amount of circumferential stretch is needed to reach the same amount of stress seen in the artery pretreatment. These results are consistent with those seen in Converse and Monson (2021), which showed that applied loads cause softening in the direction of the load (6-9). A visual inspection of the stress-stretch responses and stretches during angioplasty suggests that a larger circumferential stretch may cause a greater degree of softening in the artery.

The quantitative measurements support the observations seen in the stress-stretch curves. A significant increase ($p=0.0015$) in the in vivo circumferential stretch was seen posttreatment, as shown in Figure 5 and Table 1. This means that the in vivo configuration caused the artery to stretch farther posttreatment, indicating it has softened. This softening is also seen in the in vivo circumferential stress, which significantly decreased ($p=0.0094$) posttreatment, as shown in Figure 6 and Table 2. The in vivo circumferential stiffness was significantly reduced ($p=0.0109$), as seen in Figure 7 and Table 3. Posttreatment arteries also displayed less variability than pretreatment. This could be due to angioplasty causing the microstructure of the arteries to align in similar configurations, making the arteries behave more like each other. All three of these measures show that angioplasty has softened the circumferential properties of the artery and is consistent with previous studies (Converse and Monson 2021, 6-9).

Trying to correlate the softening experienced by the artery with the stretch experienced during angioplasty provided mixed results. No correlation was found between the percent change in the in vivo circumferential stress and the percent change in stretch during angioplasty (R squared=0.0007, Significance F=0.950), as seen in Figure 8 and Table 4. The percent change in the in vivo circumferential stiffness and the percent change in stretch during angioplasty also displayed a lack of correlation (R squared=0.238, Significance F=0.2199), as seen in Figure 9 and Table 5. The lack of correlation with these measures could be due to the small sample size hiding the correlation, or the relationship could be nonlinear. It could also be due to the complexities of the loading during angioplasty and the number of factors that influence the material properties of the artery.

An interesting correlation was found between the percent change in the in vivo circumferential stretch ratio and the percent change in stretch during angioplasty (R squared=0.813, Significance F=8.89E-04) shown in Figure 10 and Table 6. This suggests that the greater an artery is stretched during angioplasty, the more its in vivo circumferential stretch ratio increases posttreatment. This makes intuitive sense and shows that angioplasty can cause a significant change in the mechanical properties of the artery. Next, we investigated if there was a way to translate this correlation into something that could have clinical use. Calculating the circumferential stretch ratio would require knowing the inner and outer diameter of the artery in the load-free state, the in vivo state, and during angioplasty. Furthermore, while the percent change calculation is relatively easy, we doubt many clinicians would want to perform all these calculations during a procedure. To avoid this, we investigated if any more easily measured parameters also displayed a relationship like that between pre- and post-angioplasty circumferential stretch ratio. We found a significant linear regression (R square=0.752, Significance F=2.45E-03) between the amount the diameter increased from the in vivo configuration during angioplasty and the amount the in vivo diameter remained increased posttreatment, shown in Figure 11 and Table 7. This suggests that the increase in an artery's diameter after angioplasty is related to the change in the diameter experienced during angioplasty. These are easily measured dimensions that could help inform treatment decisions, such as the size of the angioplasty balloon and how much to inflate it. Further investigation would be needed to know the exact strength of this relationship and if it extends to healthy and diseased human tissues.

Axial Results

Axial softening was also observed post-angioplasty. The axial stress-stretch responses, seen in Figure 12, show changes similar to the circumferential curves, namely a rightward shift post-angioplasty. The main difference is that the axial response is shifted less than the circumferential response, with some samples showing almost no difference. This suggests that the axial properties were affected less than the circumferential properties, which is logical considering angioplasty mainly acts in the circumferential direction. Quantitative measures support this observation as well. The in vivo axial stretch ratio significantly increased ($p=1.76E-03$), as seen in Figure 13 and Table 8. Like the circumferential results, the arteries stretch further when placed in the in vivo configuration, suggesting softening occurred. While the change is significant, it is worth noting that the magnitude of the change is less than that seen in the circumferential direction. The in vivo axial stress also significantly decreased ($p=0.039$) following angioplasty, as shown in Figure 14 and Table 9. The in vivo axial stiffness was the same and displayed a significant decrease ($p=0.005$) following treatment, as seen in Figure 15 and Table 10. Linear regression was performed individually between the percent change in the in vivo axial stretch ratio (R square=0.023, Significance F=0.396), percent change in the in vivo axial stress (R square=5.9E-05, Significance F=0.986), and percent change in the in vivo stiffness (R square=0.081, Significance F=0.495) with the percent change in circumferential stretch during angioplasty and none displayed significance as seen in Figures 16-18 and Tables 11-13.

The results detailed above demonstrate that the axial properties of the arteries were softened despite being transverse to the loading direction during angioplasty. This is

similar to results previously reported by Convers and Monson (2021). In that study, arteries were loaded axially and displayed axial and circumferential softening, with the circumferential softening being less than axial (6-9). Angioplasty primarily loads circumferentially, which causes the circumferential properties to experience a more significant change than the axial properties. The change in axial properties is due to the circumferential loading during angioplasty, which causes the artery to stretch axially due to the Poisson effect. The exact amount of that stretch is unknown, but it is assumed to be less than the circumferential stretch. This is why the axial properties do not show as extreme changes as the circumferential properties.

Histology Results

Medial Layer Images

The histology results from the medial layer slices support the mechanical properties' data that angioplasty causes damage to arteries, specifically the microstructure. The CHP histograms, Figures 19-27, provide a qualitative glimpse at the changes following angioplasty. They suggest an increase in CHP bound to the artery following angioplasty, indicating an increased amount of damaged or denatured collagen. In every sample, the largest spike of the histogram has shifted to a higher intensity value, and the tails are more extended and taller than pretreatment. Quantitative measurements also support this conclusion. The mean pixel intensity increased significantly ($p=0.0297$) posttreatment, as shown in Figure 28 and Table 14. The change in mean pixel intensity could not be correlated with the stretch during angioplasty (R square=0.390, Significance F=0.072), as shown in Figure 29 and Table 15. The mode of the pixel intensity also

significantly increased (p=0.048), as seen in Figure 30 and Table 16. Like the mean, the change in the mode of the pixel intensity also did not correlate with the stretch during angioplasty (R square=0.001, Significance F=0.627), as shown in Figure 31 and Table 17. Both measures indicate that posttreatment arteries contain greater amounts of bound CHP, which implies greater amounts of damaged collagen. It is unclear why the change in each measure does not correlate to the stretch during the angioplasty procedure. Neither measure may be mathematically sensitive enough to indicate the relationship. Other experimental limitations, discussed later, may prevent the relationship from being apparent.

The bright pixel percentage does not follow the pattern of other qualitative and quantitative measures and previous research. There was no significant difference (p=0.235) between the arteries pre- and posttreatment, as seen in Figure 32 and Table 18. This does not make sense, considering the other signs of damage. This could be due to a few factors. The first is the limitations of the slicing and staining procedure. It is possible that the medial layers from the pretreatment artery do not align perfectly with the posttreatment layers, causing more considerable variations between them, or that the slices selected did not contain the part of the wall most damaged by the treatment. It is also possible that the angioplasty procedure did not stretch the tropocollagen fibers far enough to damage them and create more CHP binding sites but did stretch the fibers far enough to cause them to tighten like a braided rope being pulled and reduced the amount of available CHP binding sites, but this has not been observed previously.

Rings Images

The ring image histology results do not follow the patterns seen with the previous results. An examination of the CHP histograms, Figures 33-41, does not reveal a consistent pattern posttreatment like that seen with the medial layer slices. The mean pixel intensity (p=0.096), see Figure 42 and Table 19; mode of the pixel intensity (p=0.063), see Figure 43 and Table 20; and bright pixel percentage (p=0.069), see Figure 44 and Table 21, displayed no significant changes between the samples pre-and posttreatment. This could be due to the natural variability of the samples or the fact that collagen is either circumferentially or helically oriented in carotid arteries. When a ring is sliced off the vessel, this does not capture much of the length of the collagen fibers, reducing the number of binding sites to which CHP could attach.

The waviness ratios provided more insight into the effects of angioplasty. The waviness ratios suggest angioplasty causes the fibers to straighten out and changes how the artery responds to future loading. The waviness ratio significantly decreased (p=1.65E-05) posttreatment, as seen in Figure 45 and Table 22. This means the fibers in the artery were noticeably straighter and more extended following treatment, which may help explain the changes in the artery's behavior. The shift in waviness ratios did not show any relationship with the stretch during angioplasty (R square=0.166, Significance F=0.276), as shown in Figure 46 and Table 23. This was unexpected but could be due to reasons similar to why the other comparison measures do not correlate with the stretch during angioplasty.

Limitations

There are a few limitations to the experimental procedure. The first is the sample size. Increasing the sample size would be a straightforward way to increase the strength and clarity of the experimental conclusions. The second limitation comes from ordering already dissected carotid arteries from a third party. While the samples received were reasonably consistent, it is unknown what variations existed between animals, the exact time of death, treatment during harvesting, and shipping conditions the entire time while in transit. These factors could influence how the arteries respond to the experimental procedure. The easiest way to mitigate this would be to obtain more detailed documentation from the company providing the tissue, but this may not be available. Another solution would be to obtain whole, intact animals so that every step and variable could be observed and controlled personally. This would increase the cost and difficulty of the procedure, but it would provide the necessary control and the ability to address other potential research questions.

The experimental procedure could also be improved. While global stress and strain calculations were used in this procedure, a more localized strain calculation could provide additional insight into what occurs during and after angioplasty. We were unable to find fiducial markers that functioned adequately with the arteries. Microspheres were prone to movement independent from the tissue, such as being washed away with PBS when the artery was moisturized. Nigrosin dye spots were also investigated, but they appeared to diffuse through the tissue over the course of testing, which caused doubt regarding the accuracy of the measurement. A suitable fiducial marker would allow for a more detailed analysis of the surface strains of the artery. Another limitation is that the

testing setup did not allow for calculating the stress the artery experiences during angioplasty. The procedure did not allow for the recording of the axial force during angioplasty, which is needed to calculate the stress in the artery. Also, the interaction between the angioplasty balloon and the artery wall is complicated and an area of current research. Even though the pressure that the balloon is inflated to is known, it is not known how that pressure translates to the pressure felt by the interior wall of the artery. The last limitation is the inability to measure the inner diameter of the artery while it is being evaluated. Currently, the inner diameter of the artery is calculated assuming that the artery is incompressible and maintains a constant wall volume. While this is an accurate enough assumption, being able to measure the inner diameter and how it changes during the experiment would allow for a more precise description of the artery's behavior without relying on as many of those assumptions.

Conclusion

In conclusion, it has been demonstrated that angioplasty has a statistically significant effect on the arteries that experience it. The arteries' in vivo configuration changes, lengthening axially and expanding circumferentially. The arteries also experience less stress at in vivo configurations and display a lower stiffness axially and circumferentially following angioplasty. Angioplasty also affects the artery's microstructure. The increase in CHP binding following angioplasty indicates an increase in damaged and denatured collagen. The waviness ratios also show that angioplasty stretched and straightened out other parts of the microstructure. It was also observed that the amount of circumferential deformation that remains following angioplasty correlates

to the amount of deformation the angioplasty balloon imposes on the artery while inflated. This has the potential to serve as a useful tool in clinical situations. All these observations can help explain how an artery is different following angioplasty and help improve the procedure and outcomes.

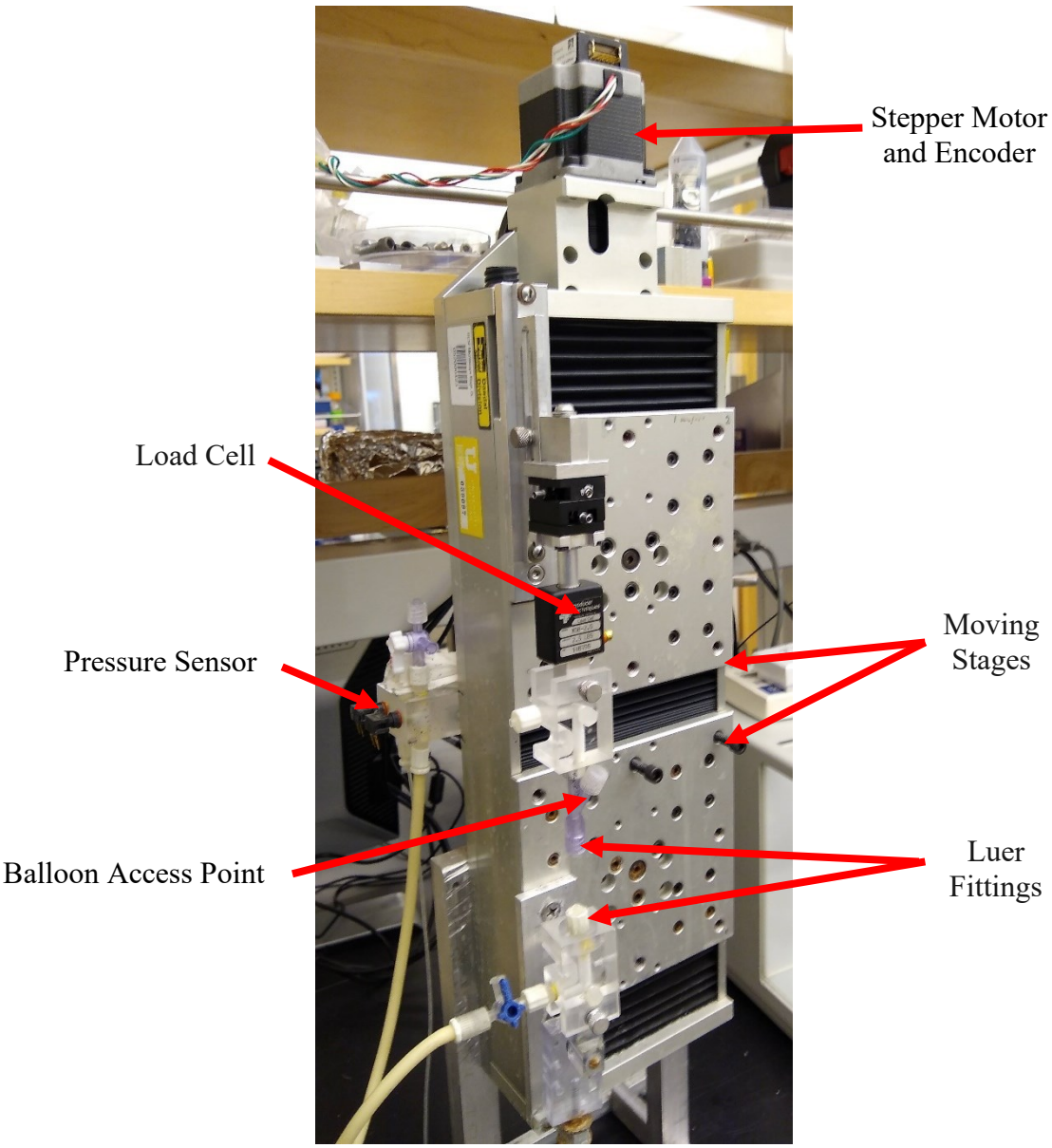

Figure 1 Photograph of custom vertical myograph with the main components labeled.

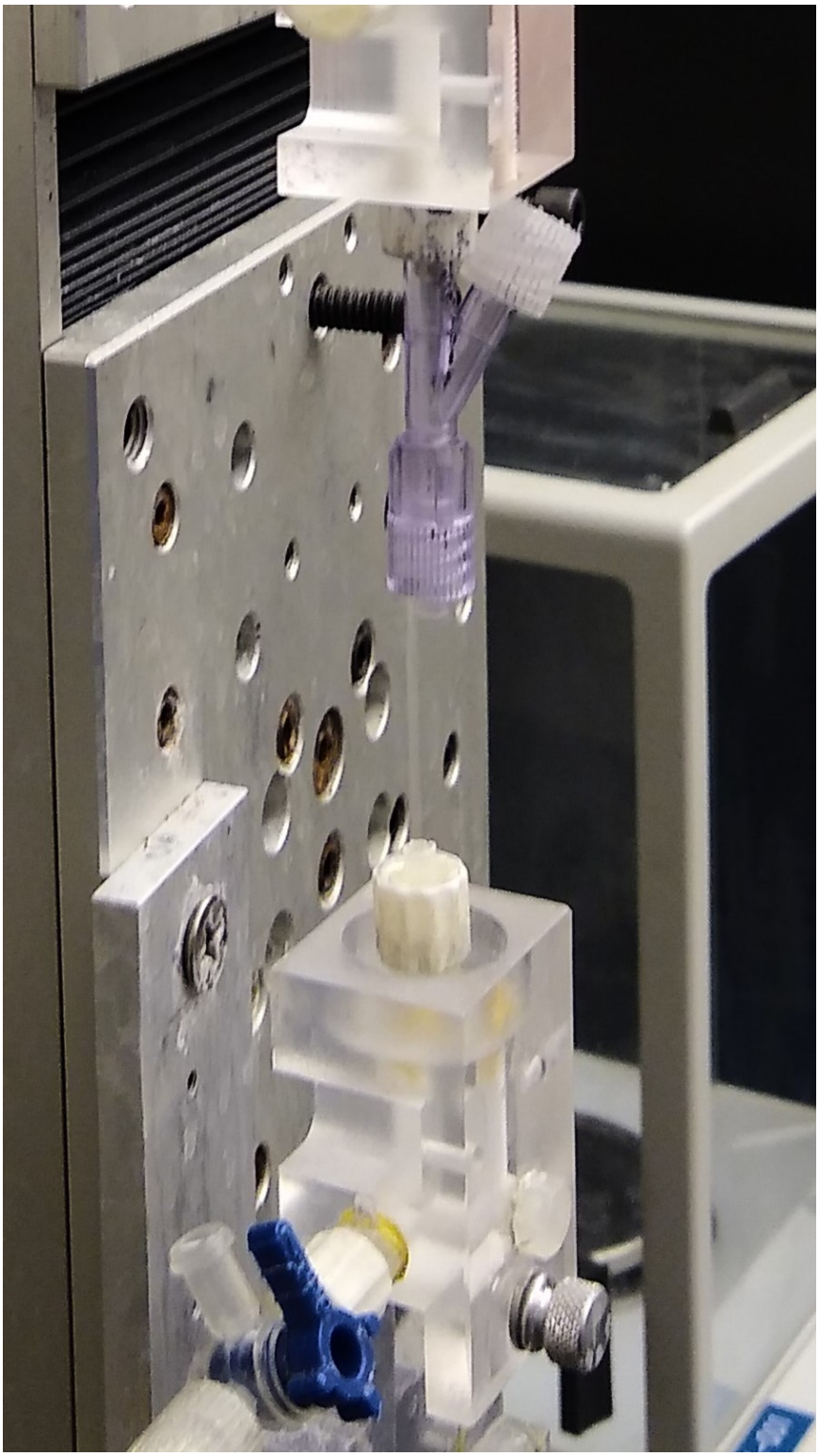

Figure 2 A zoomed-in view of the balloon access port on the vertical myograph.

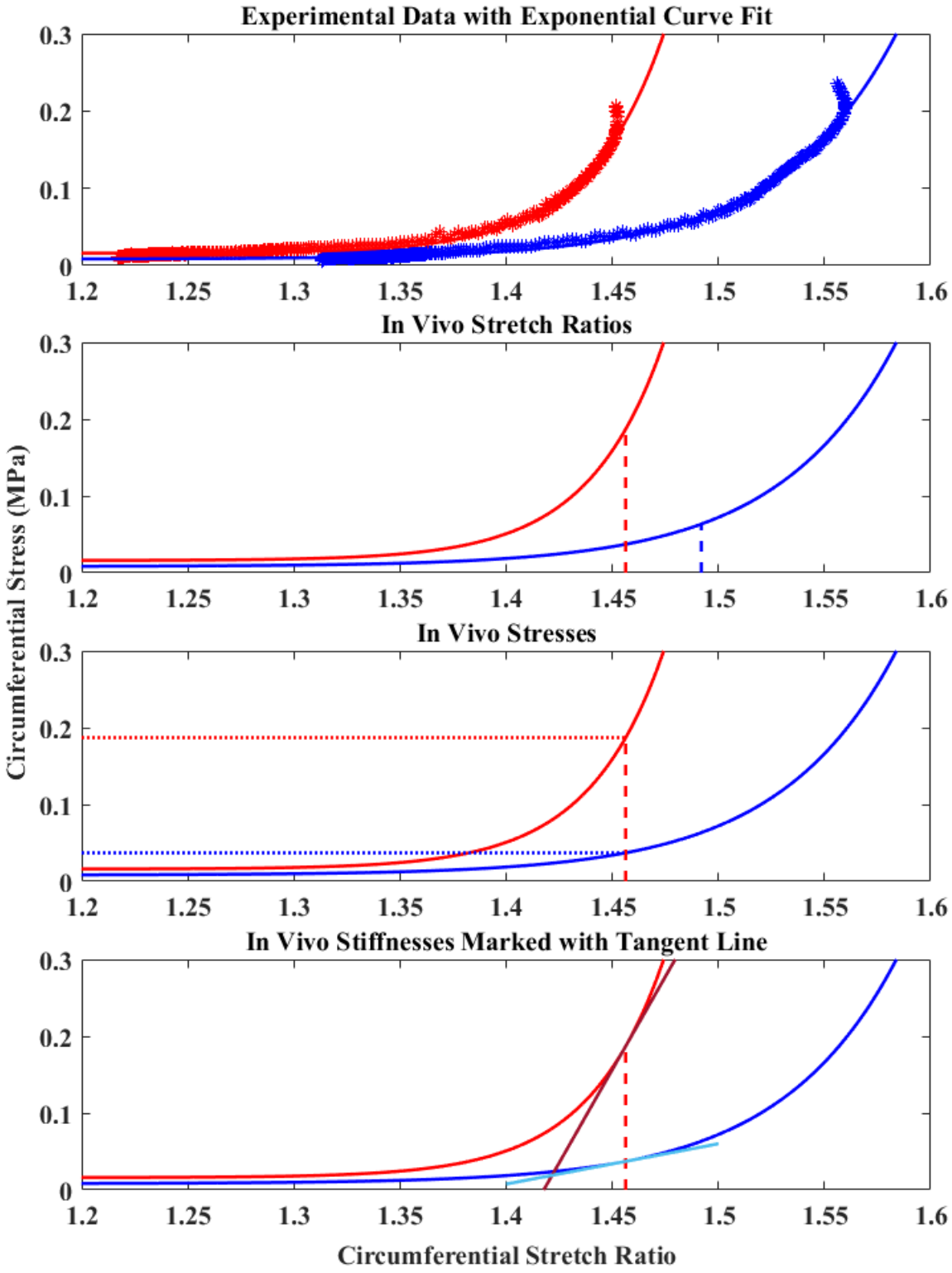

Figure 3 Stress-stretch curves with annotations demonstrating how the in vivo stretch ratio, stress, and stiffness are found and compared. The red lines indicate the sample pretreatment and the blue lines indicate the sample posttreatment.

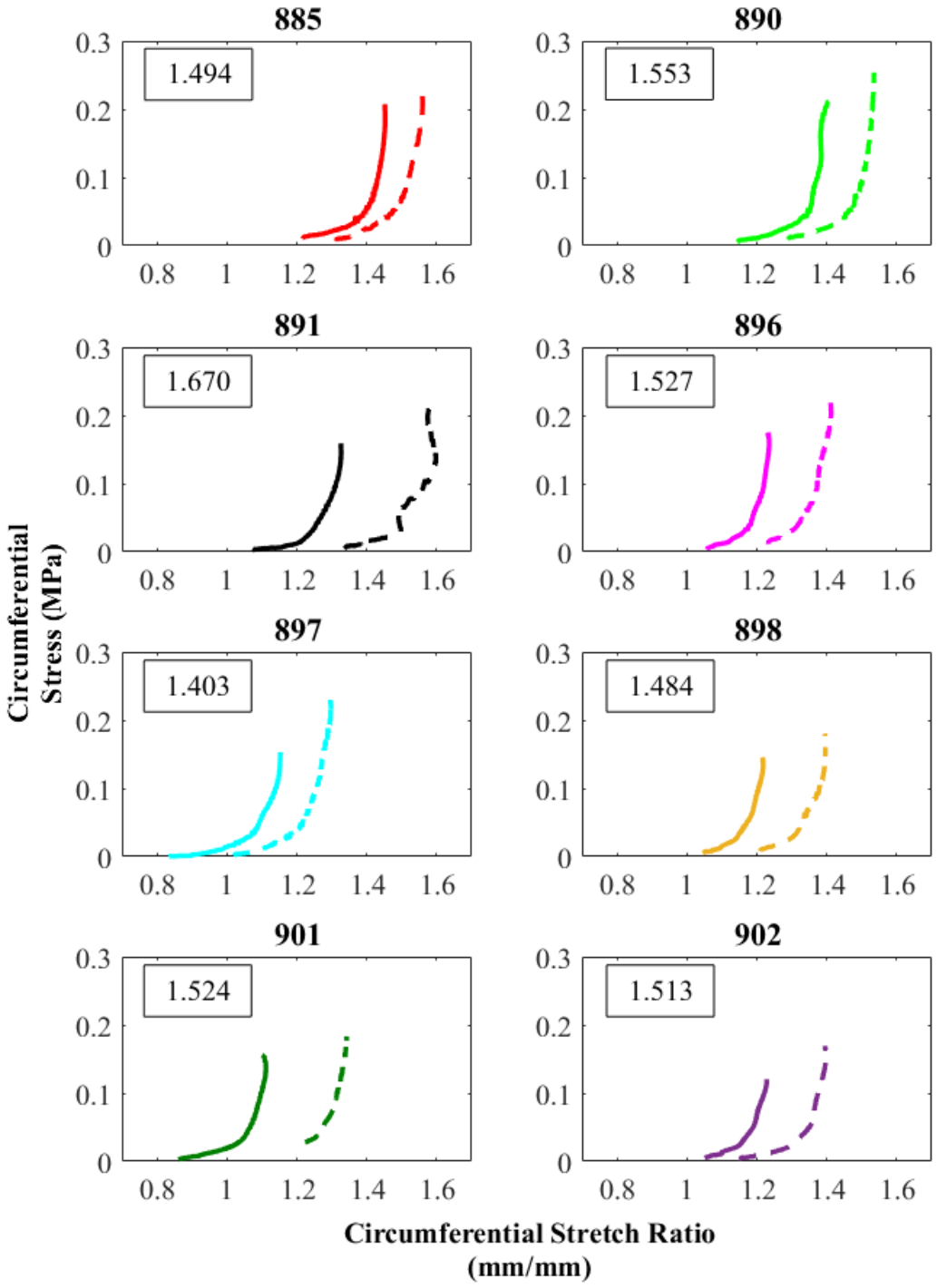

Figure 4 The circumferential stress-stretch responses of the porcine carotid arteries with an individual plot for each sample. Pretreatment is shown as a solid line and treated as a dashed line. The circumferential stretch during angioplasty is the boxed number in each plot.

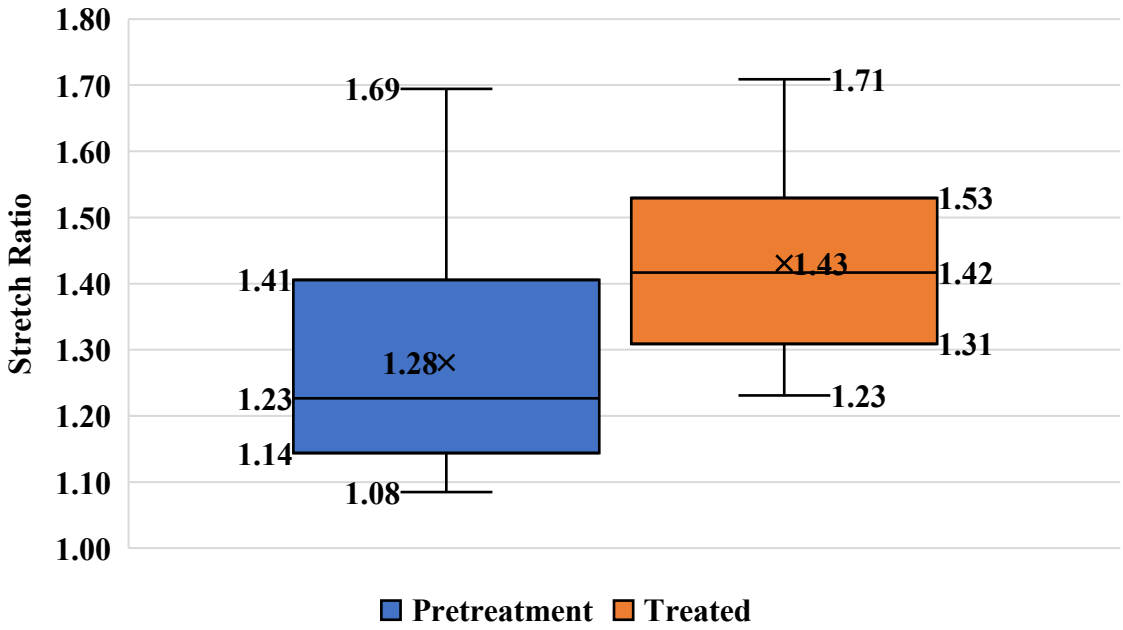

Figure 5 Box and whisker plots summarizing the circumferential in vivo stretch ratio before and after treatment.

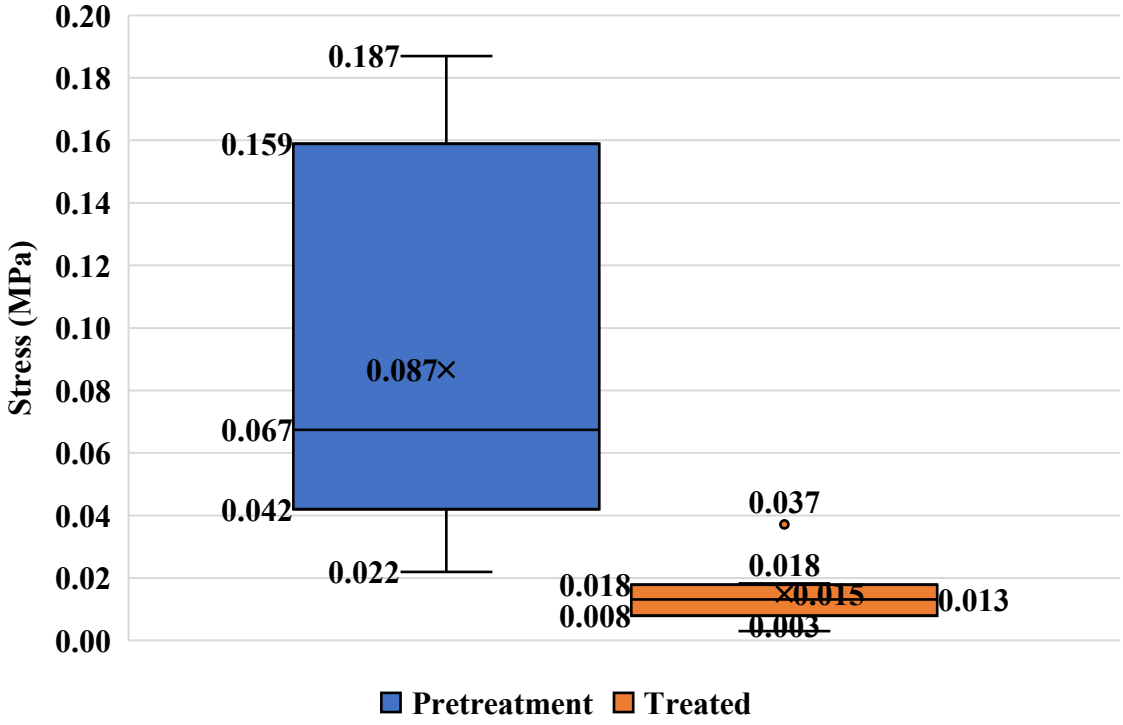

Figure 6 Box and whisker plots summarizing the circumferential stress at the in vivo configuration before and after treatment.

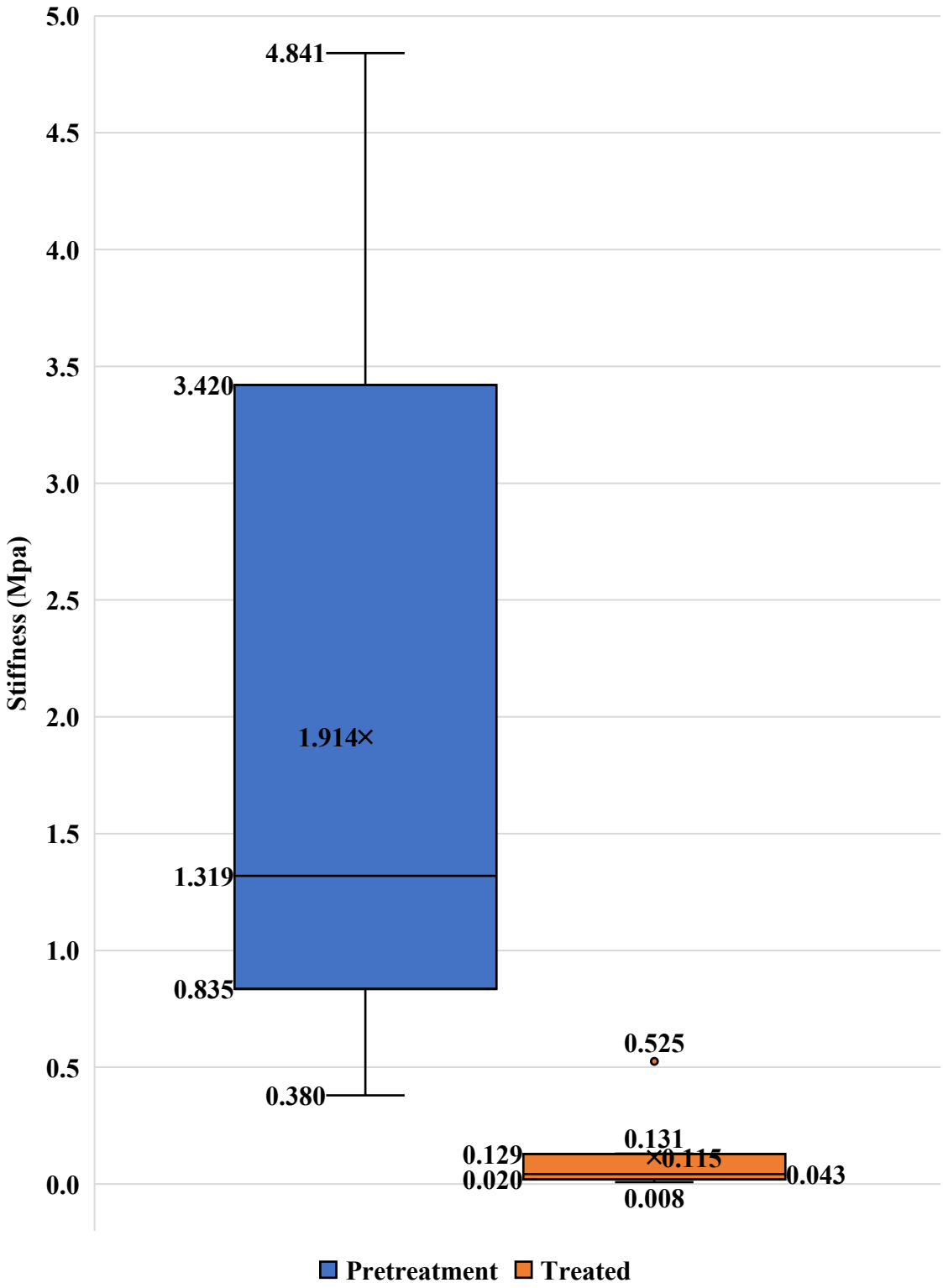

Figure 7 Box and whisker plots summarizing the circumferential in vivo stiffness before and after treatment.

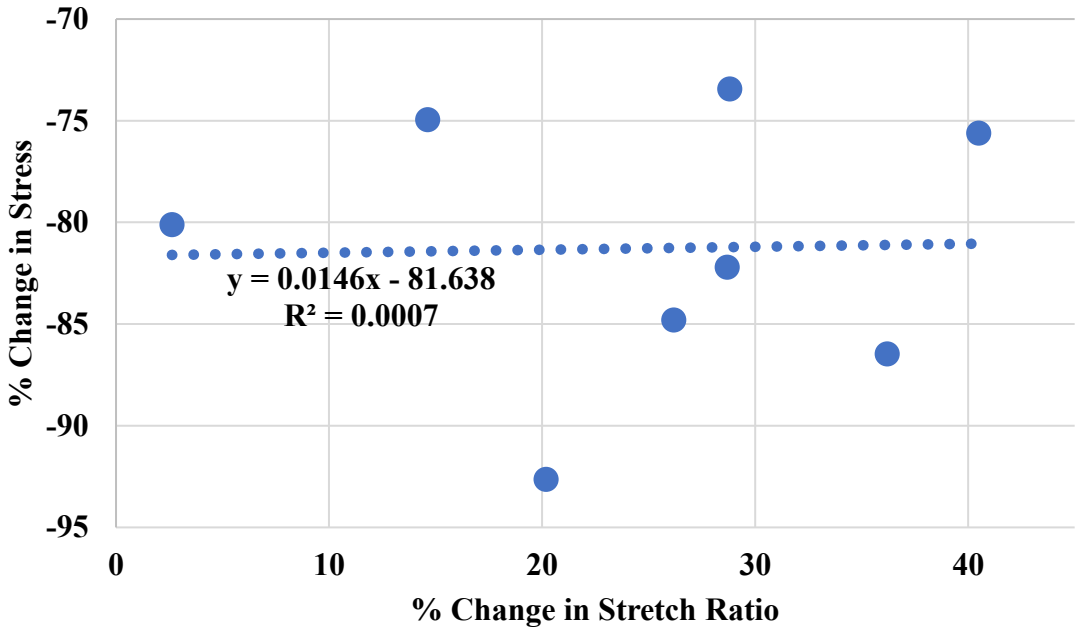

Figure 8 Scatter plot of the percent change in circumferential in vivo stress versus the percent change in the circumferential stretch ratio during angioplasty with a linear trend line and equation fit to the data.

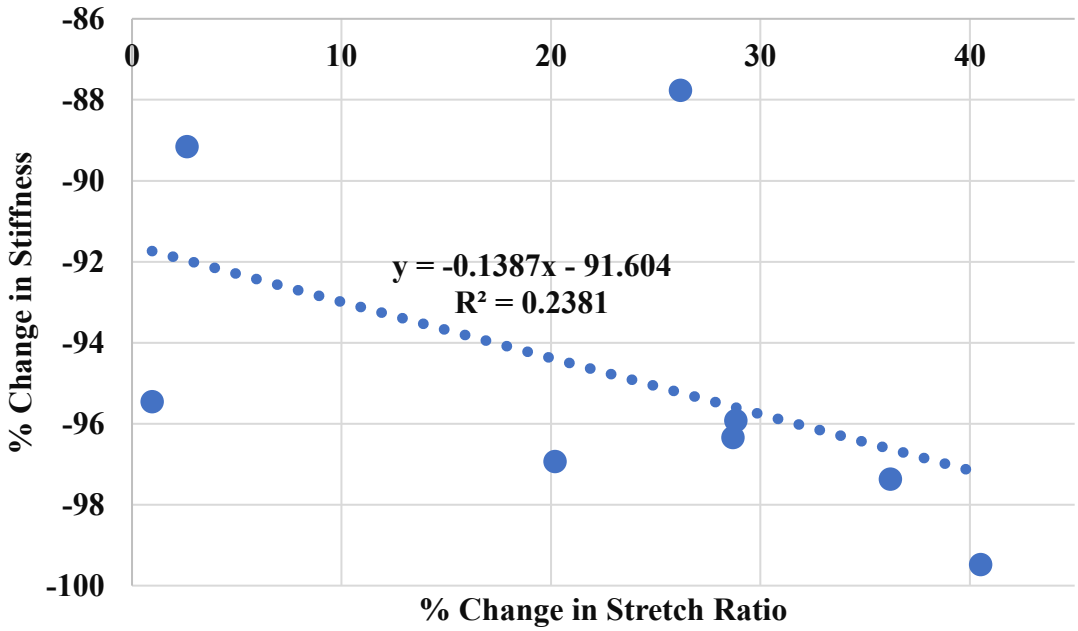

Figure 9 Scatter plot of the percent change in circumferential in vivo stiffness versus the percent change in the circumferential stretch ratio during angioplasty with a linear trend line and equation fit to the data.

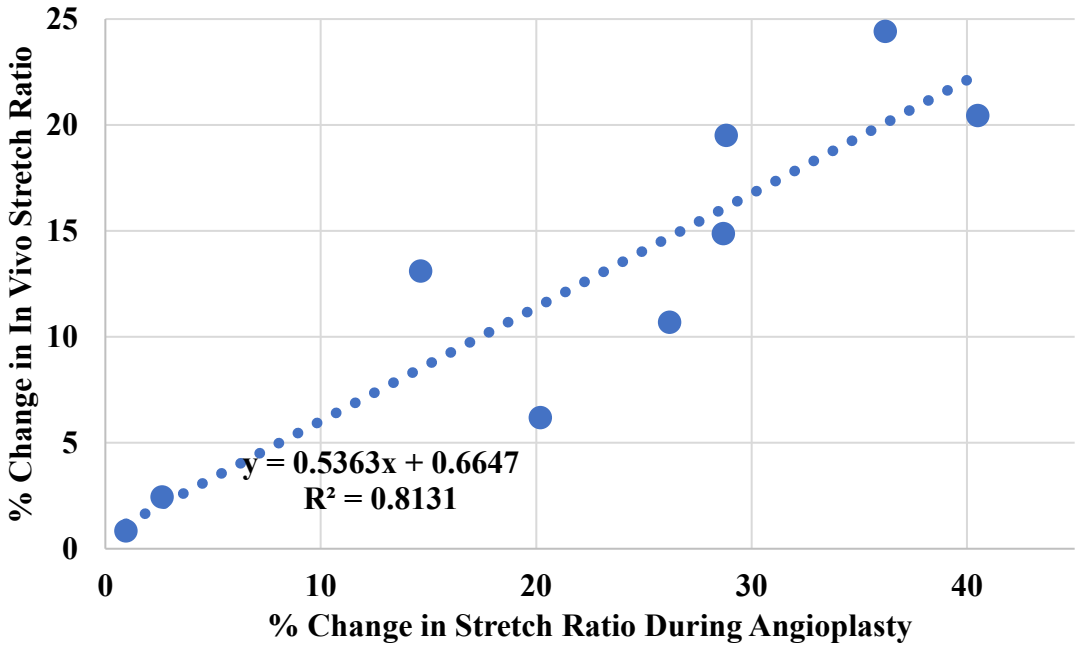

Figure 10 Scatter plot of the percent change in circumferential in vivo stretch ratio versus the percent change in the circumferential stretch ratio during angioplasty with a linear trend line and equation fit to the data.

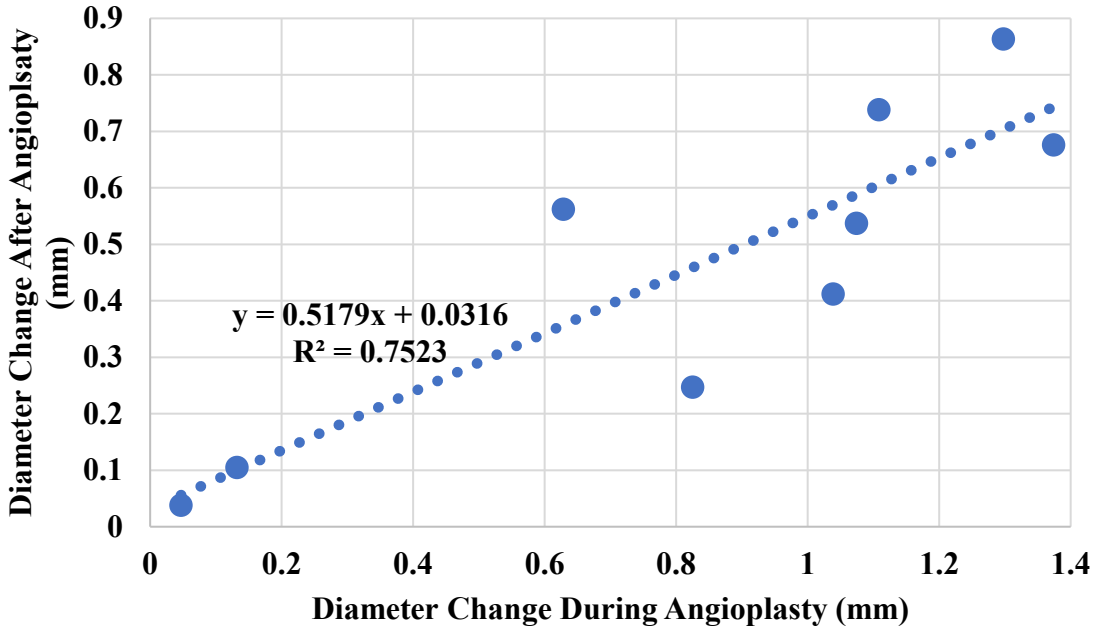

Figure 11 Scatter plot of the change in the in vivo diameter versus the change in the diameter during angioplasty with a linear trend line and equation fit to the data.

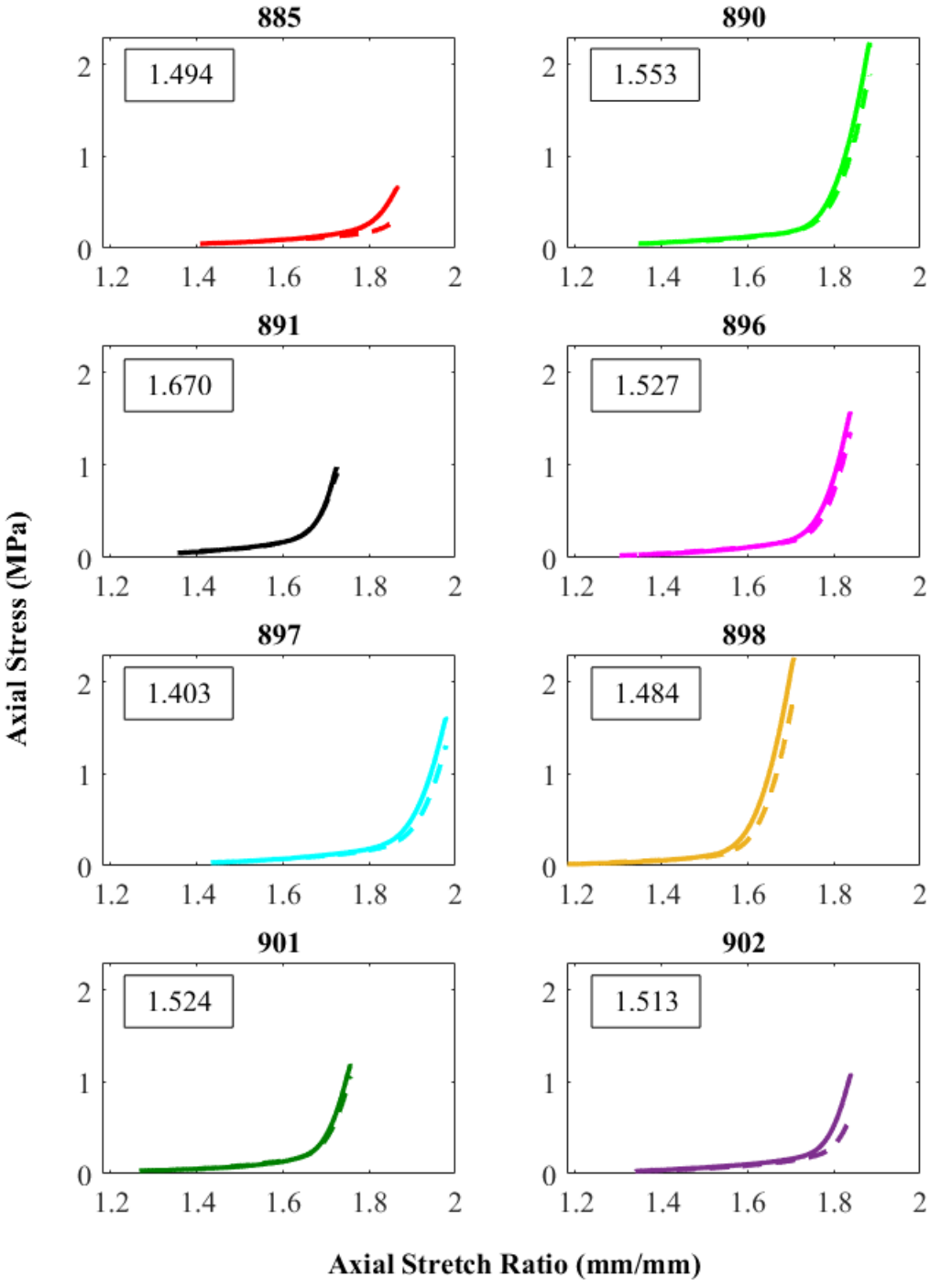

Figure 12 The axial stress-stretch responses of the porcine carotid arteries with an individual plot for each sample. Pretreatment is shown as a solid line and treated as a dashed line. The circumferential stretch during angioplasty is the boxed number in each plot.

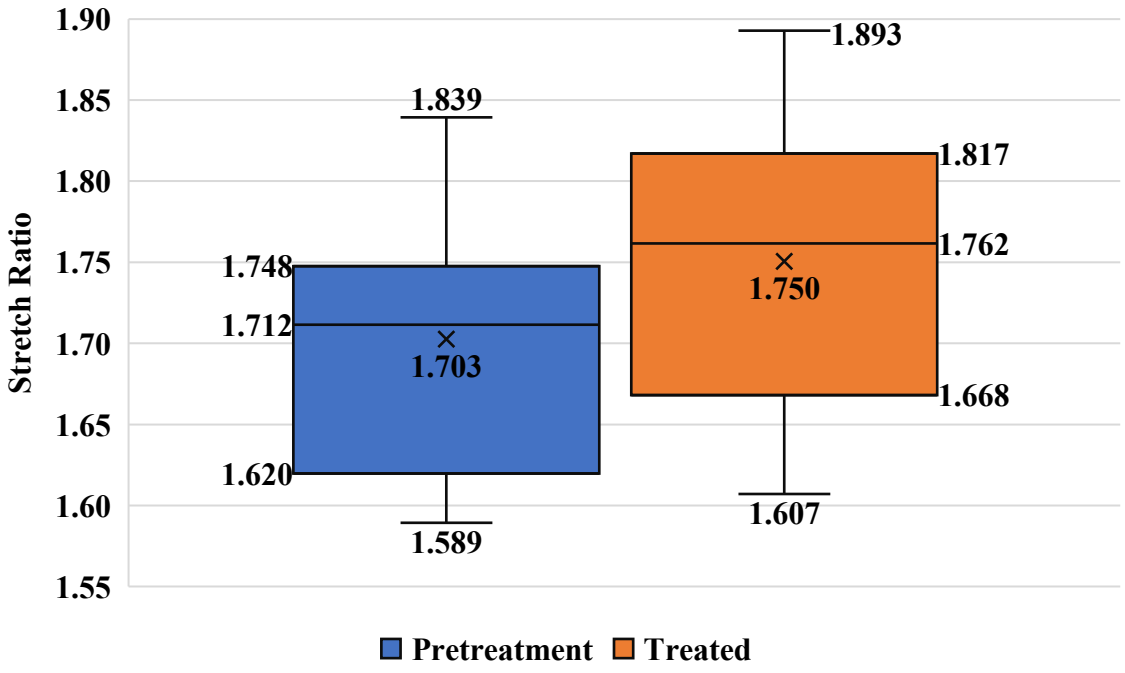

Figure 13 Box and whisker plots summarizing the in vivo axial stretch ratio before and after treatment.

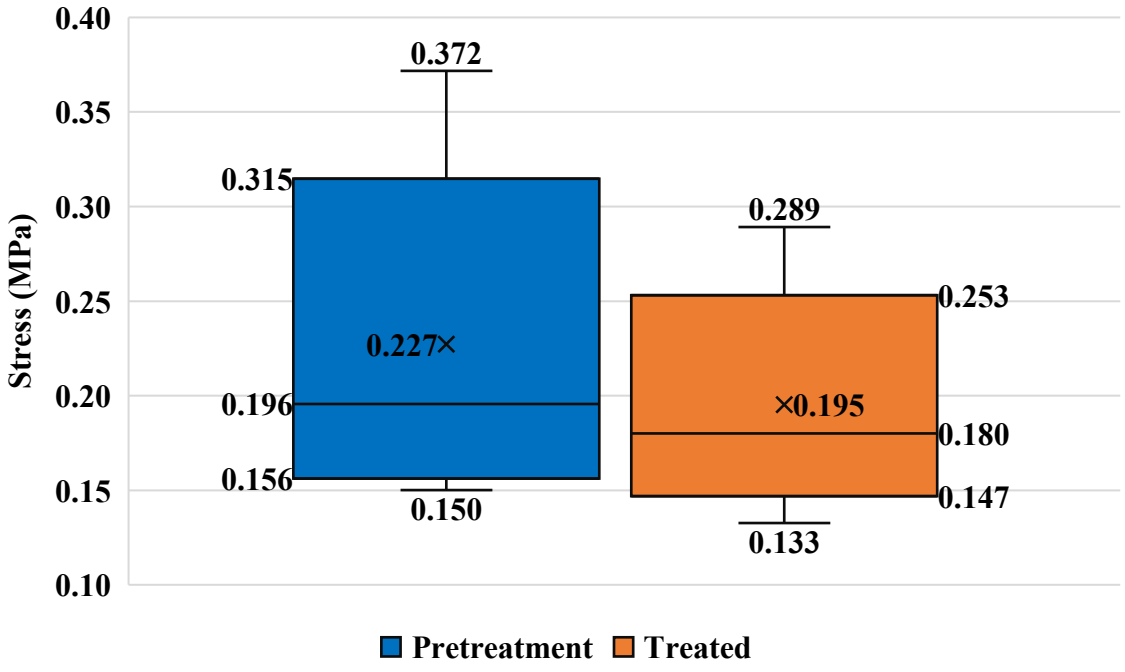

Figure 14 Box and whisker plots summarizing the axial stress at the pretreatment in vivo configuration before and after treatment.

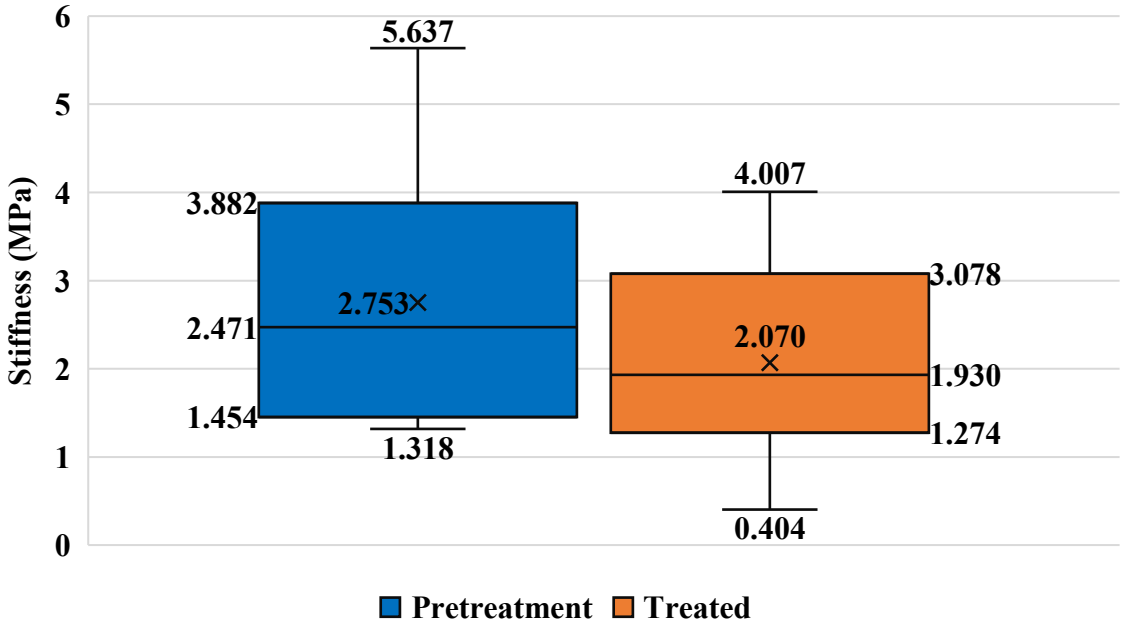

Figure 15 Box and whisker plots summarizing the axial stiffness at the pretreatment in vivo configuration before and after treatment.

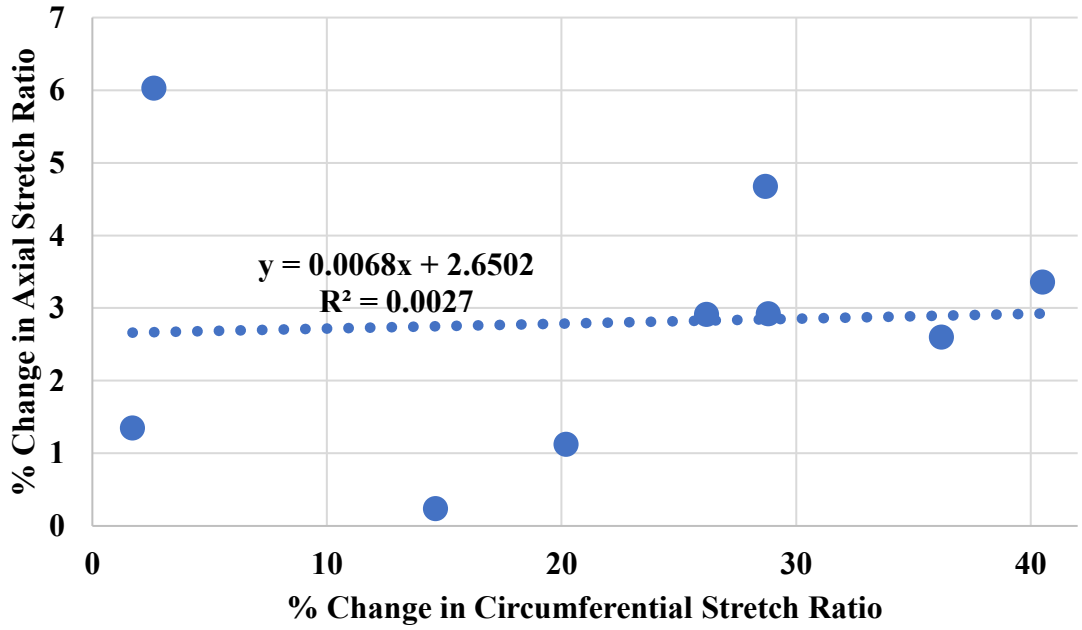

Figure 16 Scatter plot of the percent change in the axial in vivo stretch ratio versus the percent change in the circumferential stretch ratio during angioplasty with a linear trend line and equation fit to the data.

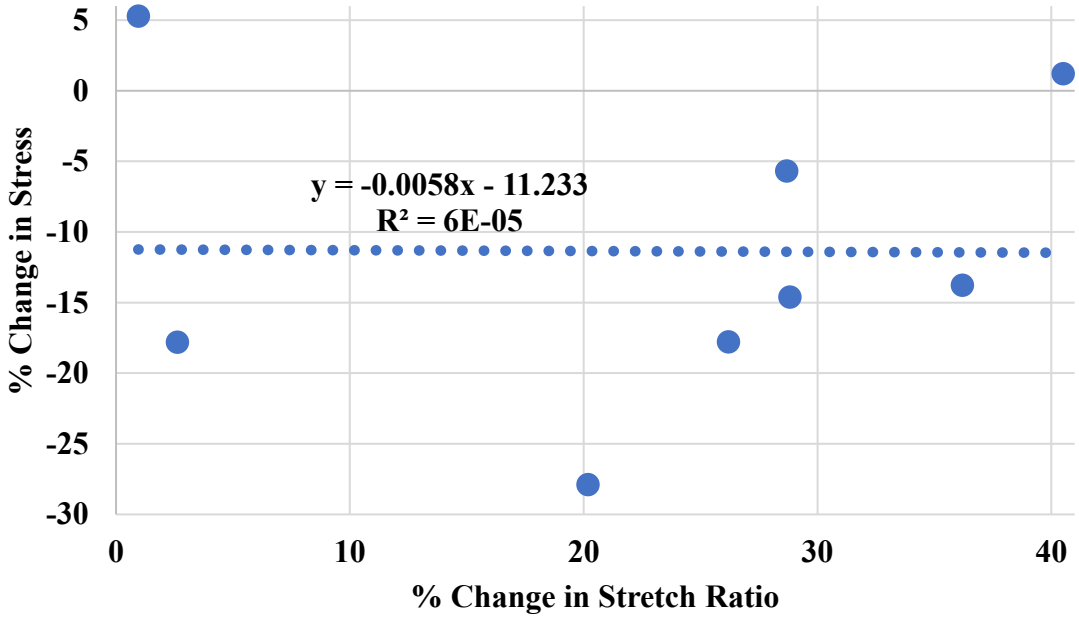

Figure 17 Scatter plot of the percent change in the axial in vivo stress versus the percent change in the circumferential stretch ratio during angioplasty with a linear trend line and equation fit to the data.

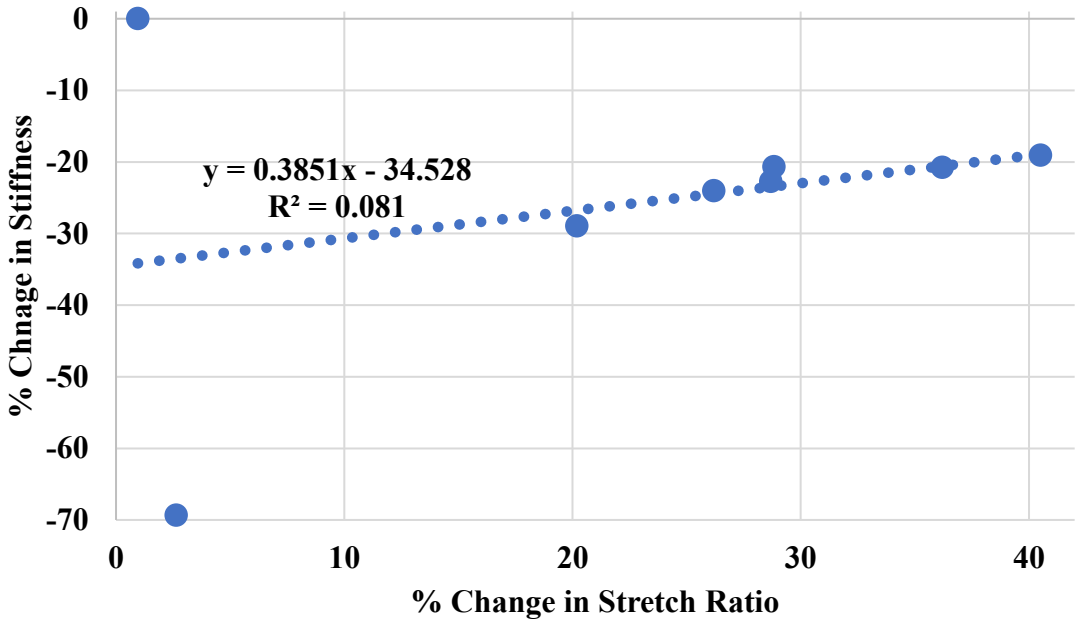

Figure 18 Scatter plot of the percent change in the axial in vivo stiffness versus the percent change in the circumferential stretch ratio during angioplasty with a linear trend line and equation fit to the data.

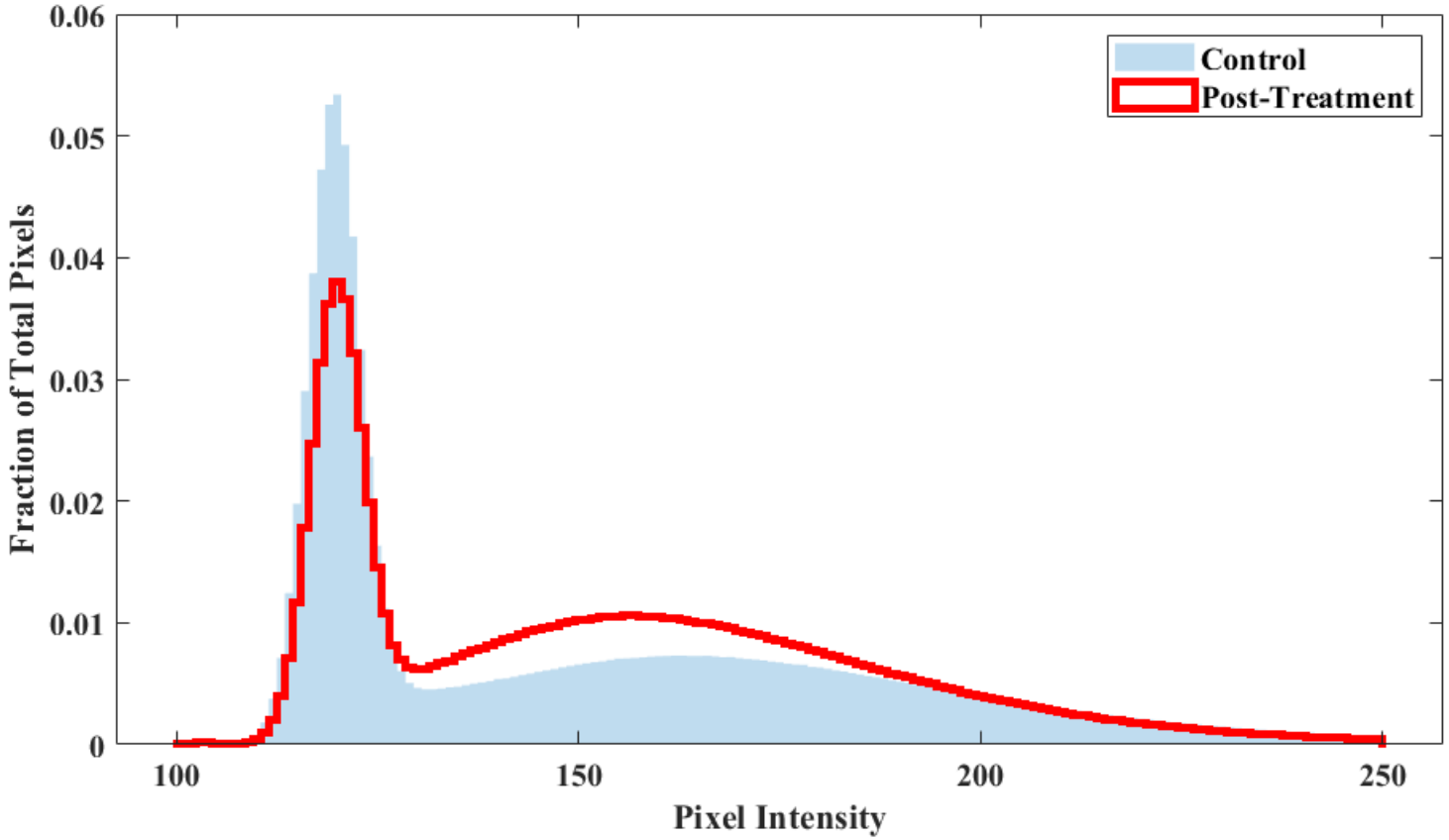

Figure 19 Histogram of pixel intensity for the control and treated CHP-stained images of the medial layer slices of artery number 885.

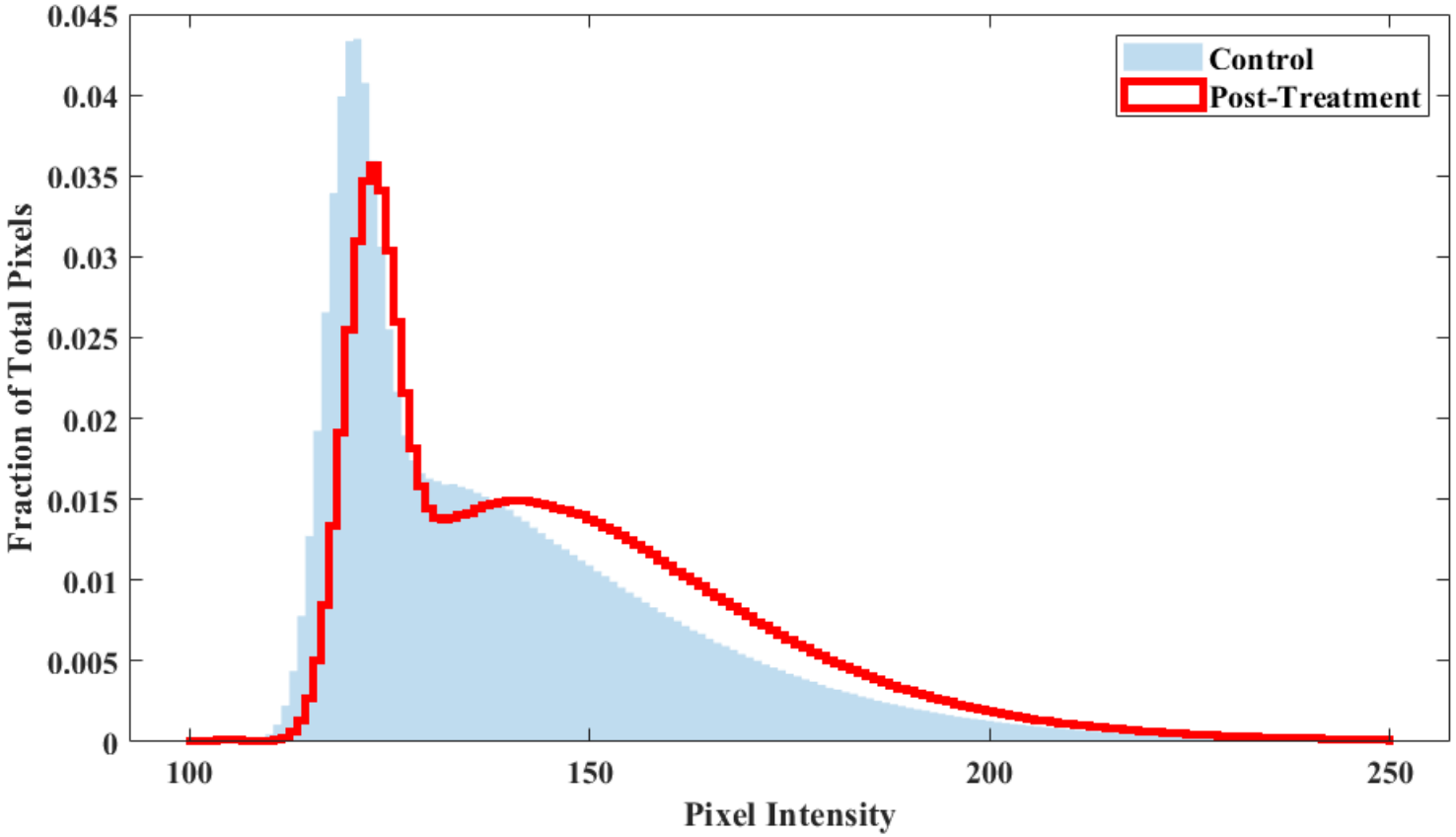

Figure 20 Histogram of pixel intensity for the control and treated CHP-stained images of the medial layer slices of artery number 890.

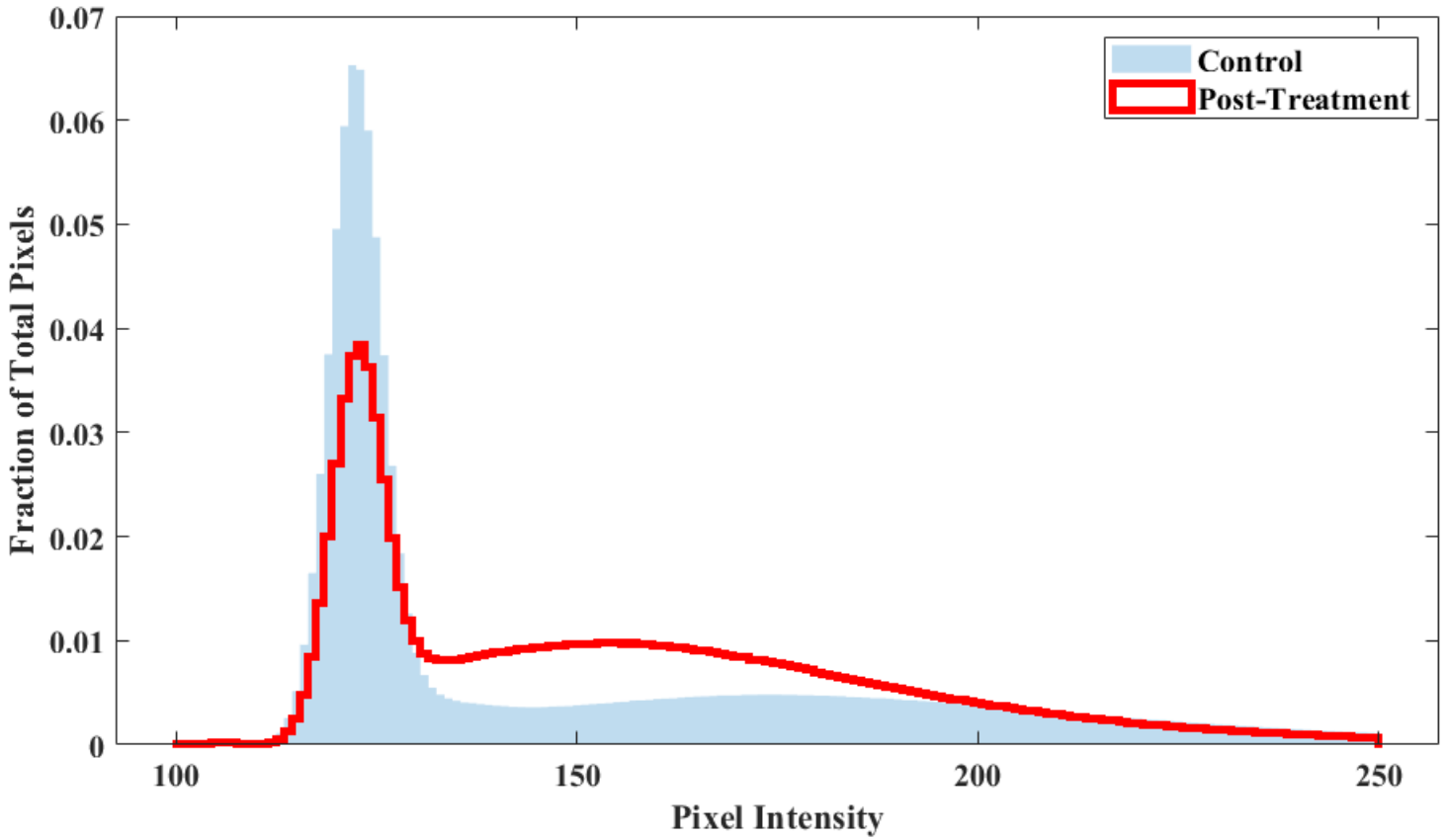

Figure 21 Histogram of pixel intensity for the control and treated CHP-stained images of the medial layer slices of artery number 891.

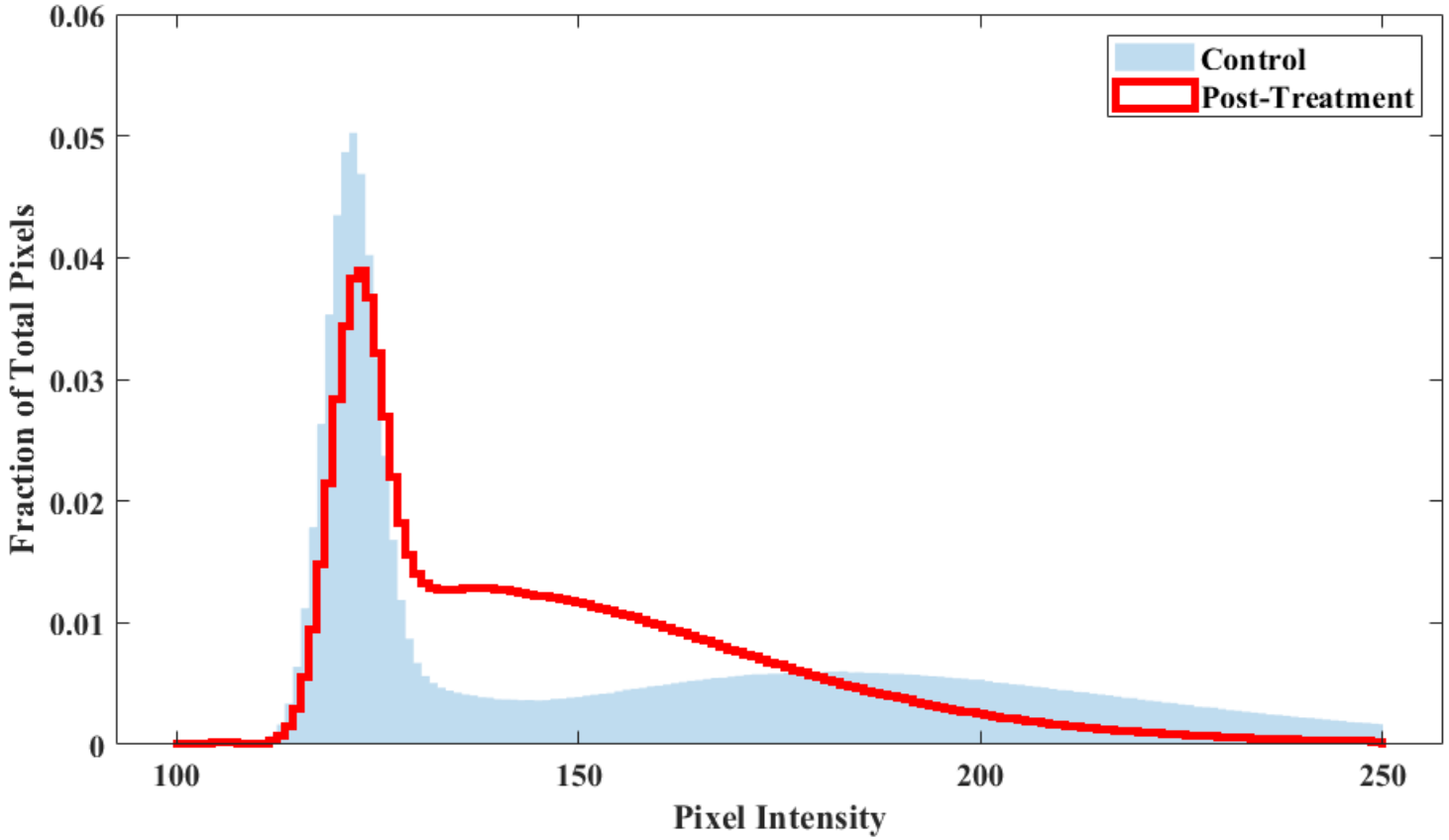

Figure 22 Histogram of pixel intensity for the control and treated CHP-stained images of the medial layer slices of artery number 892.

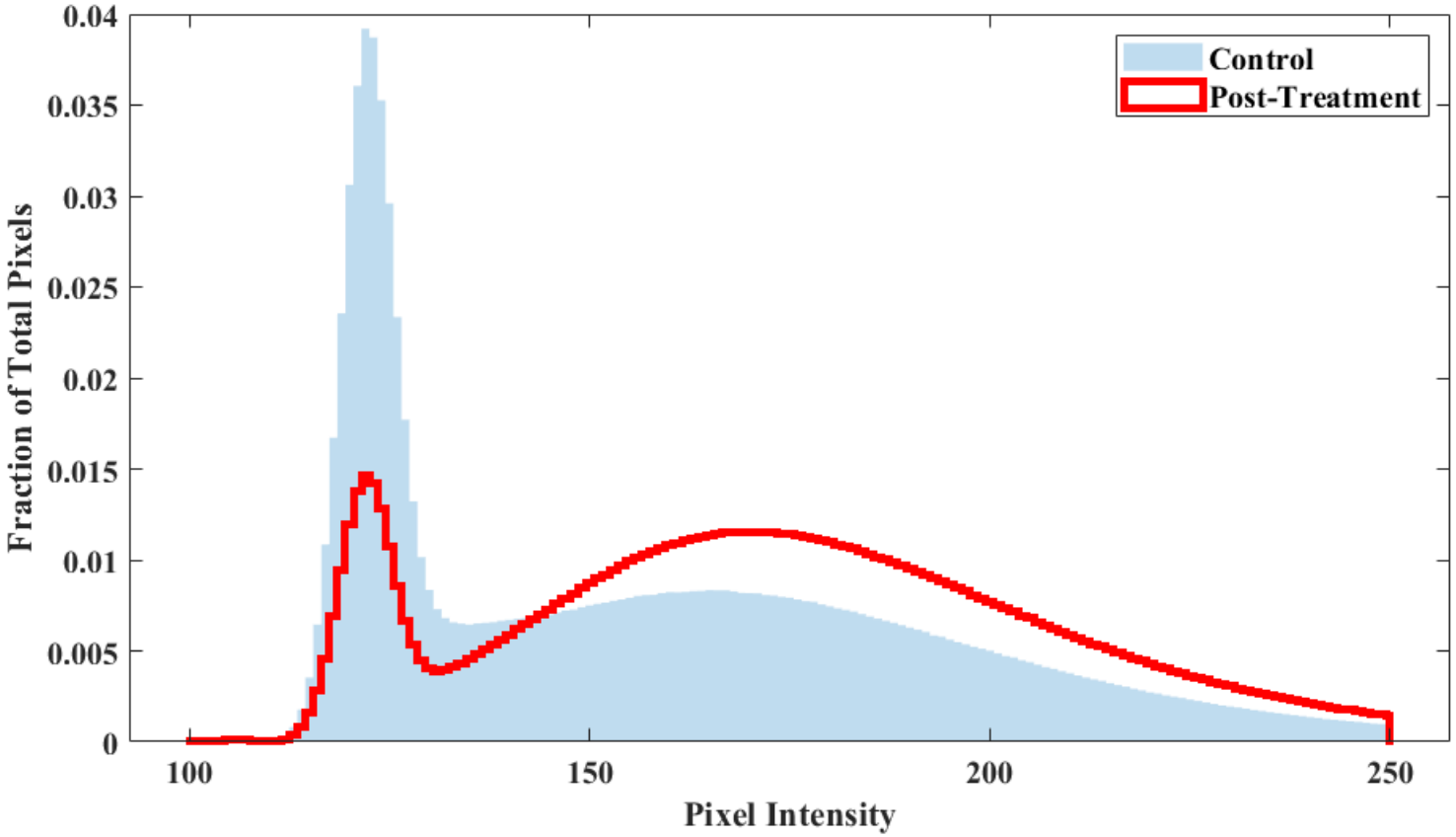

Figure 23 Histogram of pixel intensity for the control and treated CHP-stained images of the medial layer slices of artery number 896.

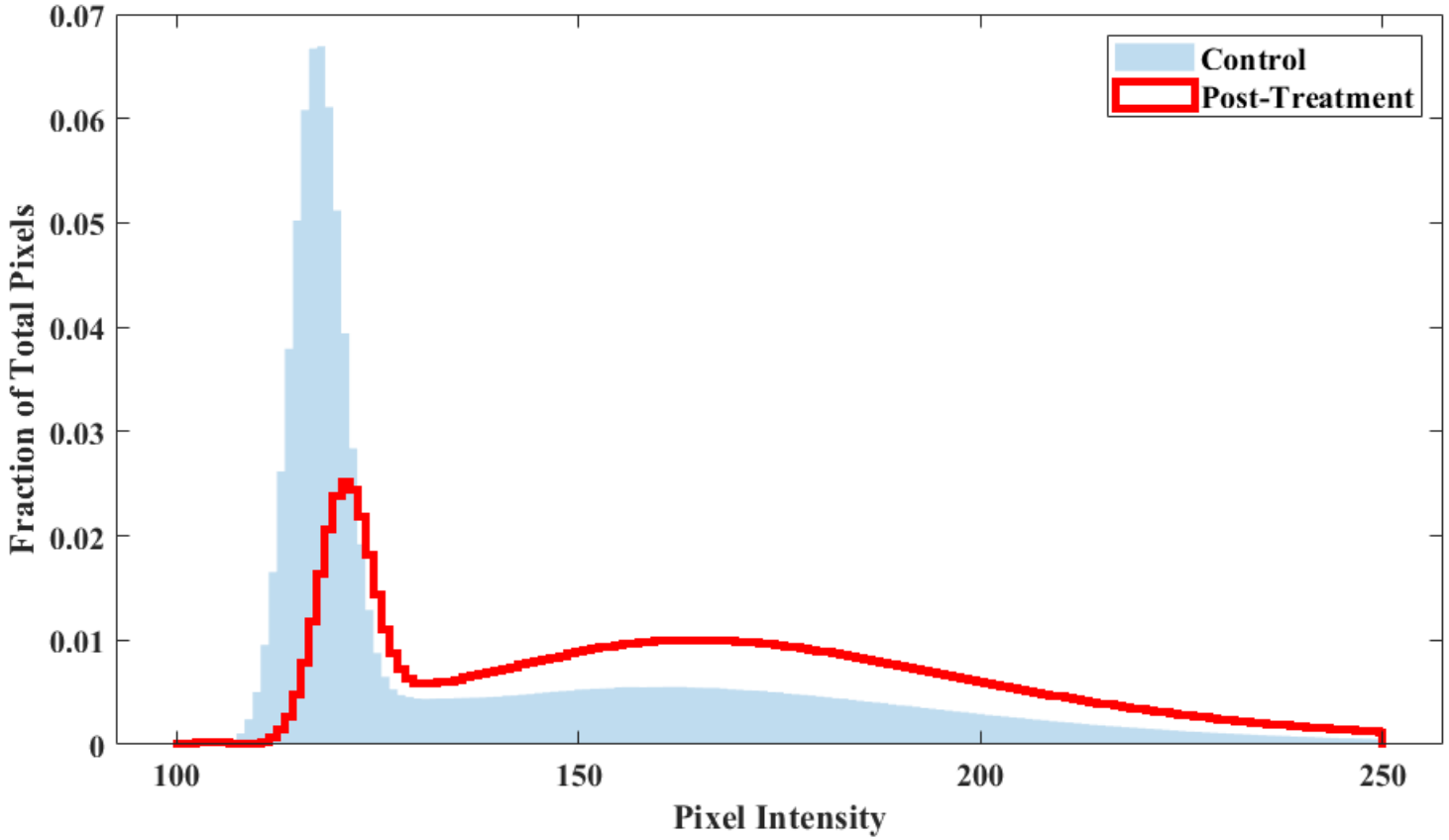

Figure 24 Histogram of pixel intensity for the control and treated CHP-stained images of the medial layer slices of artery number 897.

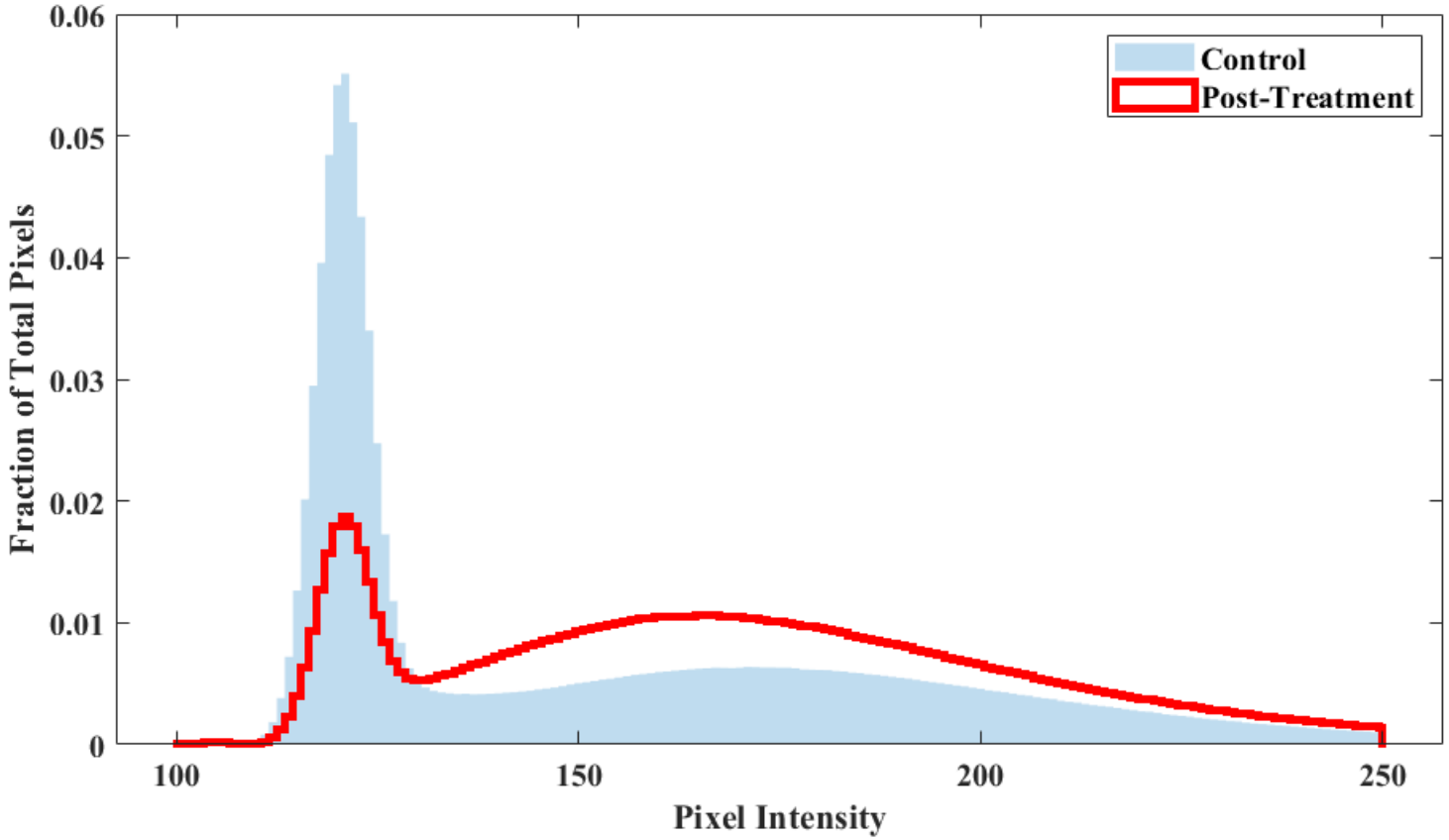

Figure 25 Histogram of pixel intensity for the control and treated CHP-stained images of the medial layer slices of artery number 898.

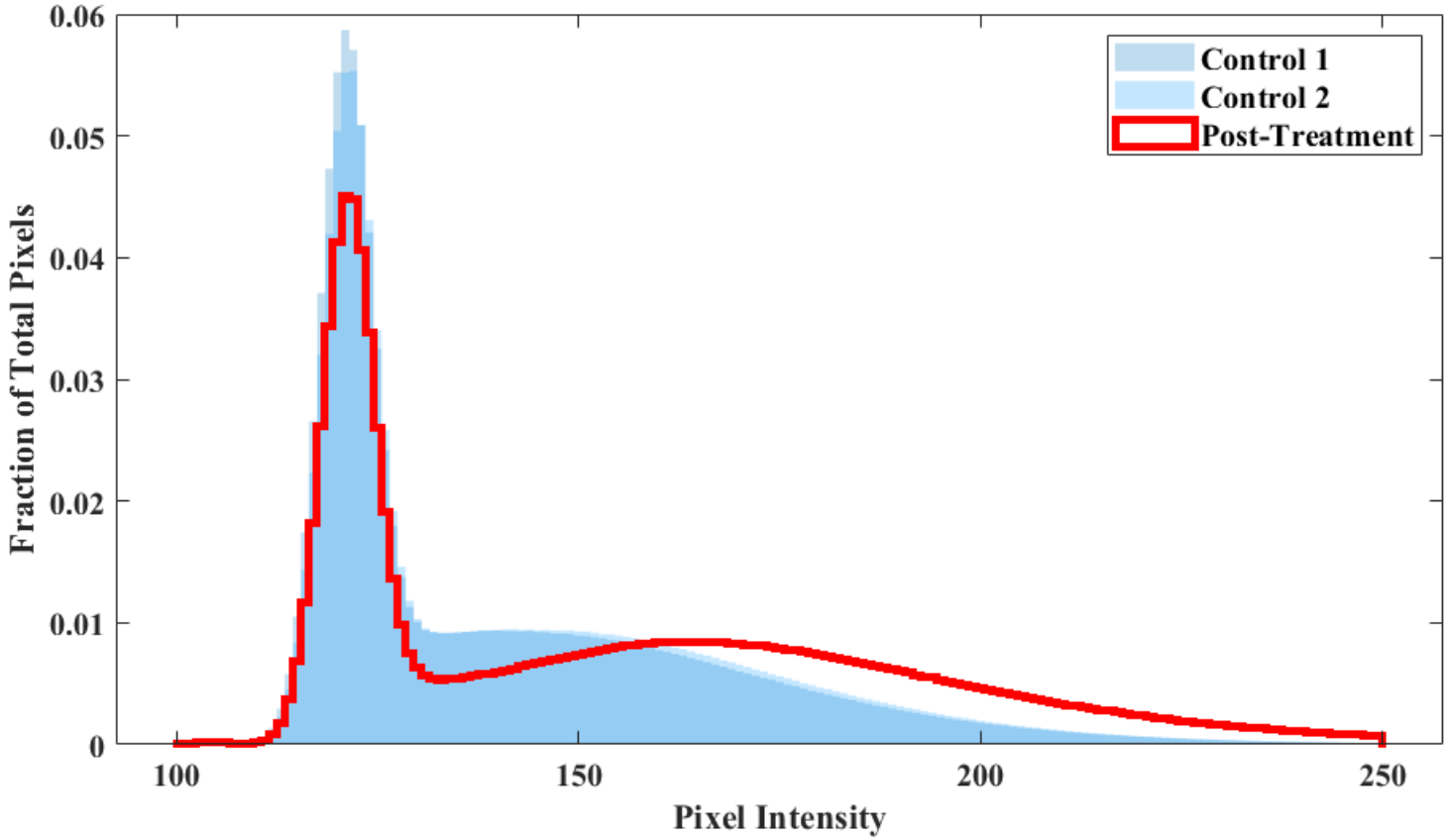

Figure 26 Histogram of pixel intensity for the control and treated CHP-stained images of the medial layer slices of artery number 901.

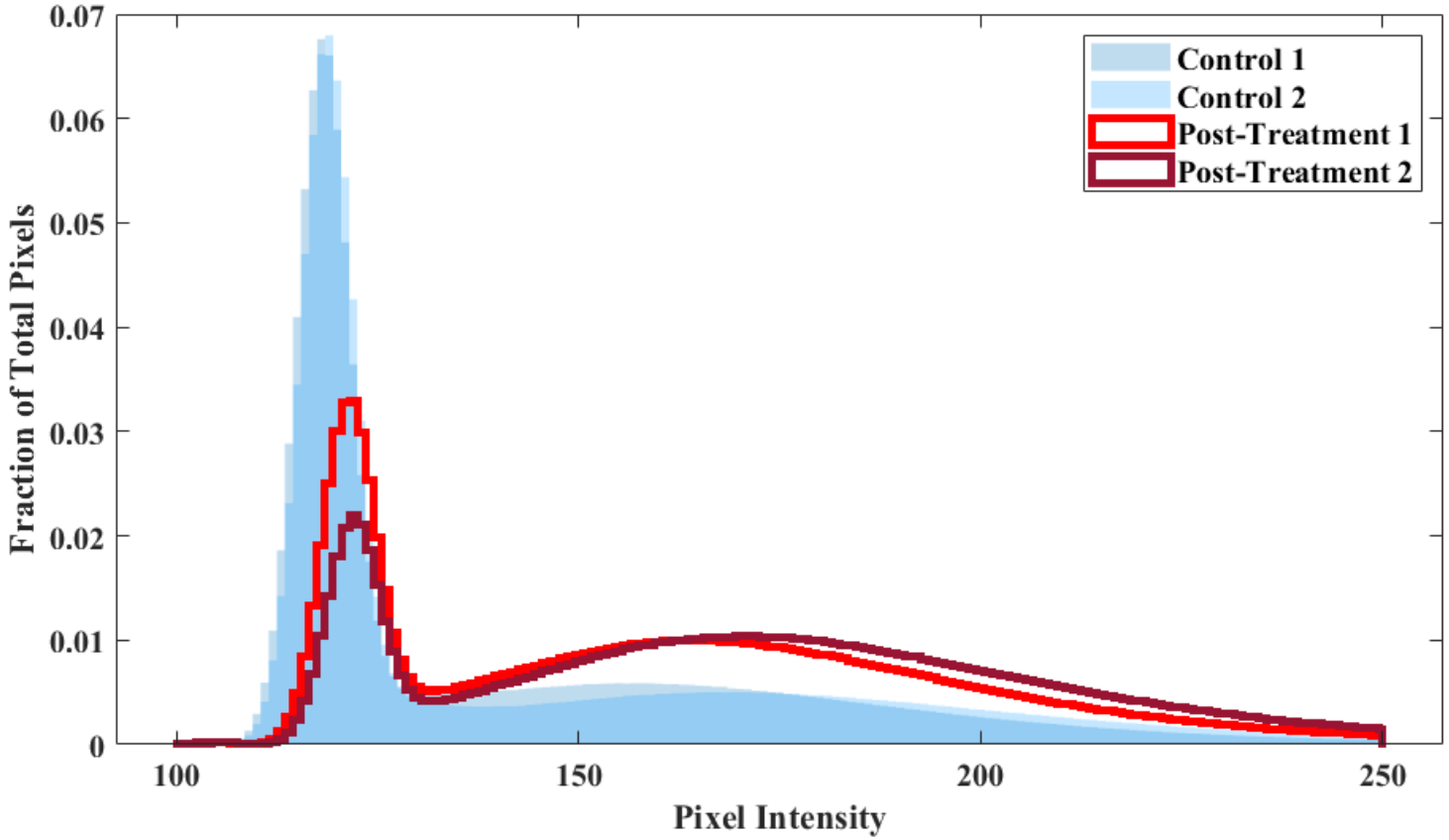

Figure 27 Histogram of pixel intensity for the control and treated CHP-stained images of the medial layer slices of artery number 902.

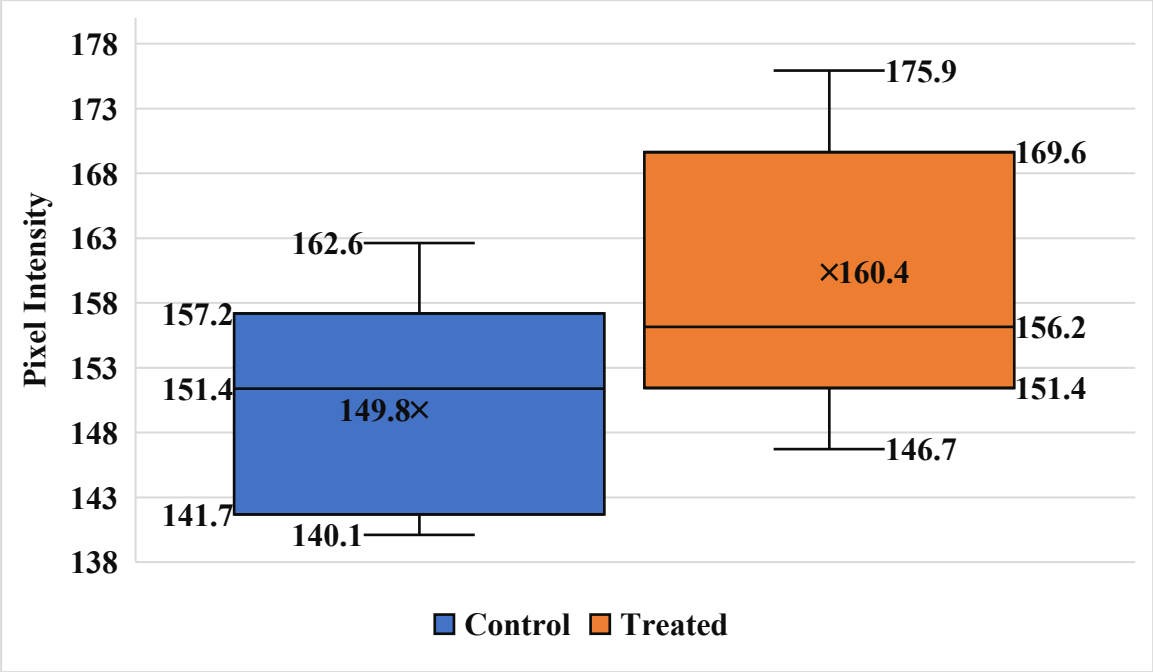

Figure 28 Box and whisker plots summarizing the mean pixel intensity of a medial layer slice of the arteries before and after treatment.

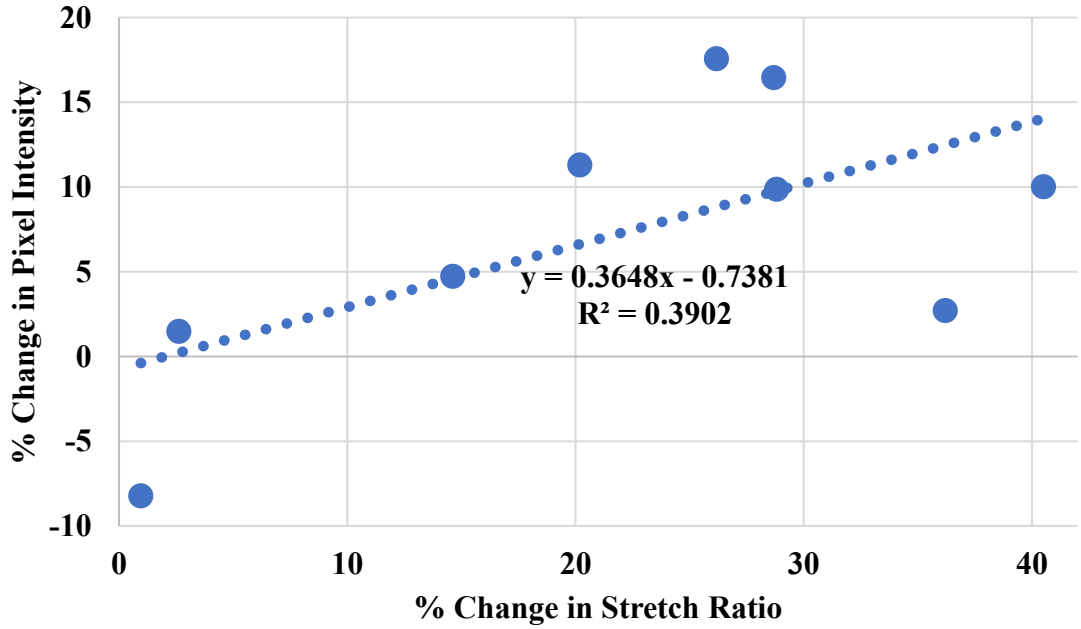

Figure 29 Scatter plot of the percent change in the mean pixel intensity of the medial layer slices versus the percent change in the circumferential stretch ratio during angioplasty with a linear trend line and equation fit to the data.

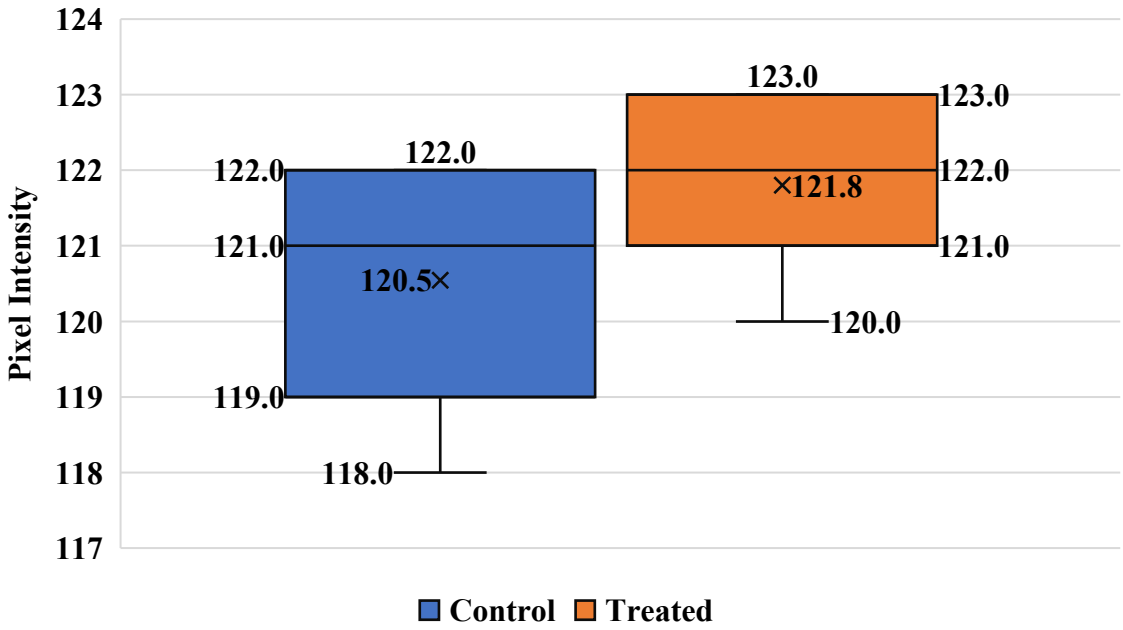

Figure 30 Box and whisker plots summarize the mode of the pixel intensity of a medial layer slice of the arteries before and after treatment.

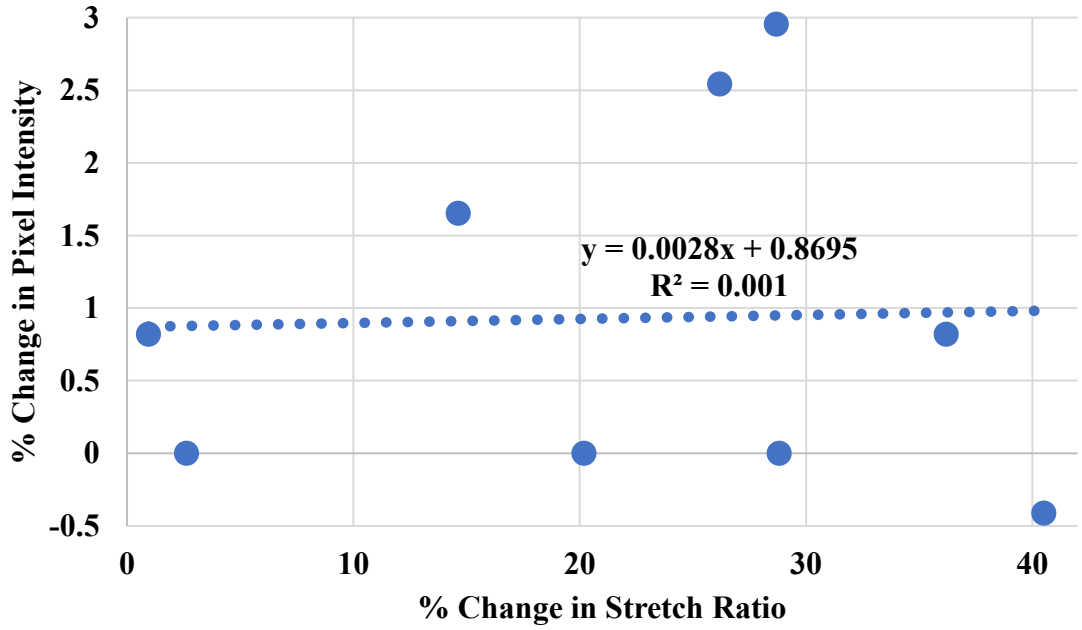

Figure 31 Scatter plot of the percent change in the mode of the pixel intensity of the medial layer slices versus the percent change in the circumferential stretch ratio during angioplasty with a linear trend line and equation fit to the data.

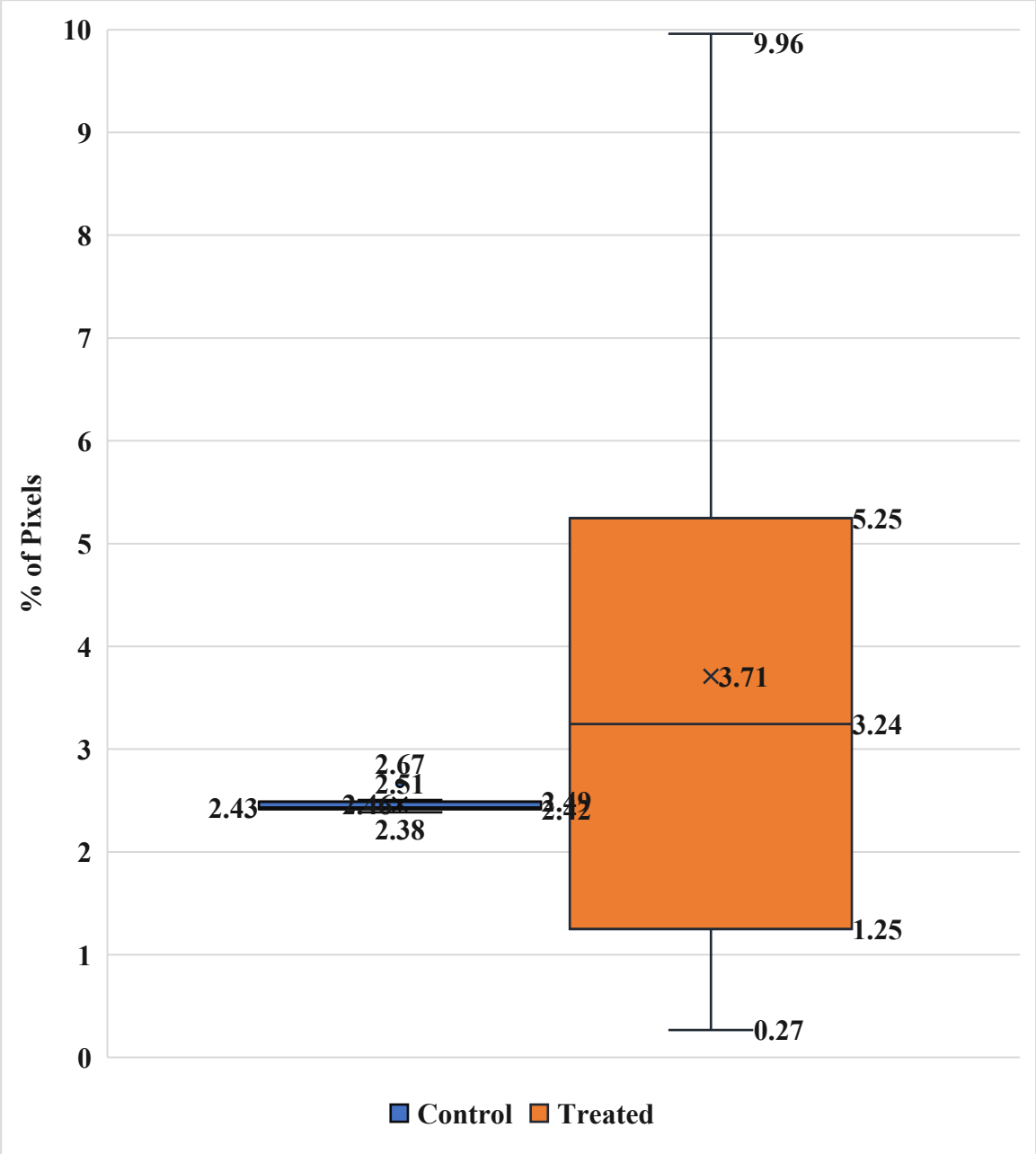

Figure 32 Box and whisker plots summarizing the bright pixels percentage of a medial layer slice of the arteries before and after treatment.

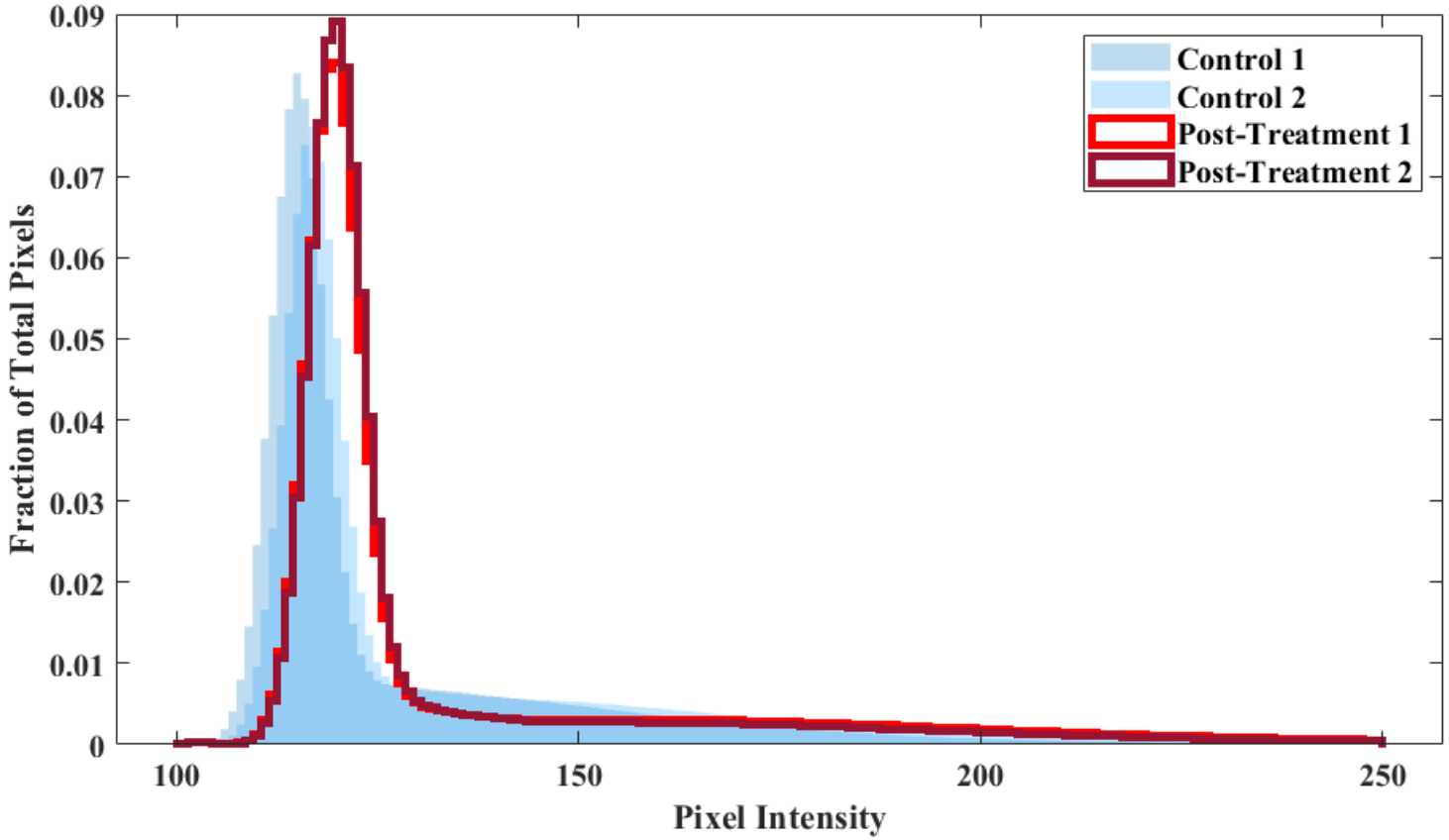

Figure 33 Histogram of pixel intensity for the control and treated CHP-stained images of the ring slices of artery number 885.

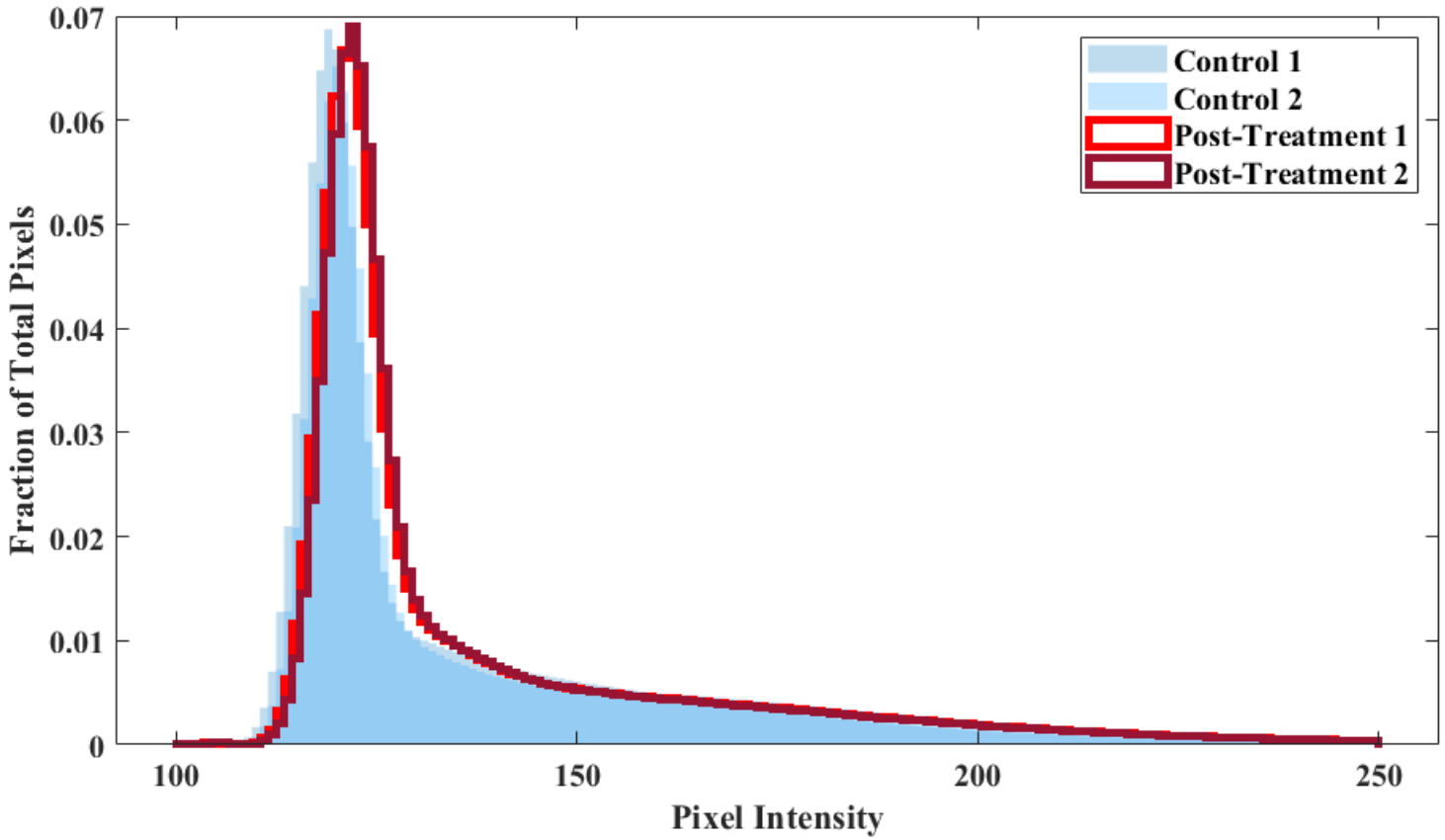

Figure 34 Histogram of pixel intensity for the control and treated CHP-stained images of the ring slices of artery number 890.

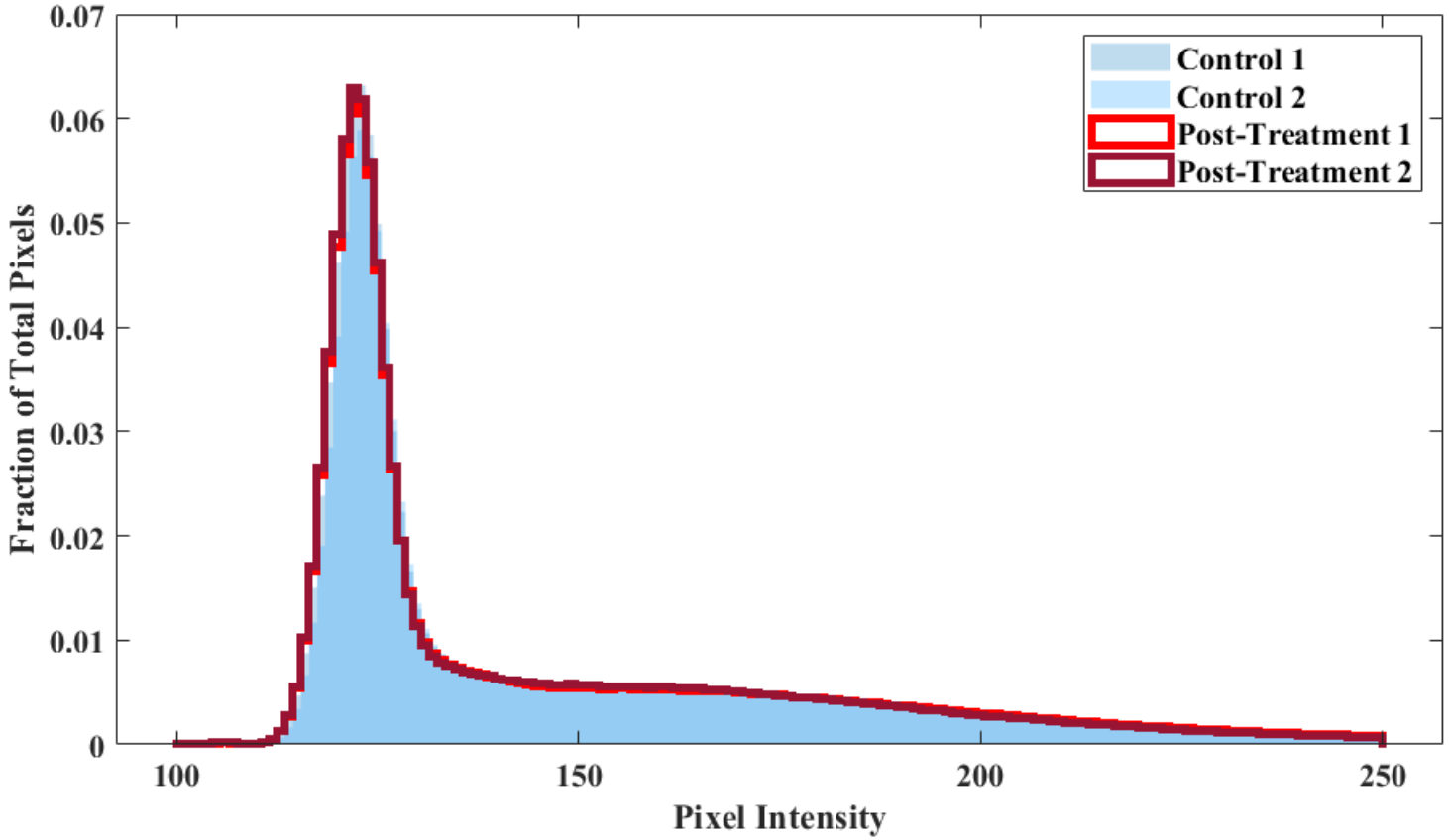

Figure 35 Histogram of pixel intensity for the control and treated CHP-stained images of the ring slices of artery number 891.

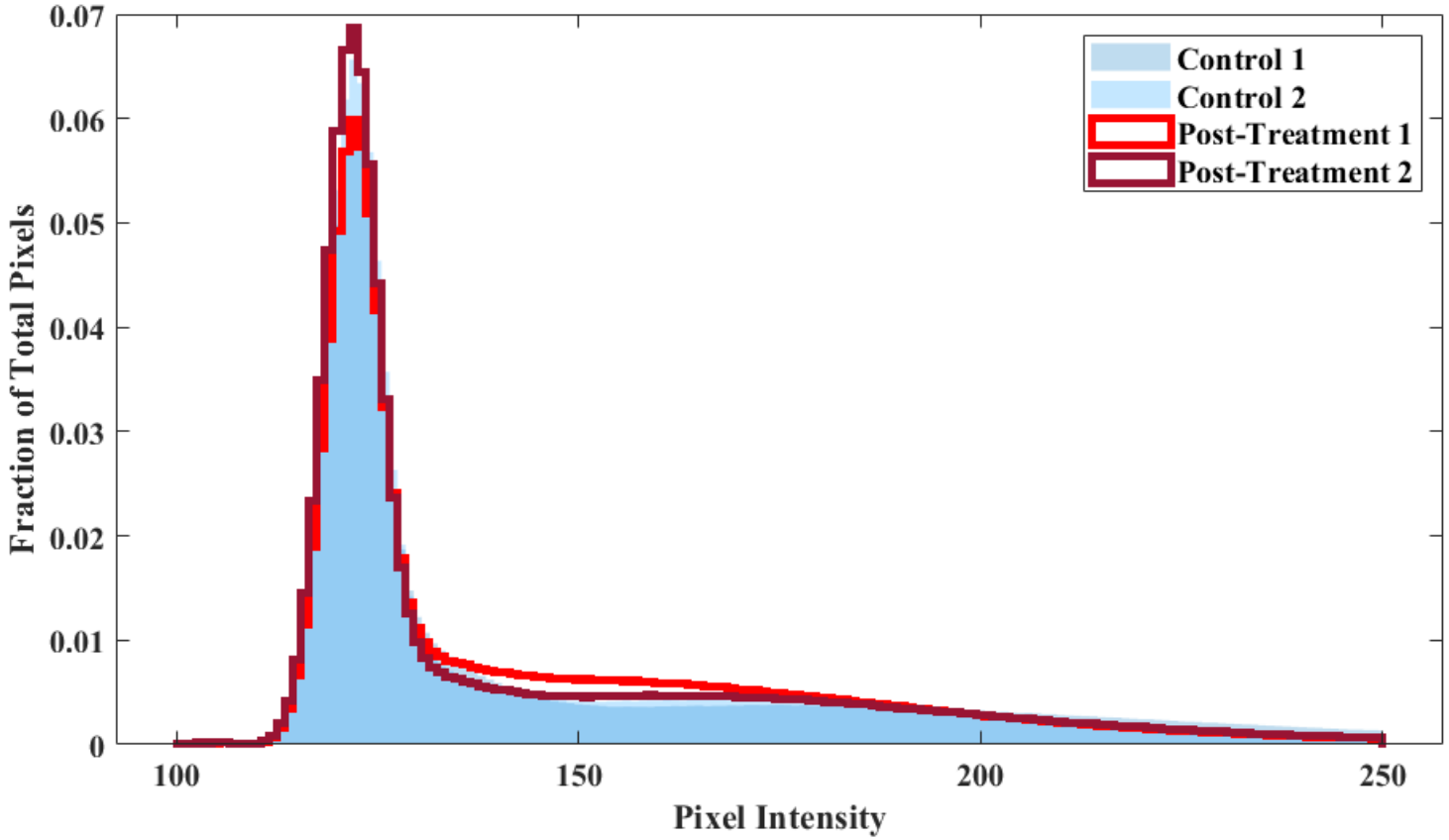

Figure 36 Histogram of pixel intensity for the control and treated CHP-stained images of the ring slices of artery number 892.

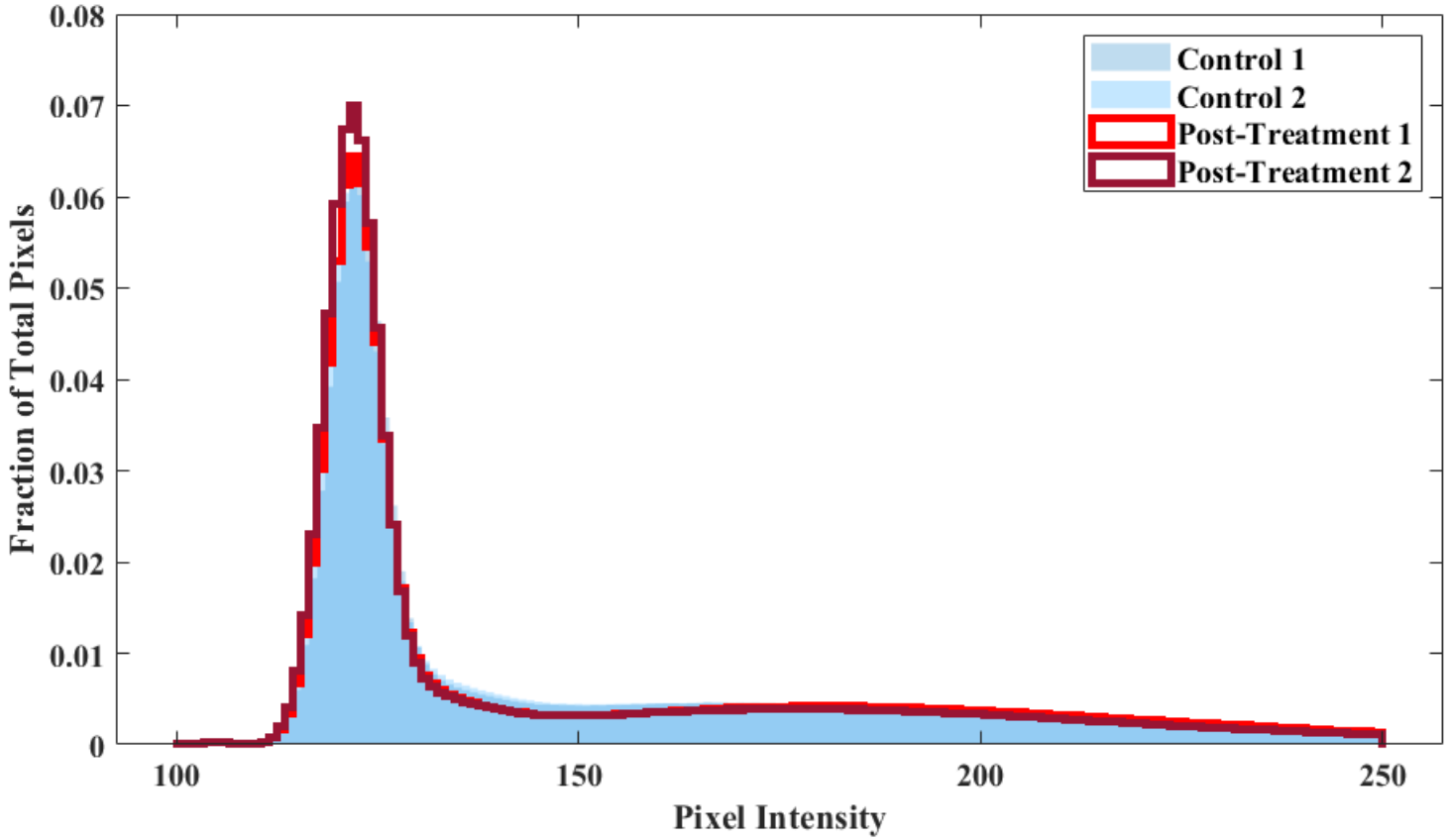

Figure 37 Histogram of pixel intensity for the control and treated CHP-stained images of the ring slices of artery number 896.

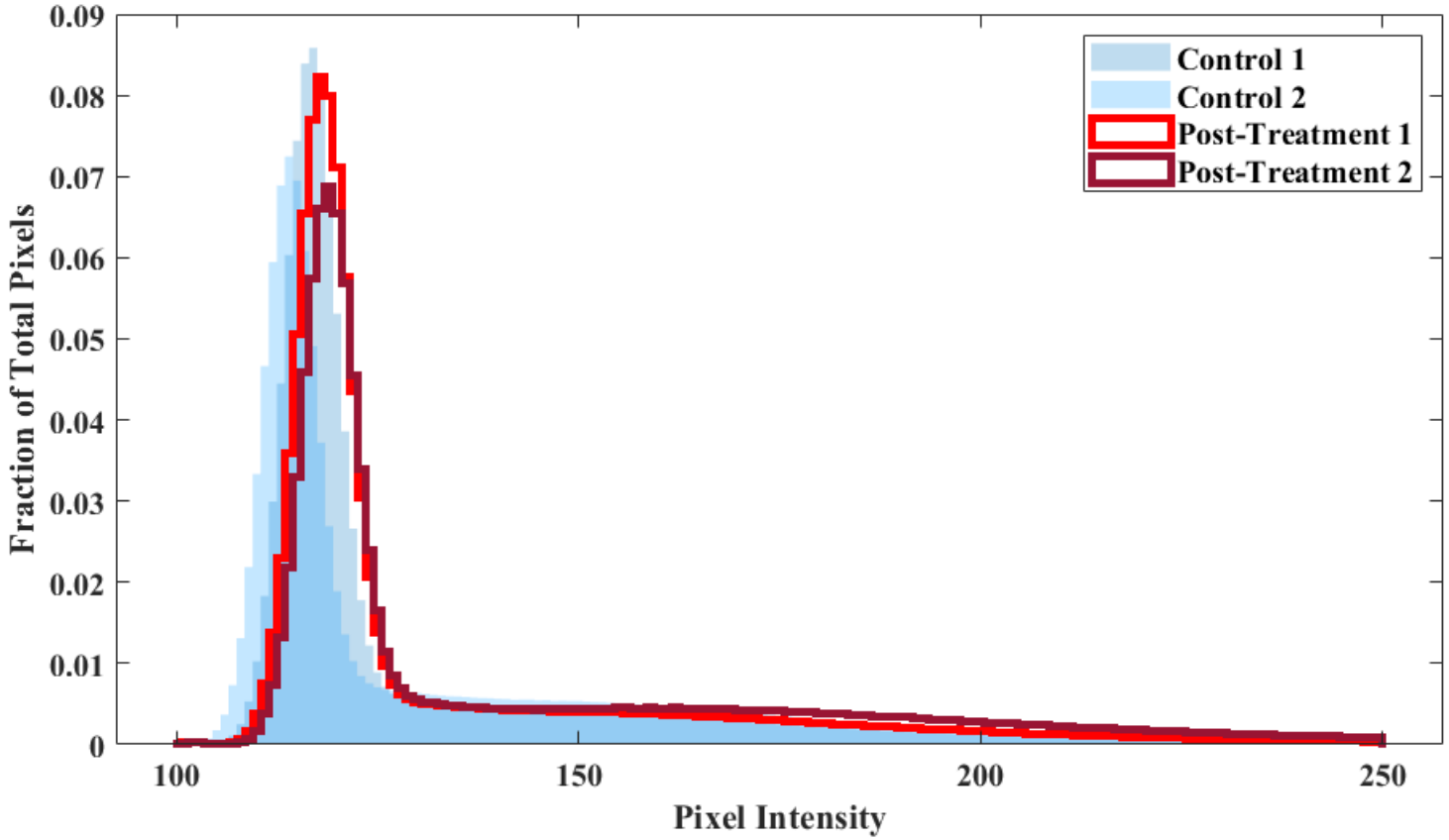

Figure 38 Histogram of pixel intensity for the control and treated CHP-stained images of the ring slices of artery number 897.

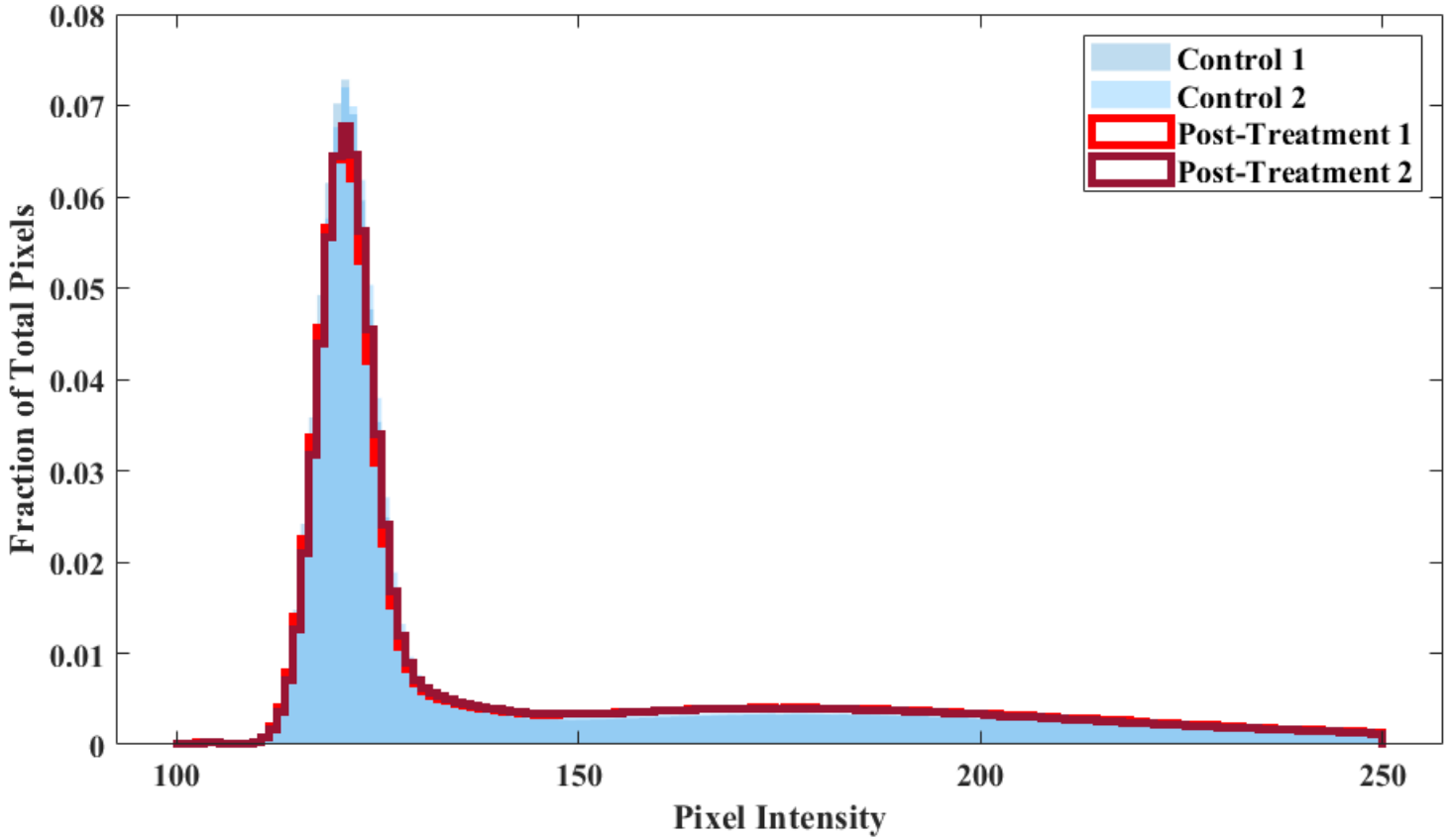

Figure 39 Histogram of pixel intensity for the control and treated CHP-stained images of the ring slices of artery number 898.

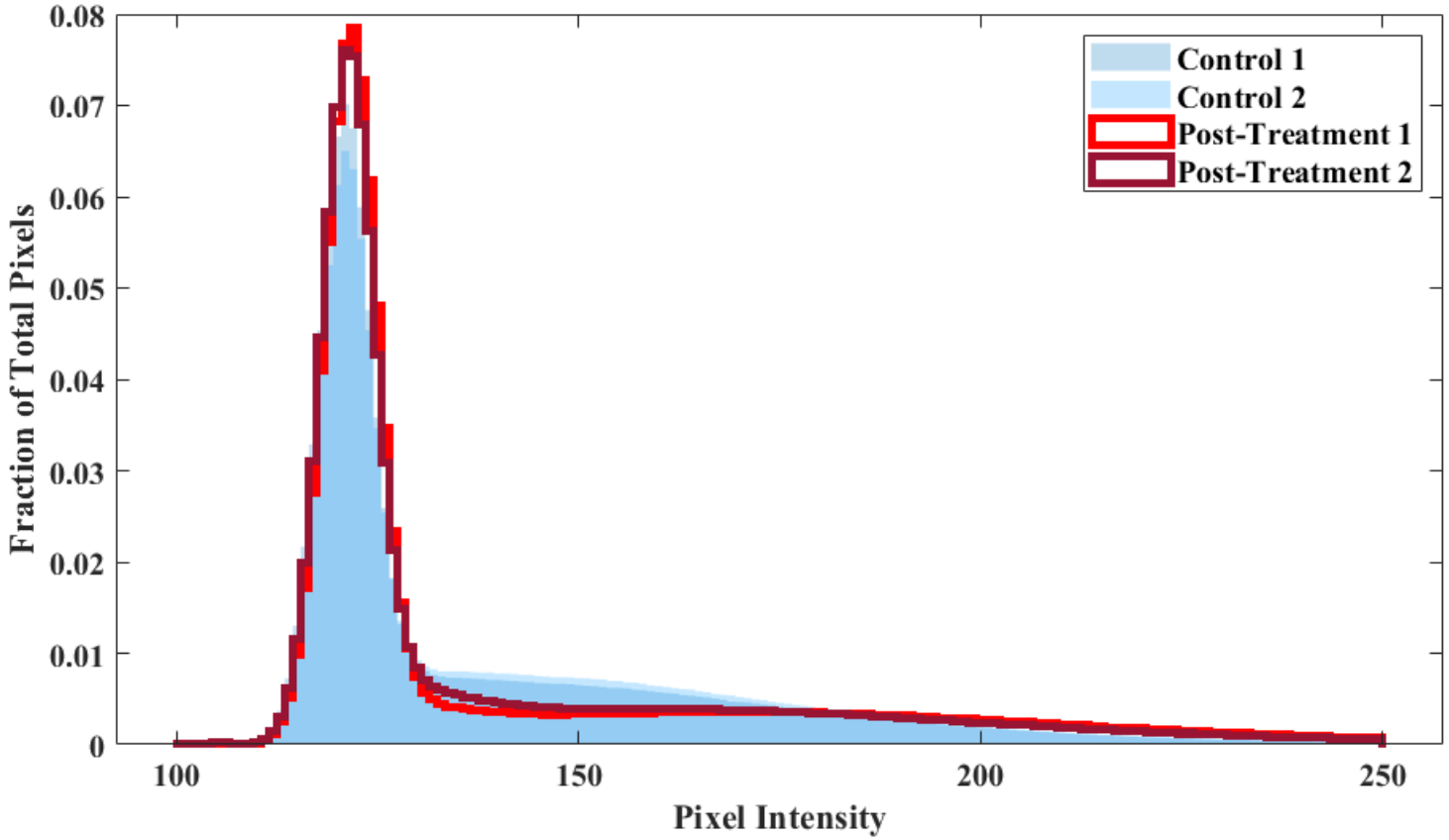

Figure 40 Histogram of pixel intensity for the control and treated CHP-stained images of the ring slices of artery number 901.

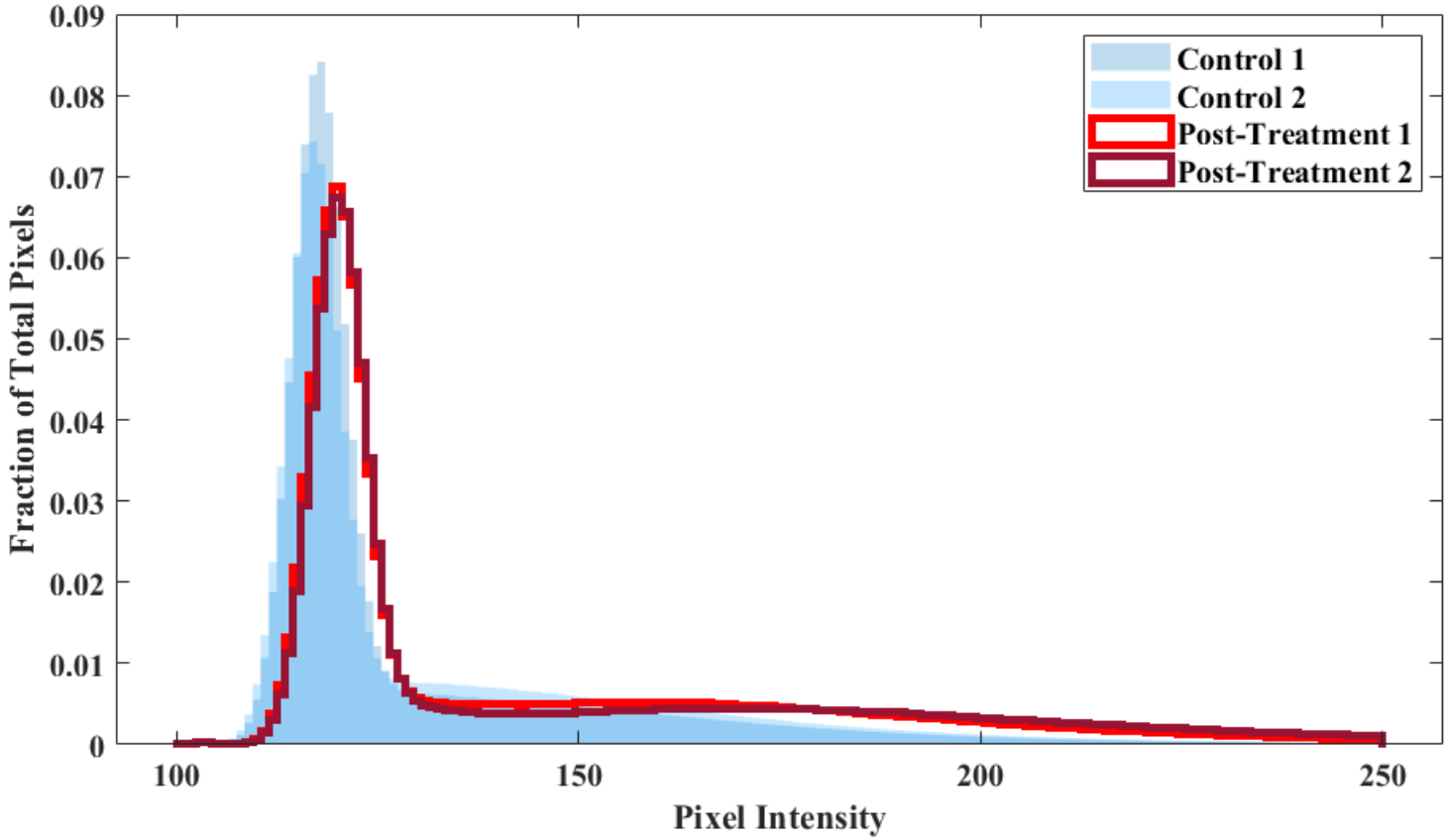

Figure 41 Histogram of pixel intensity for the control and treated CHP-stained images of the ring slices of artery number 902.

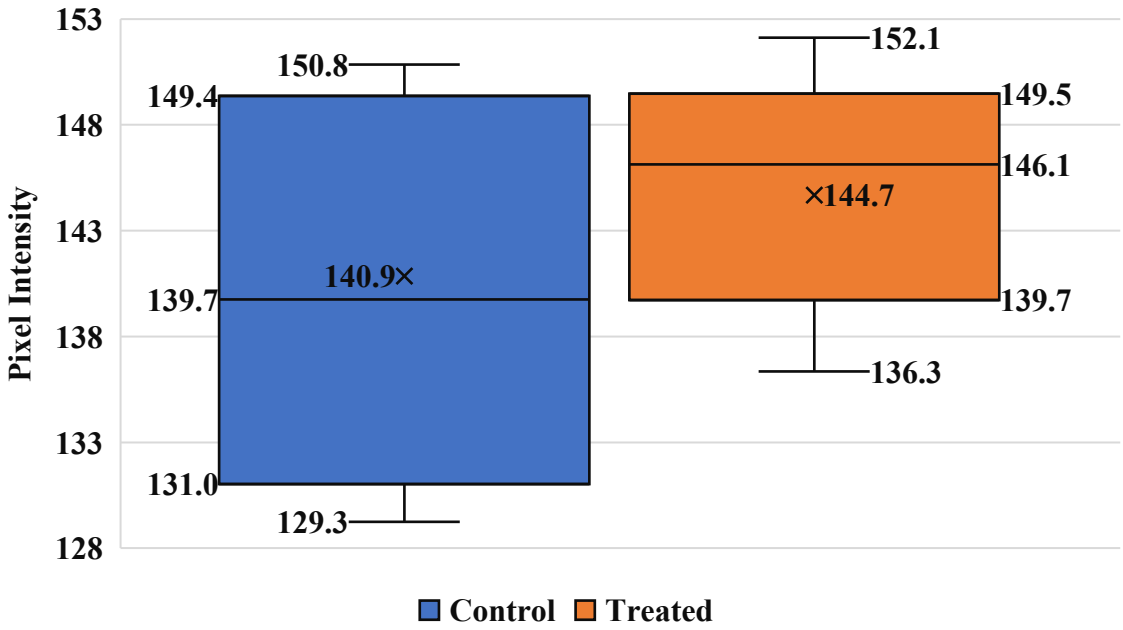

Figure 42 Box and whisker plots summarizing the ring slices' mean pixel intensity before and after treatment.

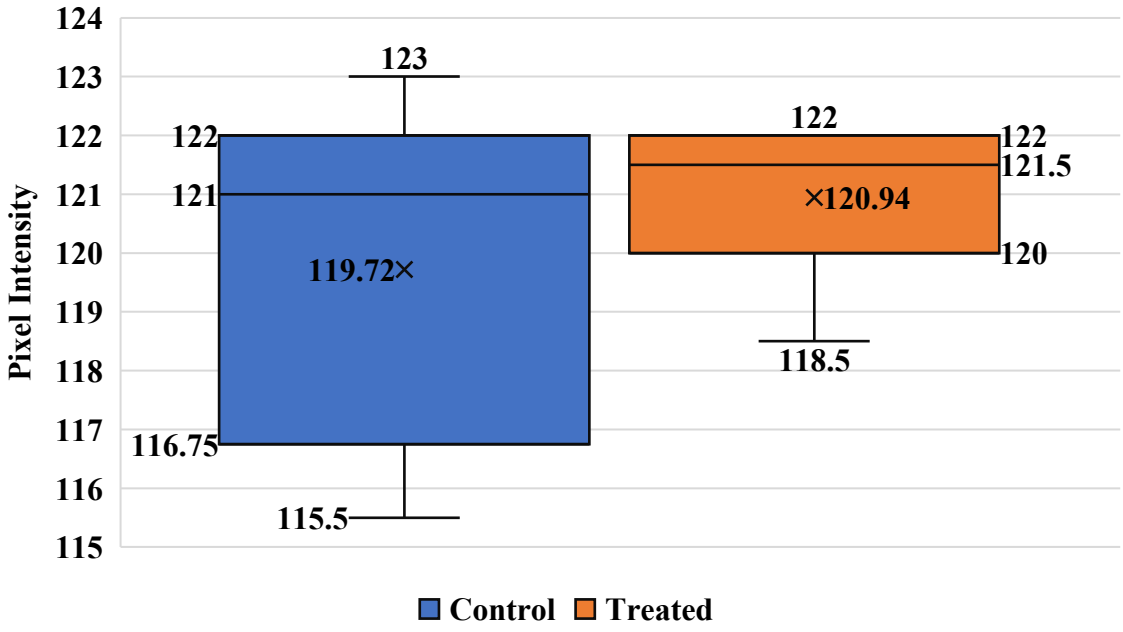

Figure 43 Box and whisker plots summarizing the mode of the pixel intensity of the ring slices before and after treatment.

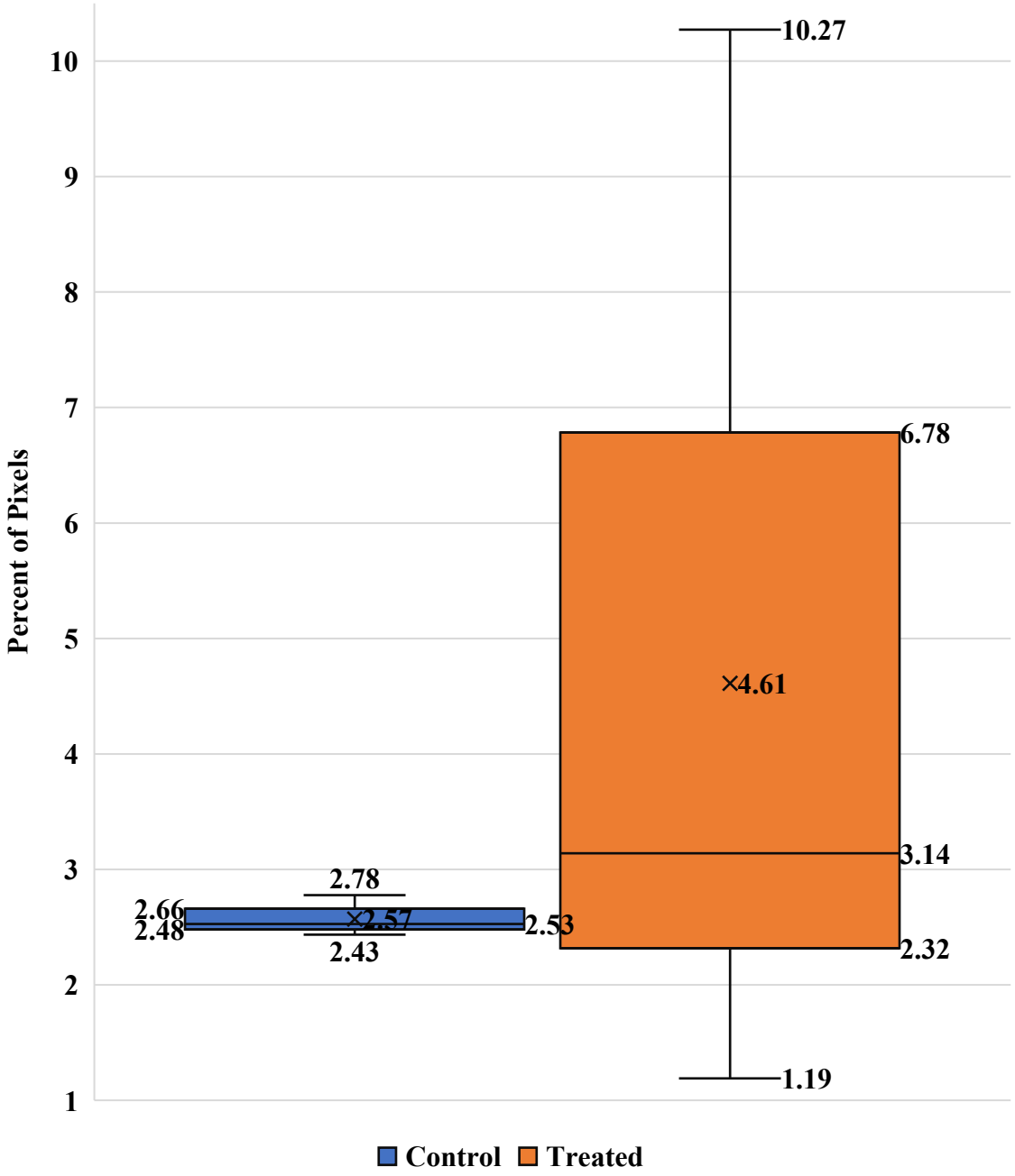

Figure 44 Box and whisker plots summarize the ring slices' bright pixel percentage before and after treatment.

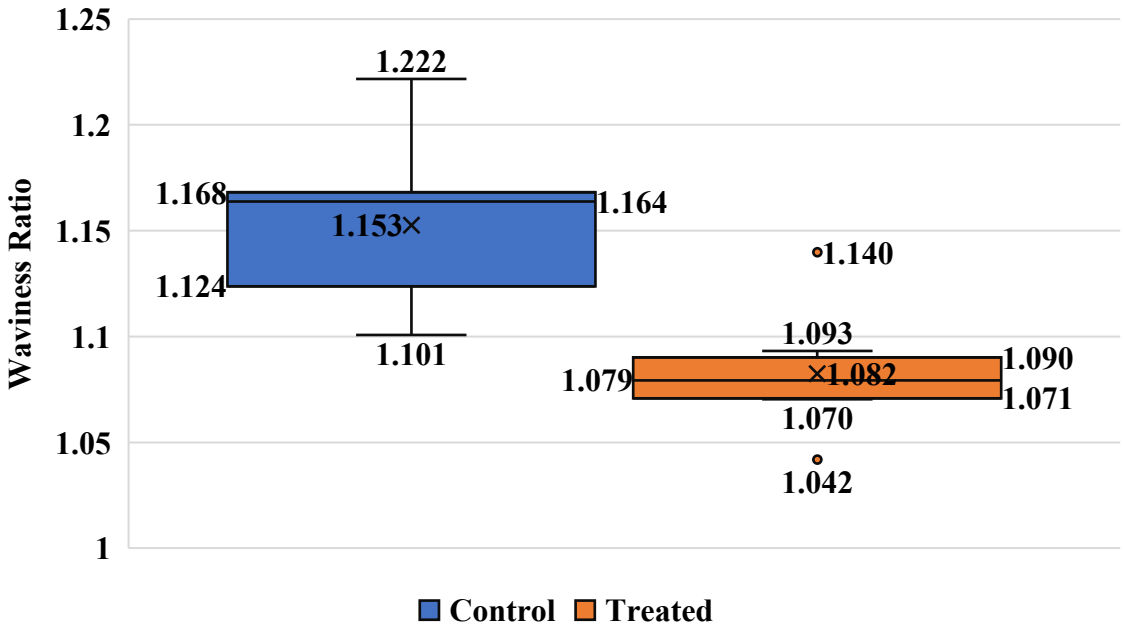

Figure 45 Box and whisker plots summarizing the waviness ratios before and after treatment.

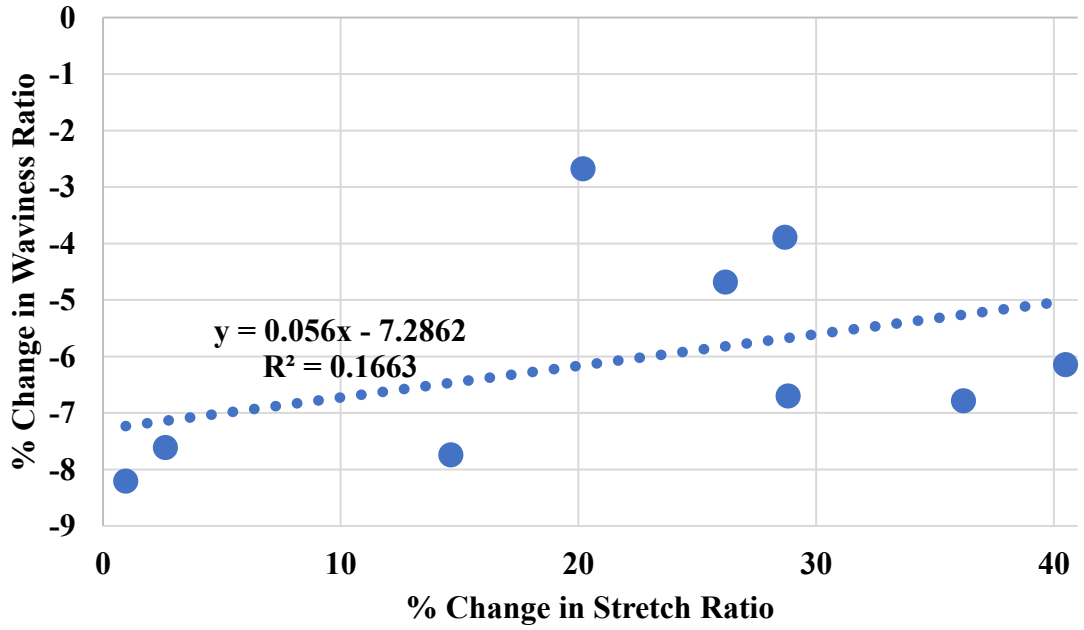

Figure 46 Scatter plot of the percent change in the waviness ratio versus the percent change in the circumferential stretch ratio during angioplasty with a linear trend line and equation fit to the data.

Table 1 Results of the paired t-test for the circumferential in vivo stretch ratio before and after treatment.

	Pretreatment In Vivo Stretch Ratio	Treated In Vivo Stretch Ratio
Mean	1.2805	1.4307
Variance	0.0375	0.0221
Degrees of Freedom	8	
t Stat	-4.7018	
P(T<=t) two-tail	0.0015	
t Critical two-tail	2.306	

Table 2 Results of the paired t-test for the circumferential in vivo stress before and after treatment.

	Pretreatment Stress (MPa)	Treated Stress (MPa)
Mean	0.0866	0.0149
Variance	0.0041	0.0001
Degrees of Freedom	7	
t Stat	3.5457	
P(T<=t) two-tail	0.0094	
t Critical two-tail	2.3646	

Table 3 Results of the paired t-test for the circumferential in vivo stiffness before and after treatment.

	Pretreatment Stiffness (MPa)	Treated Stress (MPa)
Mean	1.9142	0.1148
Variance	2.6190	0.0001
Degrees of Freedom	7	
t Stat	3.4324	
P(T<=t) two-tail	0.0109	
t Critical two-tail	2.3646	

Table 4 Regression statistics and ANOVA results between the percent change in circumferential stress and the percent change in the circumferential stretch ratio during angioplasty.

	Regression Statistics
Multiple R	0.0268
R Square	0.0007
Adjusted R Square	-0.1658
Standard Error	7.1219
Observations	8

ANOVA	**Degrees of Freedom**	**Sum of Squares**	**Mean Square**	**F**	**Significance F**
Regression	1	0.219	0.219	0.004	0.950
Residual	6	304.325	50.721		
Total	7	304.544			

Table 5 Regression statistics and ANOVA results between the percent change in circumferential stiffness and the percent change in the circumferential stretch ratio during angioplasty.

	Regression Statistics
Multiple R	0.488
R Square	0.238
Adjusted R Square	0.111
Standard Error	3.878
Observations	8

ANOVA	**Degrees of Freedom**	**Sum of Squares**	**Mean Square**	**F**	**Significance F**
Regression	1	28.200	28.200	1.875	0.220
Residual	6	90.237	15.039		
Total	7	118.437			

Table 6 Regression statistics and ANOVA results between the percent change in the circumferential in vivo stretch ratio and the percent change in the circumferential stretch ratio during angioplasty.

	Regression Statistics
Multiple R	0.902
R Square	0.813
Adjusted R Square	0.786
Standard Error	3.799
Observations	9

ANOVA	**Degrees of Freedom**	**Sum of Squares**	**Mean Square**	**F**	**Significance F**
Regression	1	439.591	439.591	30.451	8.89E-04
Residual	7	101.053	14.436		
Total	8	540.644			

Table 7 Regression statistics and ANOVA results between the diameter increase post-angioplasty and the diameter increase during angioplasty.

	Regression Statistics
Multiple R	0.867
R Square	0.752
Adjusted R Square	0.717
Standard Error	0.152
Observations	9

ANOVA	**Degrees of Freedom**	**Sum of Squares**	**Mean Square**	**F**	**Significance F**
Regression	1	0.492	0.492	21.260	2.45E-03
Residual	7	0.162	0.023		
Total	8	0.654			

Table 8 Results of the paired t-test for the in vivo axial stretch ratio before and after treatment.

	Pretreatment In Vivo Stretch Ratio	Treated In Vivo Stretch Ratio
Mean	1.7027	1.7505
Variance	6.40E-03	8.26E-03
Degrees of Freedom	8	
t Stat	-4.5960	
P(T<=t) two-tail	1.75E-03	
t Critical two-tail	2.3060	

Table 9 Results of the paired t-test for the axial in vivo stress before and after treatment.

	Pretreatment Stress (MPa)	Treated Stress (MPa)
Mean	0.2272	0.1953
Variance	0.0075	0.0033
Degrees of Freedom	7	
t Stat	2.537	
P(T<=t) two-tail	0.039	
t Critical two-tail	2.365	

Table 10 Results of the paired t-test for the axial in vivo stiffness before and after treatment.

	Pretreatment Stiffness (MPa)	Treated Stiffness (MPa)
Mean	2.753	2.070
Variance	2.300	1.353
Degrees of Freedom	7	
t Stat	3.984	
P(T<=t) two-tail	0.005	
t Critical two-tail	2.365	

Table 11 Regression statistics and ANOVA results between the percent change in the axial in vivo stretch ratio and the percent change in circumferential stretch ratio during angioplasty.

	Regression Statistics
Multiple R	0.052
R Square	0.003
Adjusted R Square	-0.140
Standard Error	1.917
Observations	9

ANOVA	**Degrees of Freedom**	**Sum of Squares**	**Mean Square**	**F**	**Significance F**
Regression	1	0.069	0.069	0.019	0.895
Residual	7	25.725	3.675		
Total	8	25.793			

Table 12 Regression statistics and ANOVA results between the percent change in the axial in vivo stress and the percent change in circumferential stretch ratio during angioplasty.

	Regression Statistics
Multiple R	7.65E-03
R Square	5.85E-05
Adjusted R Square	-0.167
Standard Error	11.831
Observations	8

ANOVA	**Degrees of Freedom**	**Sum of Squares**	**Mean Square**	**F**	**Significance F**
Regression	1	0.049	0.049	3.51E-04	0.986
Residual	6	839.873	139.979		
Total	7	839.922			

Table 13 Regression statistics and ANOVA results between the percent change in the axial in vivo stiffness and the percent change in circumferential stretch ratio during angioplasty.

	Regression Statistics
Multiple R	0.285
R Square	0.081
Adjusted R Square	-0.072
Standard Error	20.275
Observations	8

ANOVA	**Degrees of Freedom**	**Sum of Squares**	**Mean Square**	**F**	**Significance F**
Regression	1	217.302	217.302	0.529	0.495
Residual	6	2466.515	411.086		
Total	7	2683.817			

Table 14 Results of the paired t-test for the mean pixel intensity of the medial layer slices before and after treatment.

	Pretreatment Pixel Intensity	**Treated Pixel Intensity**
Mean	149.7585	160.3807
Variance	69.84692	107.8916
Degrees of Freedom	8	
t Stat	-2.64038	
P(T<=t) two-tail	0.029696	
t Critical two-tail	2.306004	

Table 15 Regression statistics and ANOVA results between the percent change in the mean pixel intensity of the medial layer slices and the percent change in circumferential stretch ratio during angioplasty.

	Regression Statistics
Multiple R	0.625
R Square	0.390
Adjusted R Square	0.303
Standard Error	6.740
Observations	9

ANOVA	Degrees of Freedom	Sum of Squares	Mean Square	F	Significance F
Regression	1	203.424	203.424	4.478	0.072
Residual	7	317.957	45.422		
Total	8	521.381			

Table 16 Results of the paired t-test for the mode of the pixel intensity of the medial layer slices before and after treatment.

	Pretreatment Pixel Intensity	Treated Pixel Intensity
Mean	120.667	121.778
Variance	2.313	1.194
Degrees of Freedom	8	
t Stat	-2.329	
P(T<=t) two-tail	0.048	
t Critical two-tail	2.306	

Table 17 Regression statistics and ANOVA results between the percent change in the mode of the pixel intensity of the medial layer slices and the percent change in circumferential stretch ratio during angioplasty.

	Regression Statistics
Multiple R	0.032
R Square	0.001
Adjusted R Square	-0.142
Standard Error	1.289
Observations	9

ANOVA	Degrees of Freedom	Sum of Squares	Mean Square	F	Significance F
Regression	1	0.012	0.012	0.007	0.935
Residual	7	11.624	1.661		
Total	8	11.636			

Table 18 Results of the paired t-test for the bright pixel percentage of the medial layer slices before and after treatment.

	Pretreatment Bright Pixel Percentage	Treated Bright Pixel Percentage
Mean	2.462	3.708
Variance	0.007	8.605
Degrees of Freedom	8	
t Stat	-1.286	
P(T<=t) two-tail	0.235	
t Critical two-tail	2.306	

Table 19 Results of the paired t-test for the mean pixel intensity of the ring slices before and after treatment.

	Pretreatment Pixel Intensity	Treated Pixel Intensity
Mean	140.8626	144.6808
Variance	81.23872	29.92584
Degrees of Freedom	8	
t Stat	-1.88825	
P(T<=t) two-tail	0.095683	
t Critical two-tail	2.306004	

Table 20 Results of the paired t-test for the mode of the pixel intensity of the ring slices before and after treatment.

	Pretreatment Pixel Intensity	Treated Pixel Intensity
Mean	119.72	120.94
Variance	7.63	1.47
Degrees of Freedom	8	
t Stat	-2.160	
P(T<=t) two-tail	0.063	
t Critical two-tail	2.306	

Table 21 Results of the paired t-test for the bright pixel percentage of the ring slices before and after treatment.

	Pretreatment Bright Pixel Percentage	Treated Bright Pixel Percentage
Mean	2.571	4.613
Variance	0.013	8.694
Degrees of Freedom	8	
t Stat	-2.096	
P(T<=t) two-tail	0.069	
t Critical two-tail	2.306	

Table 22 Results of the paired t-test for the waviness ratios before and after treatment.

	Pretreatment Waviness Ratio	Treated Waviness Ratio
Mean	1.153	1.082
Variance	1.31E-03	6.76E-04
Degrees of Freedom	8	
t Stat	9.140	
P(T<=t) two-tail	1.65E-05	
t Critical two-tail	2.306	

Table 23 Regression statistics and ANOVA results between the percent change in the waviness ratios and the percent change in circumferential stretch ratio during angioplasty.

	Regression Statistics
Multiple R	0.408
R Square	0.166
Adjusted R Square	0.047
Standard Error	1.852
Observations	9

ANOVA	Degrees of Freedom	Sum of Squares	Mean Square	F	Significance F
Regression	1	4.792	4.792	1.397	0.276
Residual	7	24.018	3.431		
Total	8	28.810			

CHAPTER 3

EXPLORATORY IN VIVO EXPERIMENTS

Purpose of Study

After observing the effects of in vitro angioplasty on porcine carotid arteries, we wanted to explore the effects of in vivo angioplasty on carotid and other peripheral arteries. We also wanted to see how the effects of angioplasty are recovered over time and collect data to guide further research. This was accomplished by performing in vivo angioplasty on Göttingen minipigs and harvesting arteries at different times post-angioplasty.

Experimental Procedure

This procedure, which involved live animals, was approved by the University of Utah Animal Care and Use Committee. Göttingen minipigs were anesthetized, and ultrasound was used to locate and gain initial access to the femoral or iliac artery. A guide wire was then inserted and guided with fluoroscopy angiography to different locations within the vasculature. To help locate each treatment site, its position relative to anatomical landmarks, such as arterial branches or skeletal features, was recorded. When a desired location in the vasculature was reached, an angioplasty balloon was guided along the wire to the area and then inflated for one minute. It was then deflated and

removed. The balloon and guide wire were removed through the access point, which was then closed. All angioplasty procedures were performed by Dr. Matthew Alexander, a neurointerventional surgeon who regularly performs similar procedures in humans. The pigs were allowed to recover for eight or twelve days after the procedure. After the recovery period had passed, the pigs were euthanized by phenytoin/pentobarbital overdose, and the arteries were harvested.

The remainder of the sample preparation, mechanical evaluation, and histology followed the preparation outlined in Chapter 2. While all arteries harvested were imaged, only the carotid arteries were large and straight enough to be mechanically evaluated. The resulting mechanical and histological sample sizes were too small for statistical testing.

Results

After the experiment's conclusion, one pig was harvested after an eight-day recovery period and another after a twelve-day recovery. The eight-day recovery pig had the following arteries treated and harvested: left and right carotid, left and right internal iliac, left and right external iliac, and left and right subclavian. For the twelve-day recovery pig, the arteries on the right side of the body did not experience angioplasty but were harvested and evaluated to serve as baseline samples. The left carotid, left external iliac, and left subclavian arteries were treated and harvested. The right external iliac was not harvested to serve as the pretreatment sample because it was used to access the vasculature and was damaged during access. The left internal iliac artery was also not harvested because the guide wire could not be maneuvered into the artery. To have iliac artery samples representing pretreatment, eight days posttreatment, and twelve days

posttreatment, all iliac arteries were combined into a singular comparison group due to their similar location, size, and function.

Mechanical Properties

The carotid arteries display the same softening pattern found in the in vivo study, as seen in the circumferential stress-stretch curves in Figure 47. The eight- and twelve-day curves are shifted to the right compared to the pretreatment, suggesting the arteries had softened. The twelve-day curve almost matches the pretreatment artery, suggesting that recovery had occurred by then. The in vivo circumferential stress, seen in Figure 48, follows the trend in the stress-stretch curves. The stress is decreased in the eight-day sample and returned to pretreatment levels in the twelve-day sample. This also suggests that angioplasty causes circumferential softening, which the artery mostly recovers from within twelve days after treatment. The same pattern is also present in the in vivo circumferential stiffness, seen in Figure 49, except that the twelve-day sample has an increased stiffness compared to the pretreatment carotids. This could be caused by remodeling in the artery or natural variance in the samples. The circumferential in vivo stretch ratio, seen in Figure 50, does not follow the pattern observed in the other mechanical properties. The stretch ratio decreased following treatment and is still decreased after twelve days of recovery. The in vitro studies showed that angioplasty-induced softening causes the in vivo stretch ratio to increase, not decrease. This discrepancy could be due to in vivo conditions differing from in vitro conditions. In vivo, the carotid artery is supported by the surrounding tissues. The SMCs, which are active in vivo, also help the artery adapt to different loads and stresses. These factors could cause

the in vivo stretch ratio to change differently than what was observed during the in vitro study.

The carotid artery axial properties behaved similarly to the circumferential properties. The stress-stretch curves in Figure 51 suggest that angioplasty-induced softening has occurred and is still present twelve days posttreatment. The eight- and twelve-day curves are shifted to the right of the pretreatment curve, and the shape of the eight-day curve is also altered. The twelve-day curve is close in shape and location to the pretreatment curve, suggesting recovery has occurred. The axial in vivo stretch ratio, shown in Figure 52, decreases following angioplasty, which does not match previous results. The in vivo stretch ratio returns to pretreatment levels by twelve days post-angioplasty, implying that the artery has begun to recover. The axial in vivo stress, seen in Figure 53, follows the expected pattern of decreasing at eight days post-angioplasty but starting to show recovery by day twelve. The axial in vivo stiffness, seen in Figure 54, deviates from the pattern. At twelve days post-angioplasty, the axial stiffness decreased to less than the pretreatment and eight-day arteries. This could be due to tissue remodeling in the carotid wall. The damaged components of the artery need to be broken down and removed before new healthy growth can occur. It is possible that this artery was in the middle of this process, meaning no new tissue had begun to be formed, and the artery was even softer than earlier in the procedure. While this is possible, further investigation would be needed to be sure.

Histology Results

Carotid Arteries

Overall, the histology results from the in vivo investigation are more challenging to parse and gather conclusions from, but they still provide helpful insights. The carotid medial and ring slices all suggest that damage from angioplasty, indicated by CHP attachment and waviness ratios, is present eight days posttreatment. However, the damage is mostly recovered by twelve days posttreatment. Both histograms, see Figures 55 and 56, show that the eight-day recovery slices are at higher intensities than the controls. The twelve-day slices are at similar or even lower intensities than the controls. The bright pixel percentage, Figures 57 and 58, mean pixel intensity, Figures 59 and 60, and the mode of the pixel intensity, Figures 61 and 62, for both the ring and layers slices show similar behavior. The values are elevated eight days posttreatment and then return to near control levels by twelve days posttreatment. This suggests a greater amount of damage is present in the artery on day eight, which is then repaired by day twelve. The carotid artery waviness ratios in Figure 63 also support this conclusion. The waviness ratios decreased on day eight, meaning angioplasty had stretched and straightened the carotid's microstructure. On day twelve, the waviness ratios were elevated past control levels. Repair and remodeling could form new fibers that are wavier than those already in the artery. These measures suggest that in vivo angioplasty does cause microstructural damage to the carotid artery that is still present eight days post-angioplasty. However, the damage is mostly recovered at twelve days post-angioplasty.

Iliac Arteries

The histograms of the iliac arteries show the messiest signals of any sample set. Both the medial layer slices histogram, Figure 64, and the ring slices histogram, Figure 65, show that eight-day samples have elevated pixel intensities that are reduced to near control levels in the twelve-day samples. It is worth noting that the eight-day external iliac slices have intensities lower than the control samples for both the medial layer and ring slices. This could suggest that the internal and external iliac arteries are not similar enough to be in the same comparison group in future studies.

The quantitative comparisons provide further insight. The ring and medial layer slices' bright pixel percentage, Figures 66 and 67, mean pixel intensity, Figures 68 and 69, and the medial layer slices' mode of the pixel intensity, Figure 70, are increased at day eight but then return to near control levels by day twelve, which is expected based on previous histology results. The ring slices' mode of the pixel intensity, Figure 71, is an exception to this pattern. The twelve-day recovery mode values are closer to day eight levels than control levels, but all three measurements are relatively close to each other.

The waviness ratios for the iliac arteries, seen in Figure 72, increased at eight days post-angioplasty compared to the controls, which is the opposite of what was expected. The other experiments show that angioplasty decreases the waviness ratio due to stretching and straightening the microstructure, but that is not seen here. There are a few different explanations that could account for this anomaly. It is possible that remodeling in the iliac is completed before day eight, and the new components of the microstructure are naturally wavier than the preexisting components seen in the controls. It is also possible that the samples taken from the iliac artery eight days post-angioplasty did not

include the part of the artery inflated with the angioplasty balloon. This would mean the microstructure would be more like the controls due to not experiencing angioplasty. Lastly, it is also possible that the internal and external iliac arteries differ more than their similar size, location, and function would suggest, meaning that including them all in one comparison group may need to be reconsidered. At twelve days post-angioplasty, the waviness ratio has returned to control levels, which is expected. While the results of the iliac arteries are less conclusive, there is still the general pattern of angioplasty-induced microstructural damage and changes present eight days following treatment. At twelve days posttreatment, the damage and changes to the microstructure are mostly recovered.

Subclavian Arteries

The results from the subclavian arteries are cleaner, but anomalies similar to those in other in vivo results exist. The histology results suggest that angioplasty causes damage to subclavian arteries, that damage is still present eight days after treatment, and that the damage is mostly recovered by the twelfth-day post-angioplasty. It is also possible that damage is still present or that remodeling is still occurring on day twelve. This is seen in the ring histogram, see Figure 73, which shows an increased intensity at day eight that returns to a profile similar to the controls by day twelve. The medial layer histogram, see Figure 74, also shows this, except that the twelve-day recovery histogram has a taller and longer tail towards higher intensities than the other treatment levels, which suggests persistent damage or remodeling.

The bright pixel percentage for the medial layer and ring slices, Figures 75 and 76, support the conclusions drawn from the histograms. The percentage is highest on day

twelve, suggesting the continued presence of damage or remodeling. The medial layer and ring slices disagree on this pattern when looking at the mean and mode of the pixel intensities. The mean pixel intensity of the medial layer slices, Figure 77, increases throughout treatment, while the mean pixel intensity of the ring slices, Figure 78, peaks on day eight and drops below control levels on day twelve. The medial layer and ring slices display the same behavior when examining the mode of the pixel intensity, as seen in Figures 79 and 80. The mode of the pixel intensity peaks on day eight and then is at or below control levels by day twelve. These differences could be due to angioplasty primarily loading the artery circumferentially, so the ring slices may not capture the same damage or recovery seen in the medial layer slices.

The subclavian artery's waviness ratio, Figure 81, also suggests that recovery may still occur twelve days post-angioplasty. The waviness ratio decreases throughout the treatment process and is at its lowest on day twelve. This differs from the other arteries investigated but is consistent with the other histology results for the subclavian arteries. This suggests angioplasty causes microstructural damage and changes to the iliac artery, and recovery is incomplete by the twelfth-day post-angioplasty. It is worth noting that for each of these quantitative measures, each treatment group had some variability, and the differences between each group were minor. This could be obscuring the actual behavior.

Limitations and Conclusions

This experiment relied heavily on the procedures developed and outlined in Chapter 2. That means it is subject to the same shortcomings regarding the resulting mechanical and histological data. There are also other ways to improve the results of a

similar study. The first is increasing the sample size. The second is having an improved setup of the controls and different treatment levels. This would include separating the internal and external iliac arteries into their own comparison groups, collecting samples of arteries immediately after angioplasty to have another treatment level for comparison, and determining if contralateral samples are the best options to serve as controls for each arterial location. There is also the challenge of tracking the exact location subject to angioplasty throughout every stage of the treatment. Placing a long-lasting physical indicator on the section of the treated artery would ensure that it is later harvested and evaluated, removing uncertainty during evaluation. Another limitation of these exploratory experiments is that only the carotid arteries could be mechanically evaluated. Adjustment and improvement to the myograph, or utilizing a different mechanical evaluation regiment, would allow for the characterization of all the other arteries. Lastly, the artery's stretch during angioplasty could not be found due to the visual data provided by fluoroscopy. This was a useful variable and metric in the in vitro study, so developing a method to see it during in vivo treatment would help better generalize the data and make them more comparable.

Considering those limitations, valuable conclusions can still be drawn from the in vivo experiments. Mechanical softening was suggested by the observations in the carotid arteries following angioplasty. The arteries had begun to recover by the eighth-day post-angioplasty, and that recovery was also seen on the twelfth-day post-angioplasty. Collagen damage was observed eight days after angioplasty in every location tested, as indicated by the amount of CHP in the tissue samples. This was also true when investigating the other parts of the artery's microstructure, as seen with the decrease in

waviness ratios following angioplasty. The amount of remodeling and recovery varied depending on the artery's location in the body. Some arteries showed a complete recovery by day twelve, others a partial recovery, and some seemed to show an increase in microstructural damage at day twelve. These findings mostly agree with what was found in the in vitro study and suggest interesting avenues for future studies.

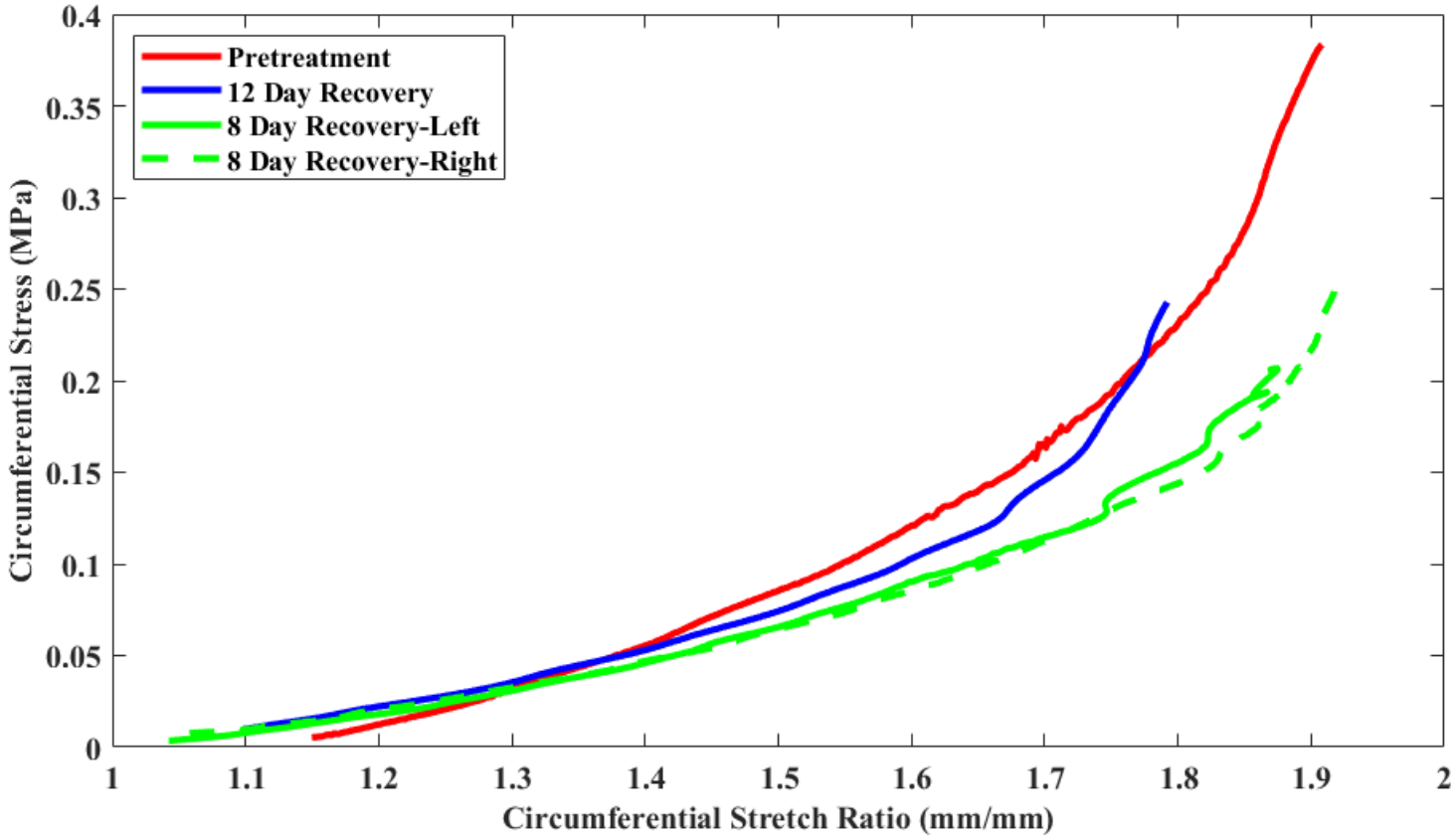

Figure 47 Circumferential stress-stretch curves of the carotid arteries throughout the exploratory experiments.

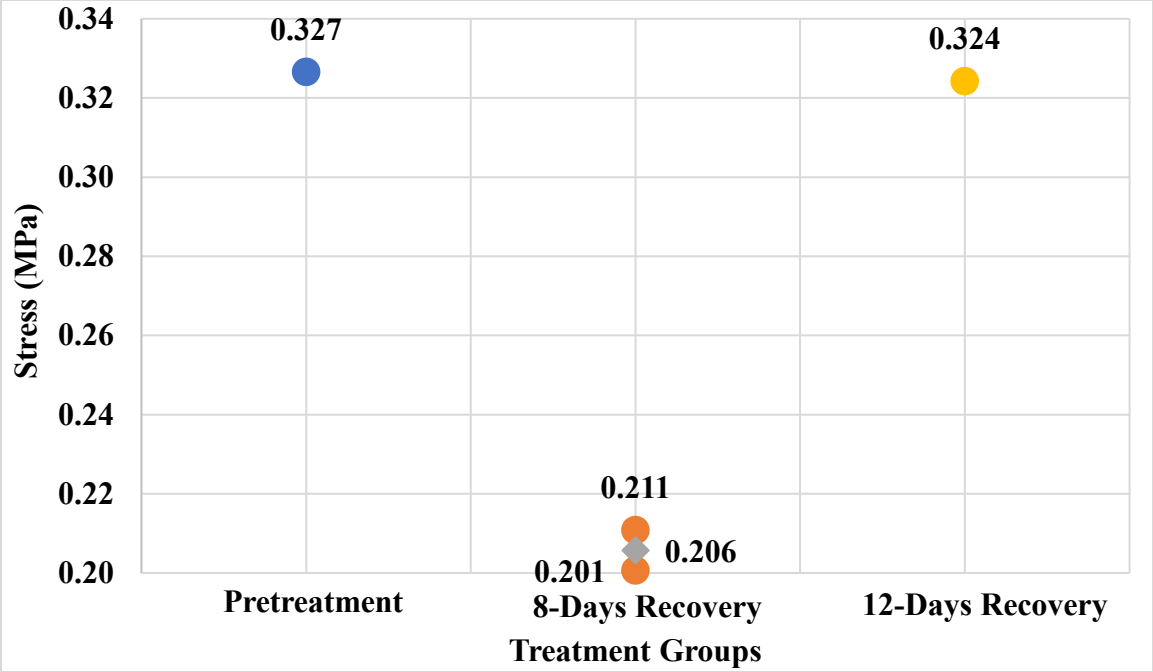

Figure 48 Values of the circumferential stress at the in vivo configuration for the carotid arteries throughout the exploratory experiments. Diamond-shaped markers indicate a group's mean value.

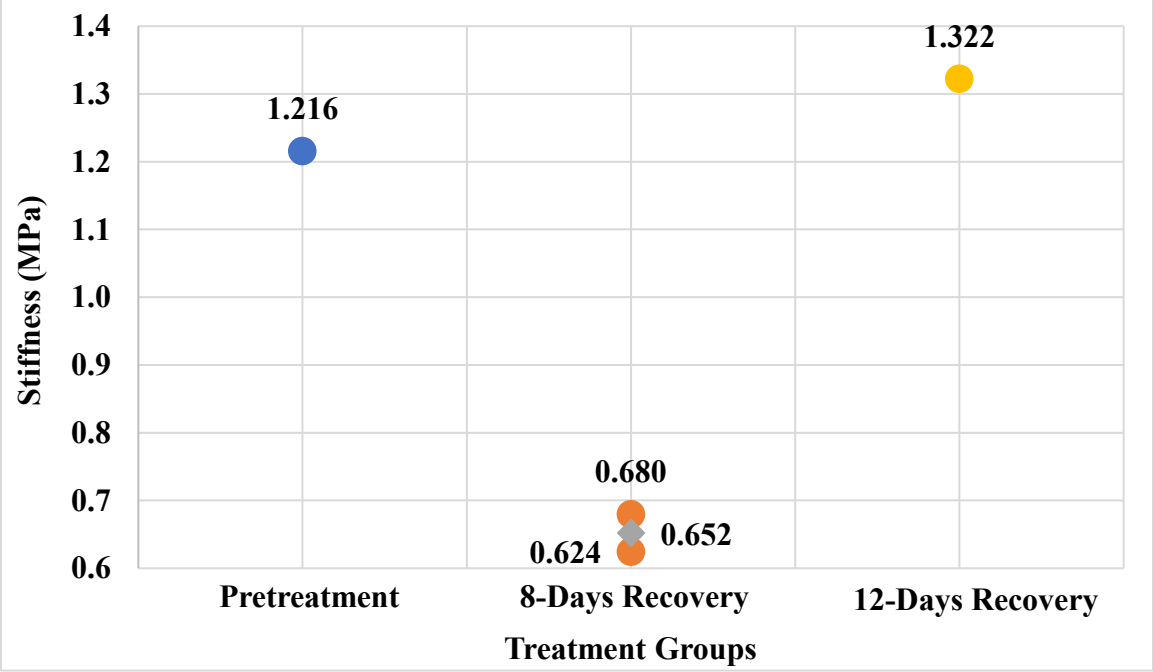

Figure 49 Values of the circumferential stiffness at the in vivo configuration for the carotid arteries throughout the exploratory experiments. Diamond-shaped markers indicate a group's mean value.

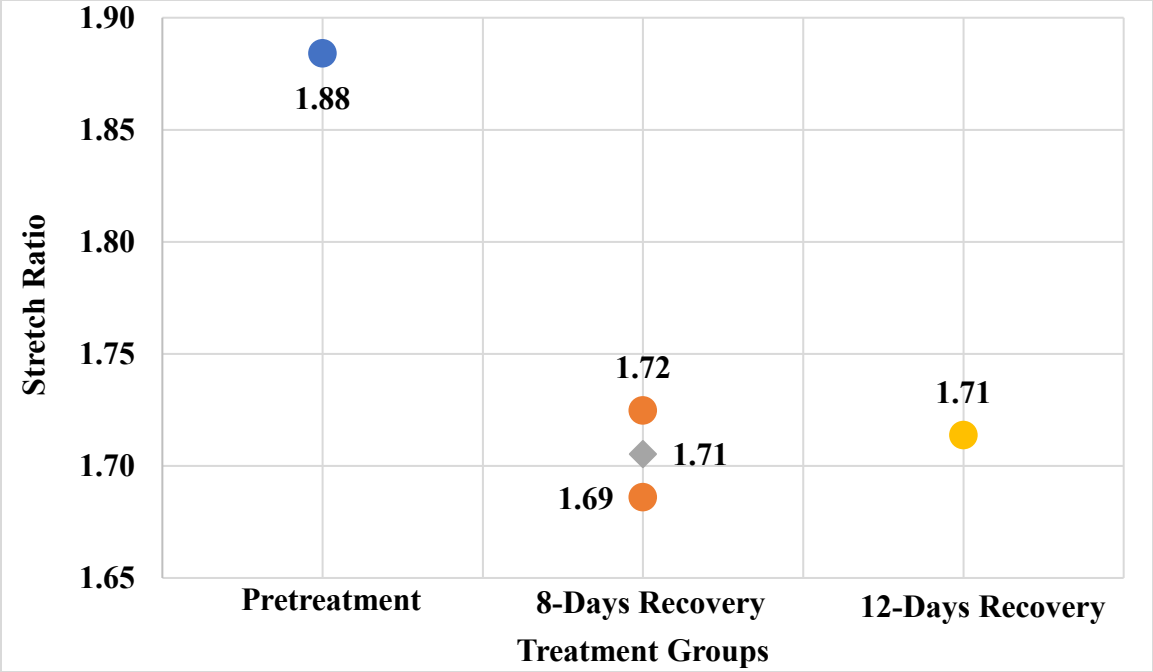

Figure 50 Values of the carotid arteries' circumferential in vivo stretch ratio throughout the exploratory experiments. Diamond-shaped markers indicate a group's mean value.

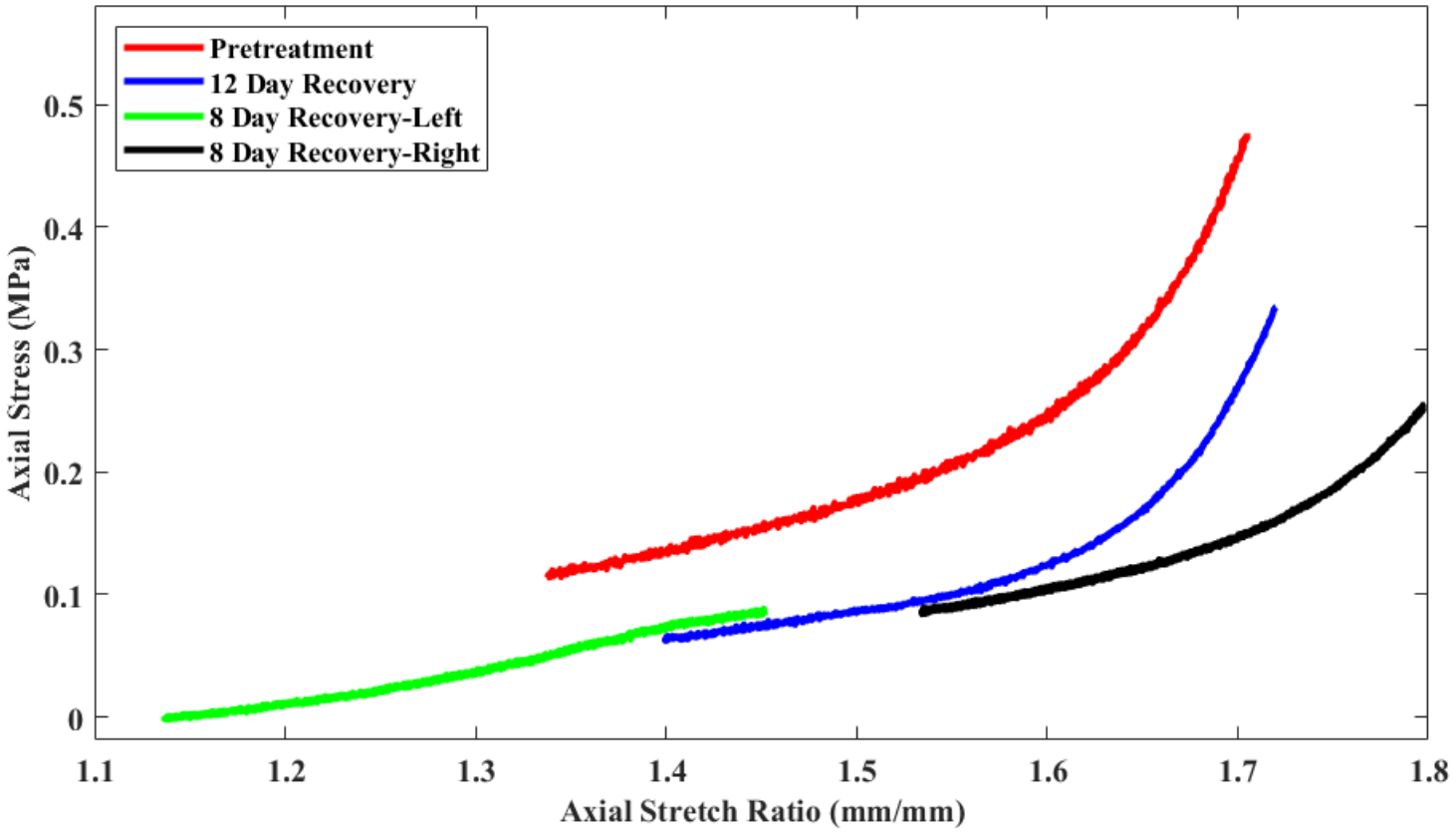

Figure 51 Axial stress-stretch curves of the carotid arteries throughout the exploratory experiments.

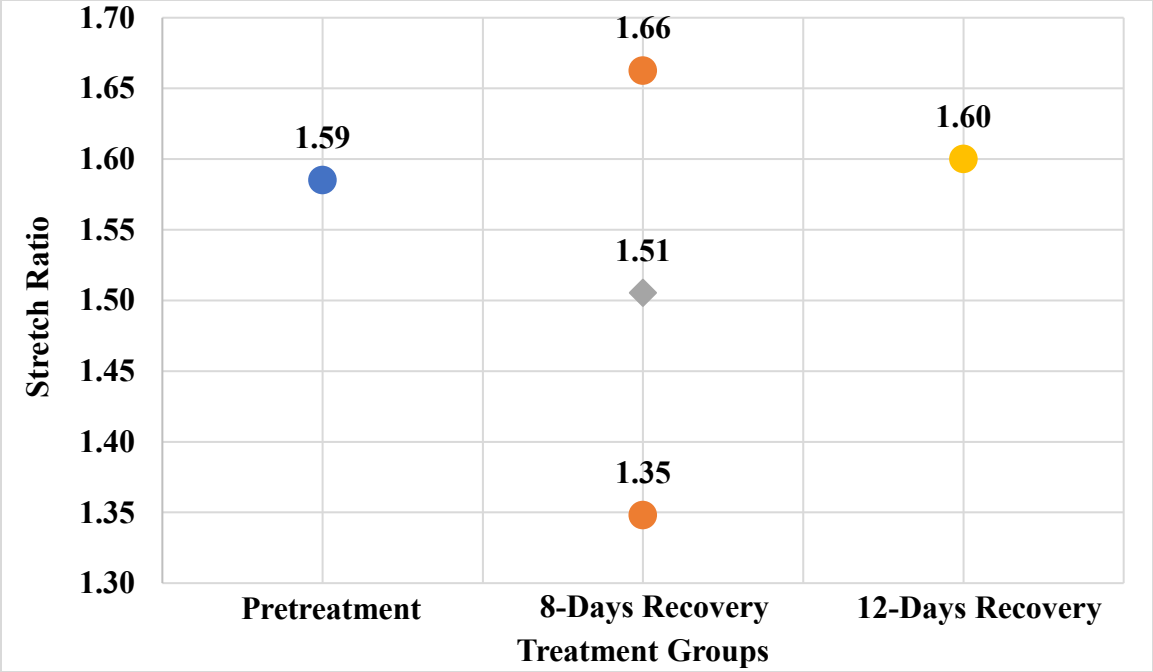

Figure 52 Values of the carotid arteries' axial in vivo stretch ratio throughout the exploratory experiments. Diamond-shaped markers indicate a group's mean value.

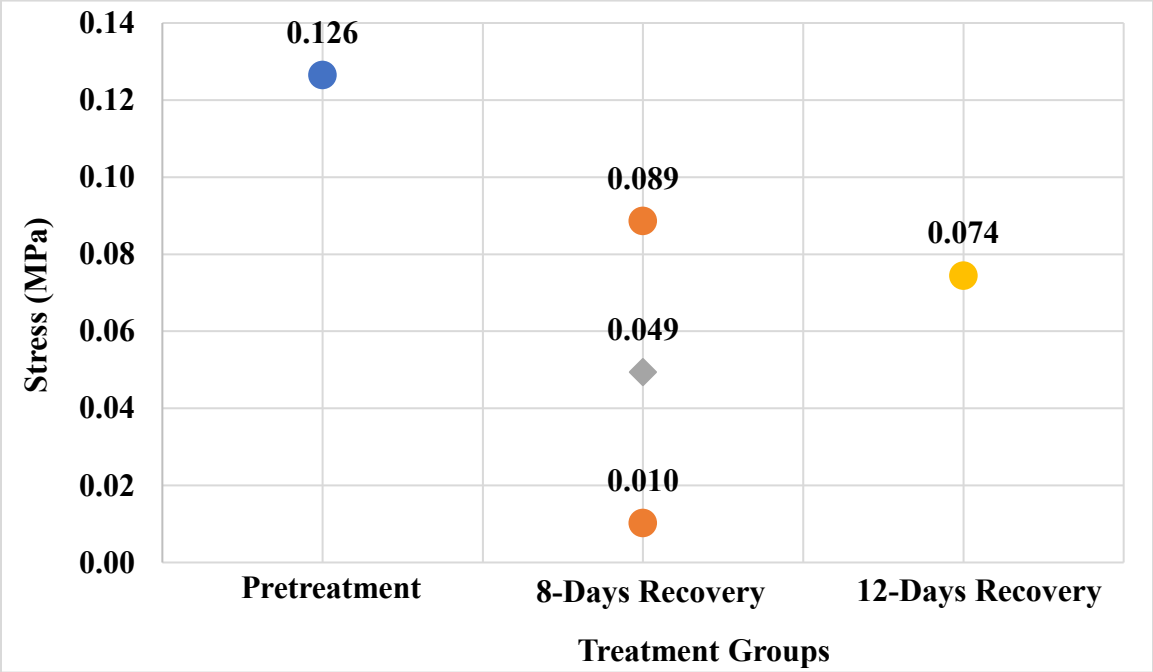

Figure 53 Values of the axial stress at the in vivo configuration for the carotid arteries throughout the exploratory experiments. Diamond-shaped markers indicate a group's mean value.

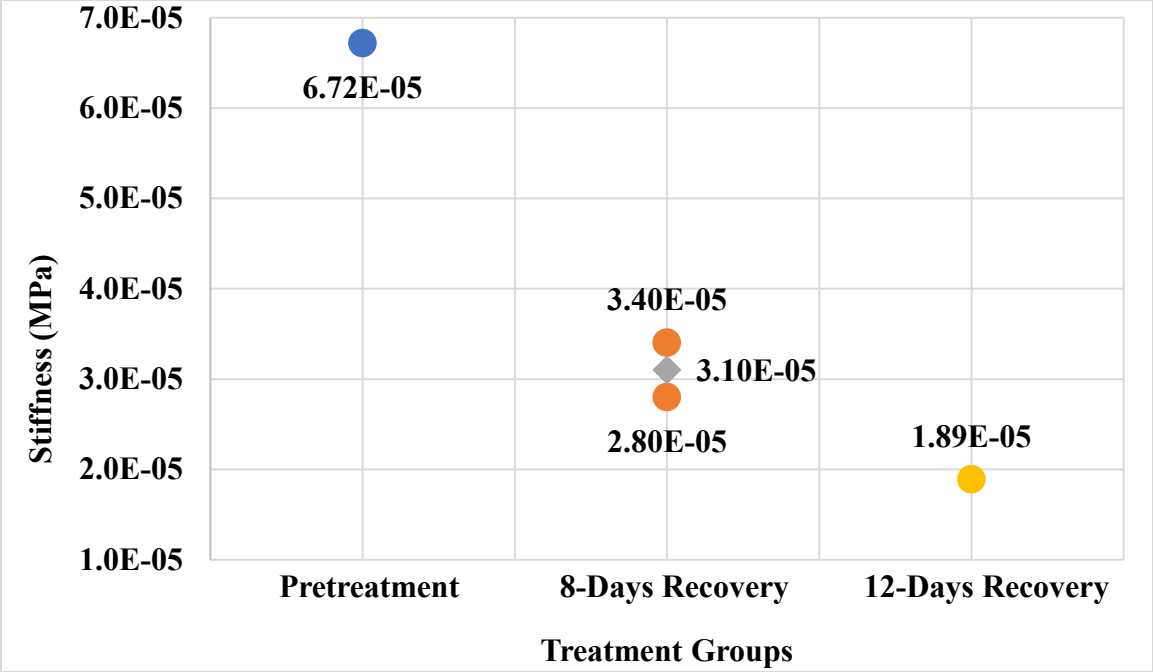

Figure 54 Values of the axial stiffness at the in vivo configuration for the carotid arteries throughout the exploratory experiments. Diamond-shaped markers indicate a group's mean value.

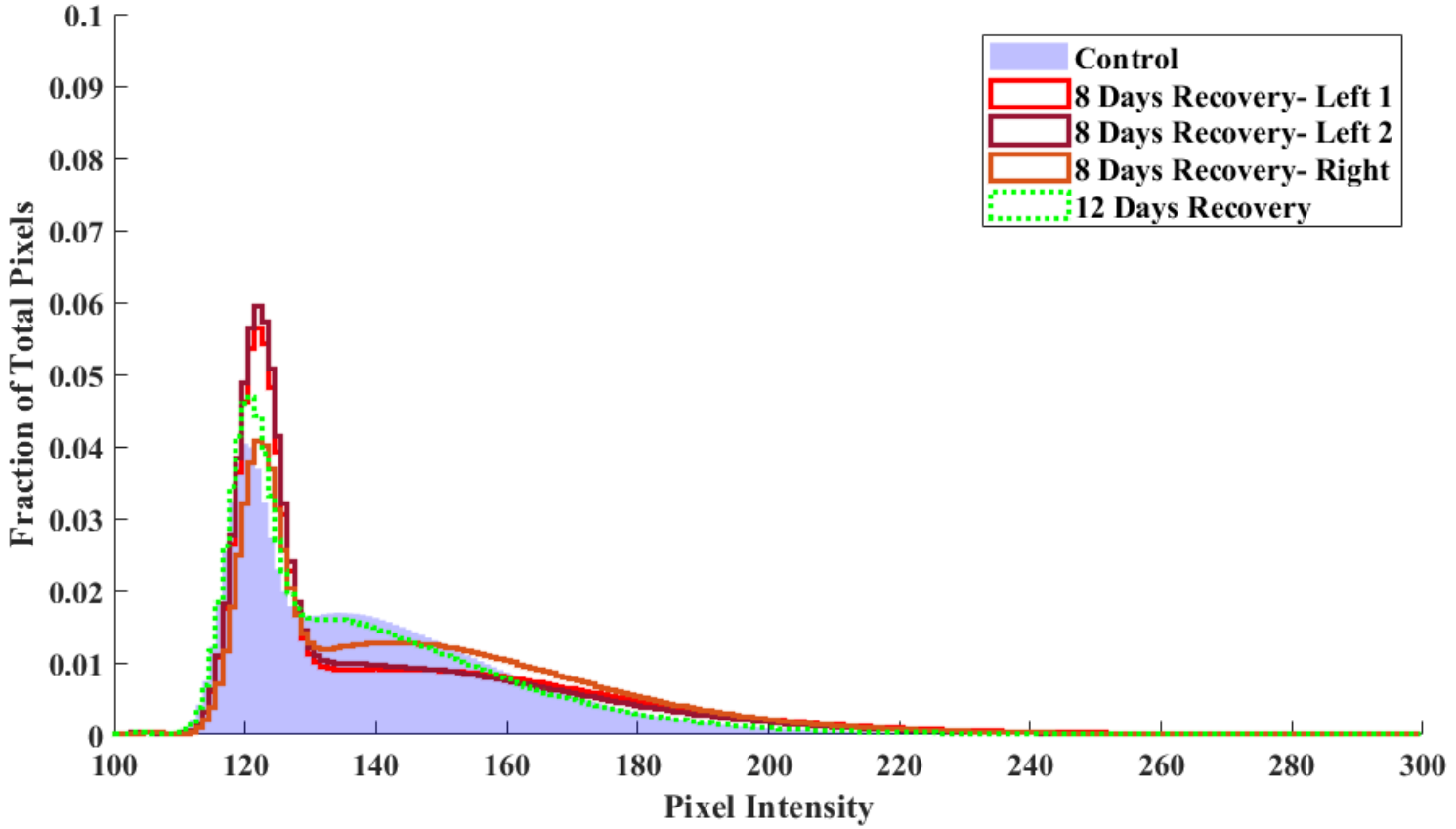

Figure 55 Histogram of pixel intensity from the CHP-stained histology images of the medial layer slices of the carotid arteries throughout the exploratory experiments.

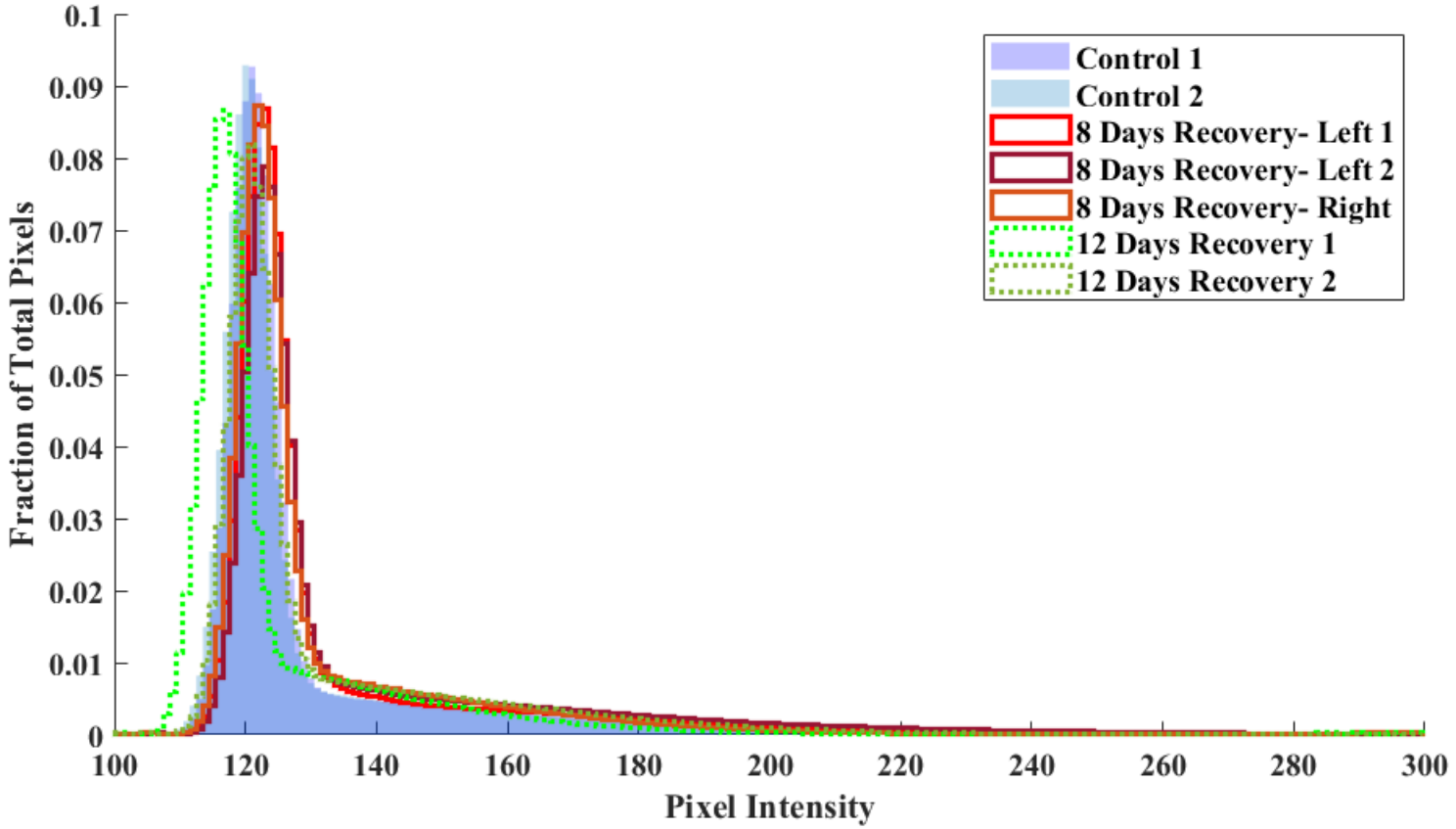

Figure 56 Histogram of pixel intensity from the CHP-stained histology images of the ring slices of the carotid arteries throughout the exploratory experiments

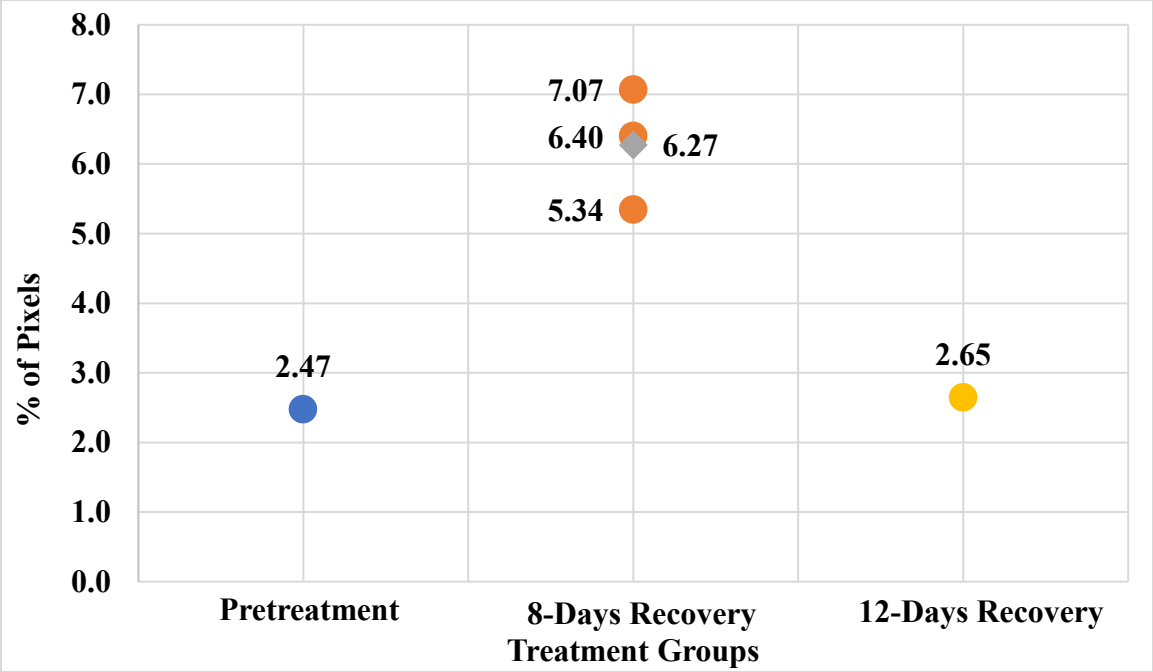

Figure 57 Values of the bright pixel percentage for the carotid medial layer slices throughout the exploratory experiments. Diamond-shaped markers indicate a group's mean value.

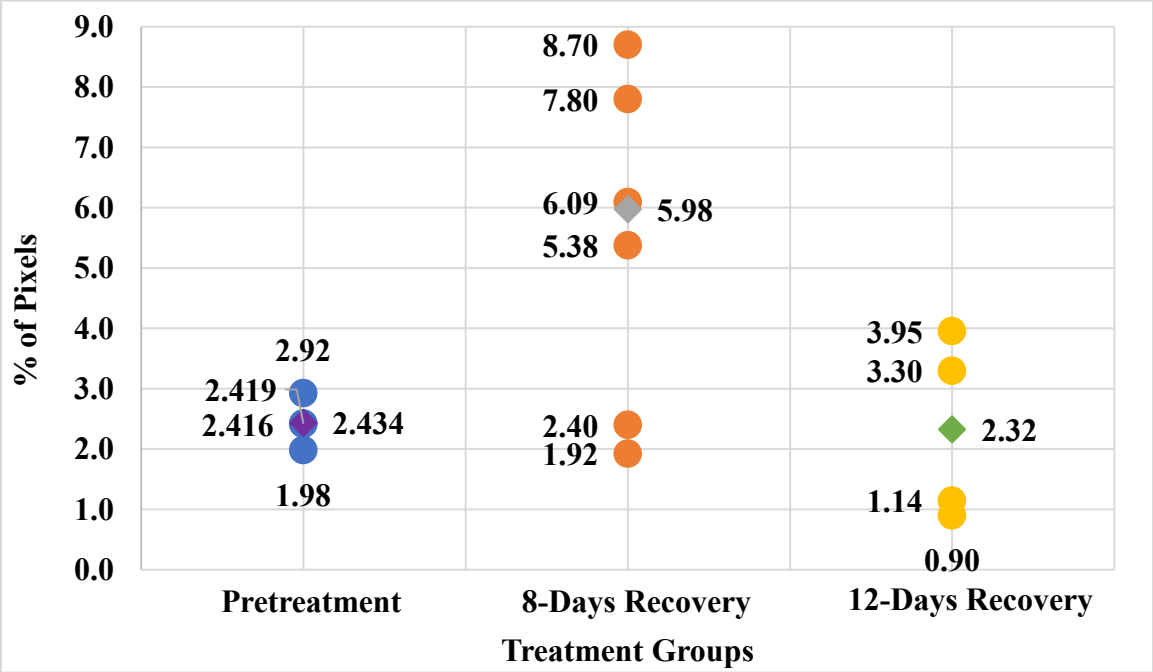

Figure 58 Values of the bright pixel percentage for the carotid ring slices throughout the exploratory experiments. Diamond-shaped markers indicate a group's mean value.

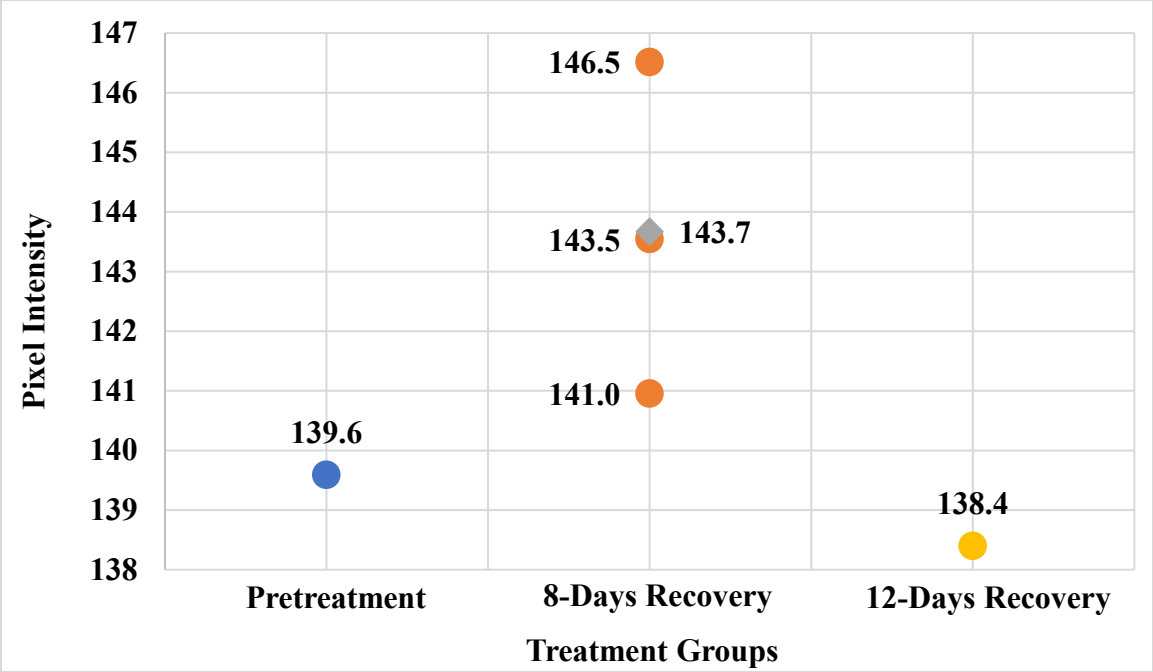

Figure 59 Values of the mean pixel intensity for the carotid medial layer slices throughout the exploratory experiments. Diamond-shaped markers indicate a group's mean value.

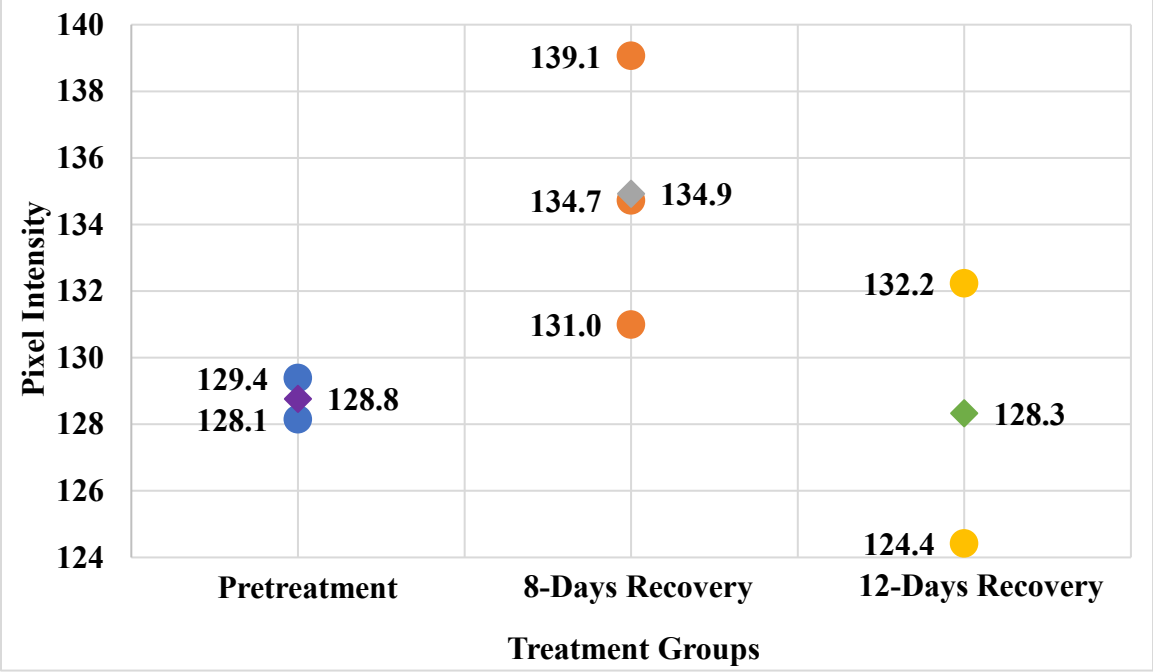

Figure 60 Values of the mean pixel intensity for the carotid ring slices throughout the exploratory experiments. Diamond-shaped markers indicate a group's mean value.

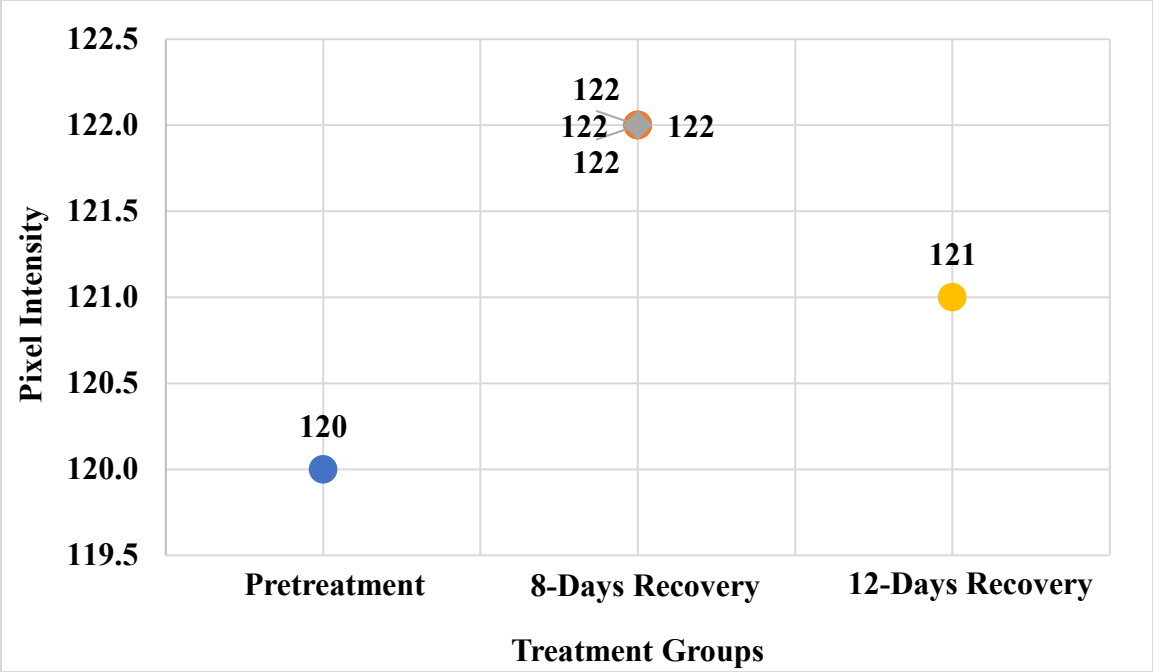

Figure 61 Values of the mode of the pixel intensity for the carotid medial layer slices throughout the exploratory experiments. Diamond-shaped markers indicate a group's mean value.

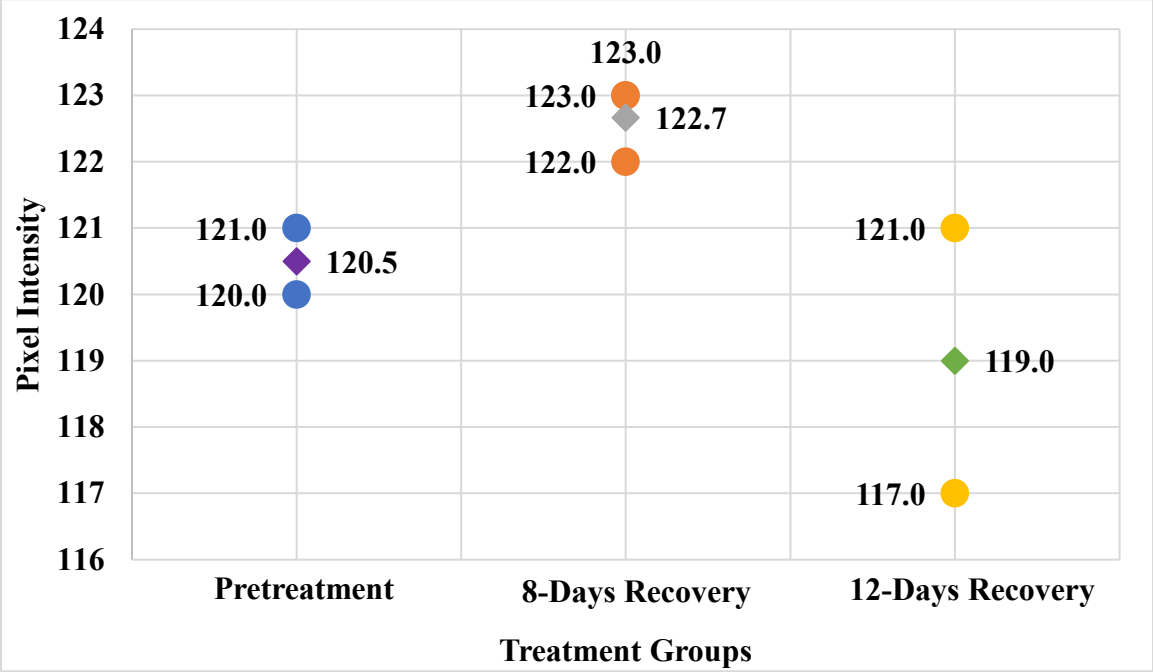

Figure 62 Values of the mode of the pixel intensity for the carotid ring slices throughout the exploratory experiments. Diamond-shaped markers indicate a group's mean value.

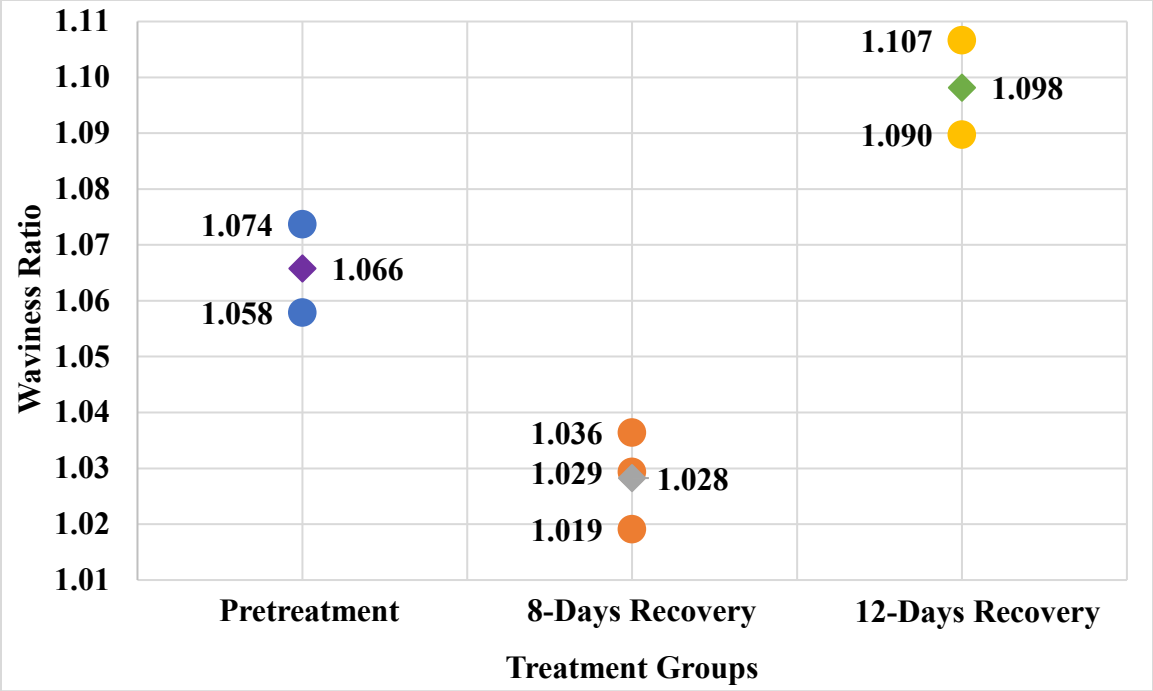

Figure 63 Values of the waviness ratios for the carotid arteries throughout the exploratory experiments. Diamond-shaped markers indicate a group's mean value.

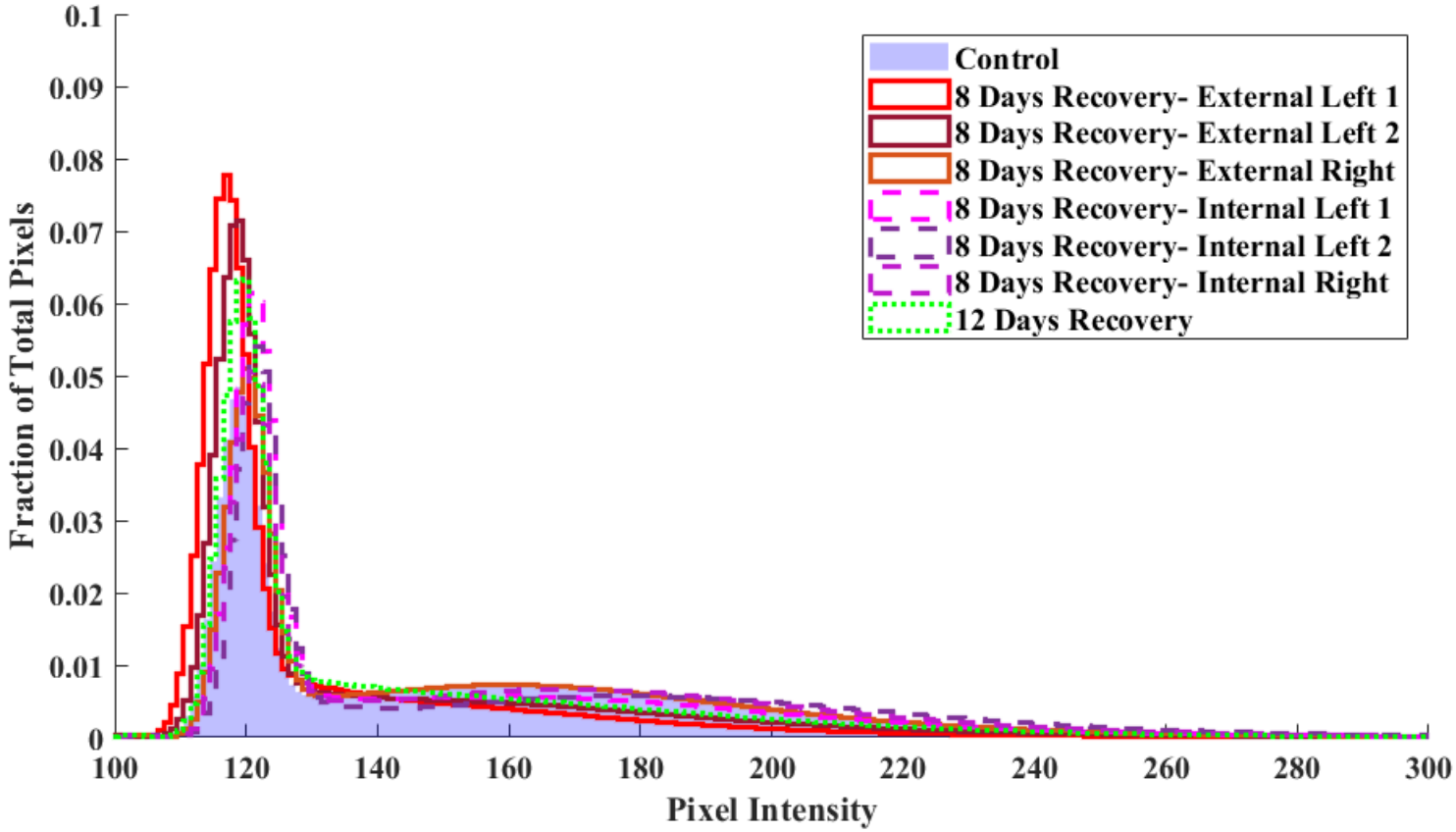

Figure 64 Histogram of pixel intensity from the CHP-stained histology images of the medial layer slices of the iliac arteries throughout the exploratory experiments.

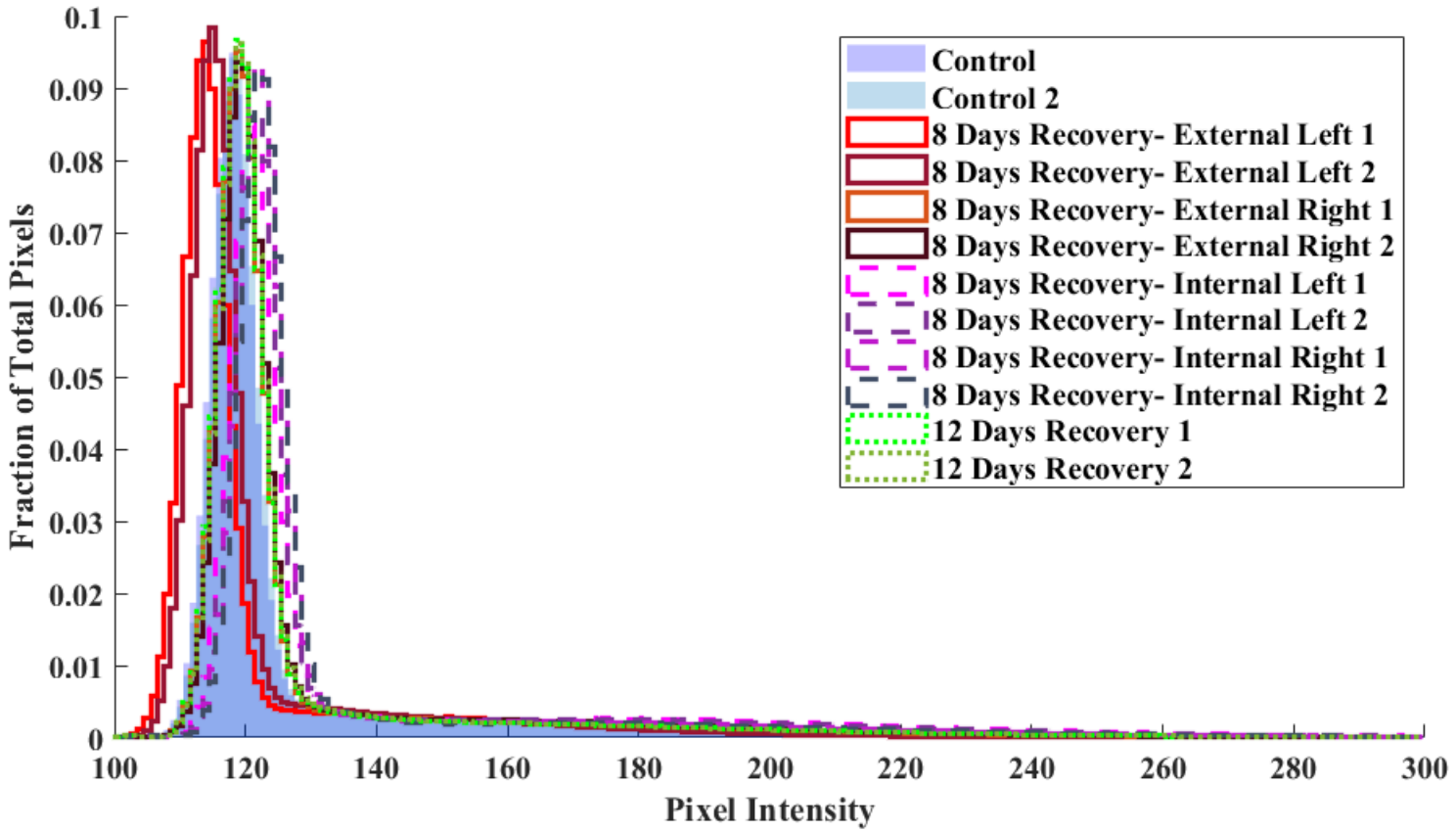

Figure 65 Histogram of pixel intensity from the CHP-stained histology images of the ring slices of the iliac arteries throughout the exploratory experiments.

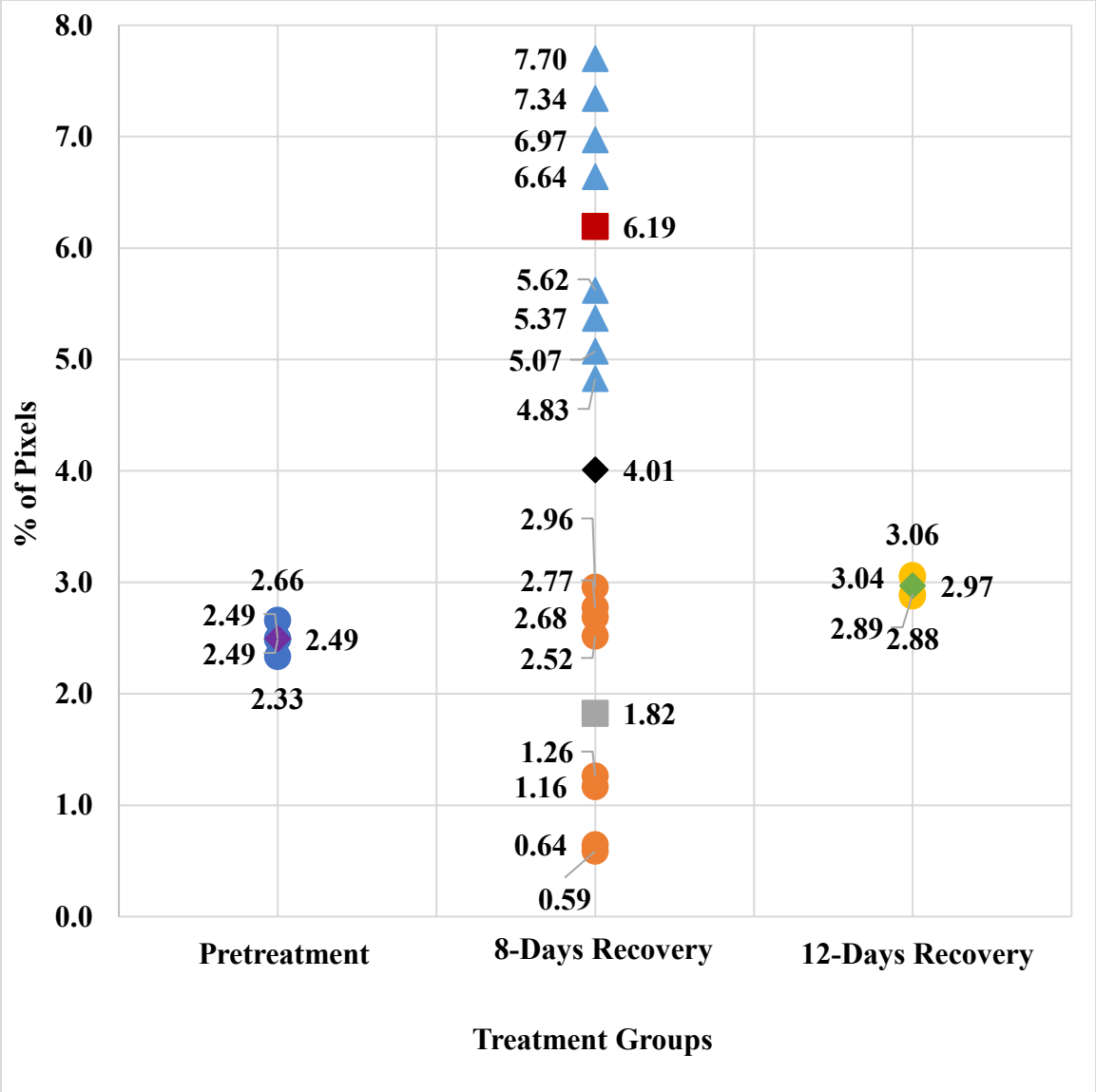

Figure 66 Values of the bright pixel percentages for the iliac ring slices throughout the exploratory experiments. For the eight-day recovery group, the triangle markers indicate the internal iliac artery, and the circle markers indicate the external artery. The square markers indicate each artery's average. Diamond-shaped markers indicate a group's mean value.

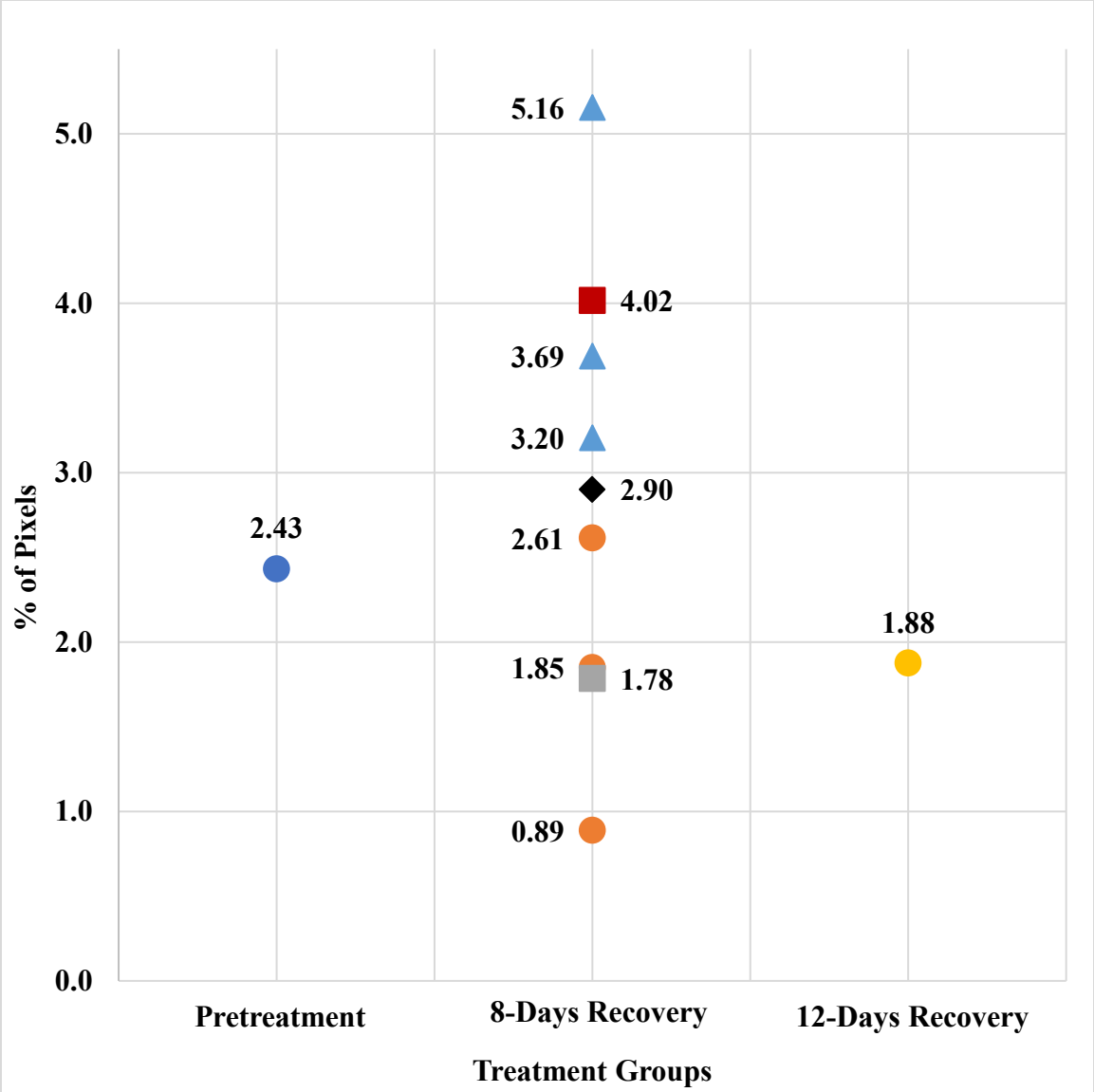

Figure 67 Values of the bright pixel percentages for the iliac medial layer slices throughout the exploratory experiments. For the eight-day recovery group, the triangle markers indicate the internal iliac artery, and the circle markers indicate the external artery. The square markers indicate each artery's average. Diamond-shaped markers indicate a group's mean value.

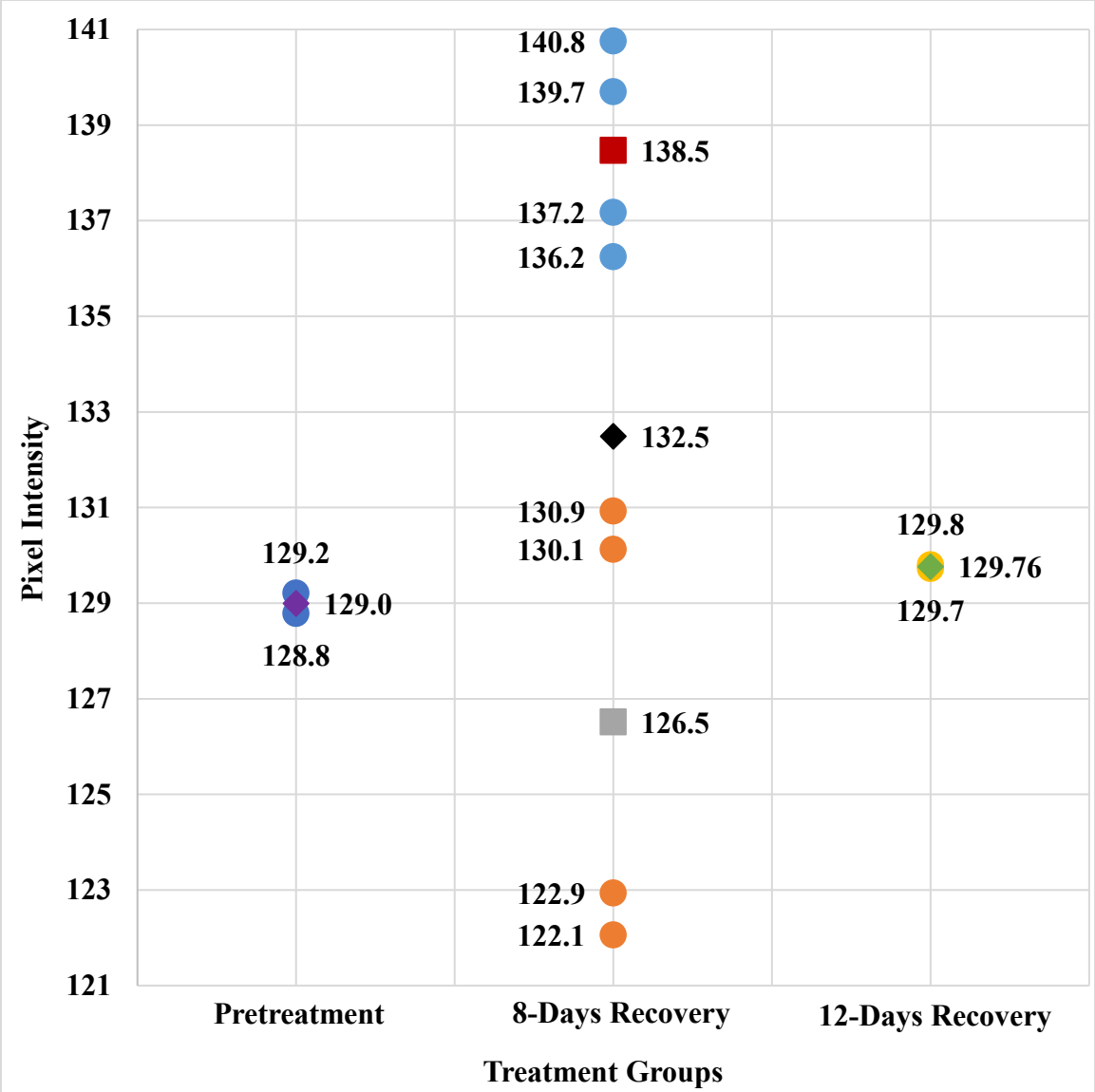

Figure 68 Values of the mean pixel intensities for the iliac ring slices throughout the exploratory experiments. For the eight-day recovery group, the triangle markers indicate the internal iliac artery, and the circle markers indicate the external artery. The square markers indicate each artery's average. Diamond-shaped markers indicate a group's mean value.

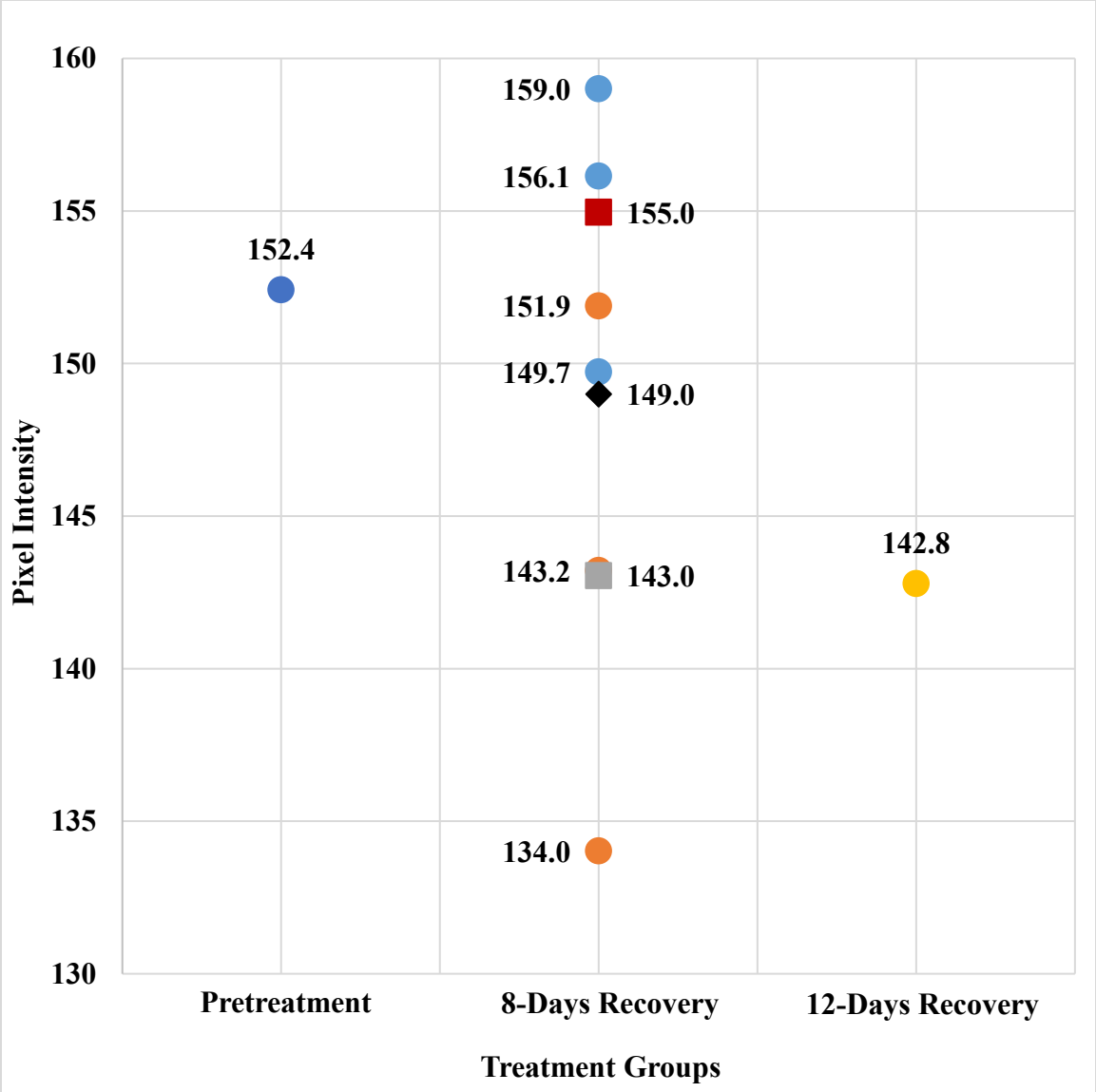

Figure 69 Values of the mean pixel intensities for the iliac medial layer slices throughout the exploratory experiments. For the eight-day recovery group, the triangle markers indicate the internal iliac artery, and the circle markers indicate the external artery. The square markers indicate each artery's average. Diamond-shaped markers indicate a group's mean value.

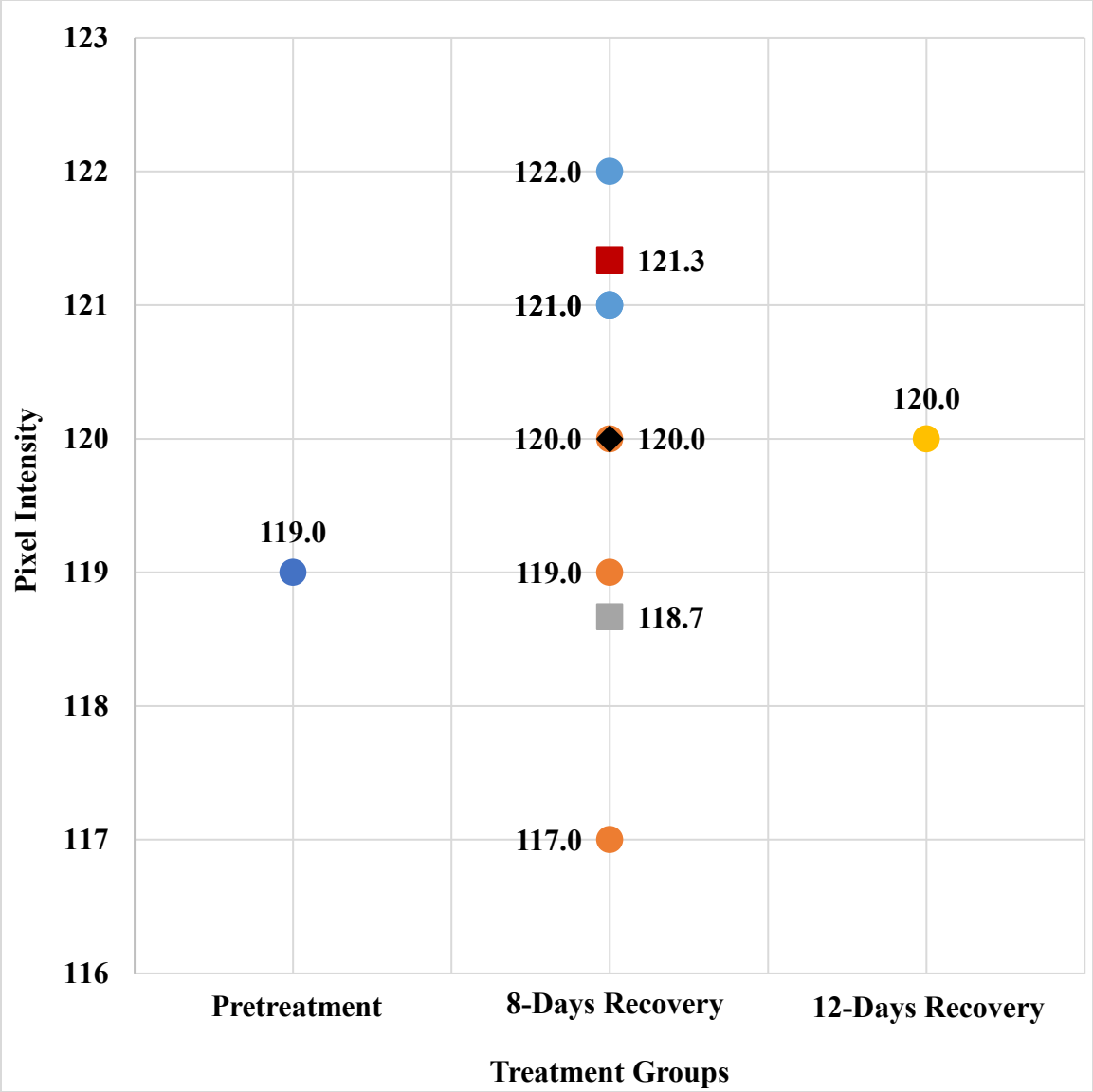

Figure 70 Values of the mode of the pixel intensities for the iliac medial layer slices throughout the exploratory experiments. For the eight-day recovery group, the triangle markers indicate the internal iliac artery, and the circle markers indicate the external artery. The square markers indicate each artery's average. Diamond-shaped markers indicate a group's mean value.

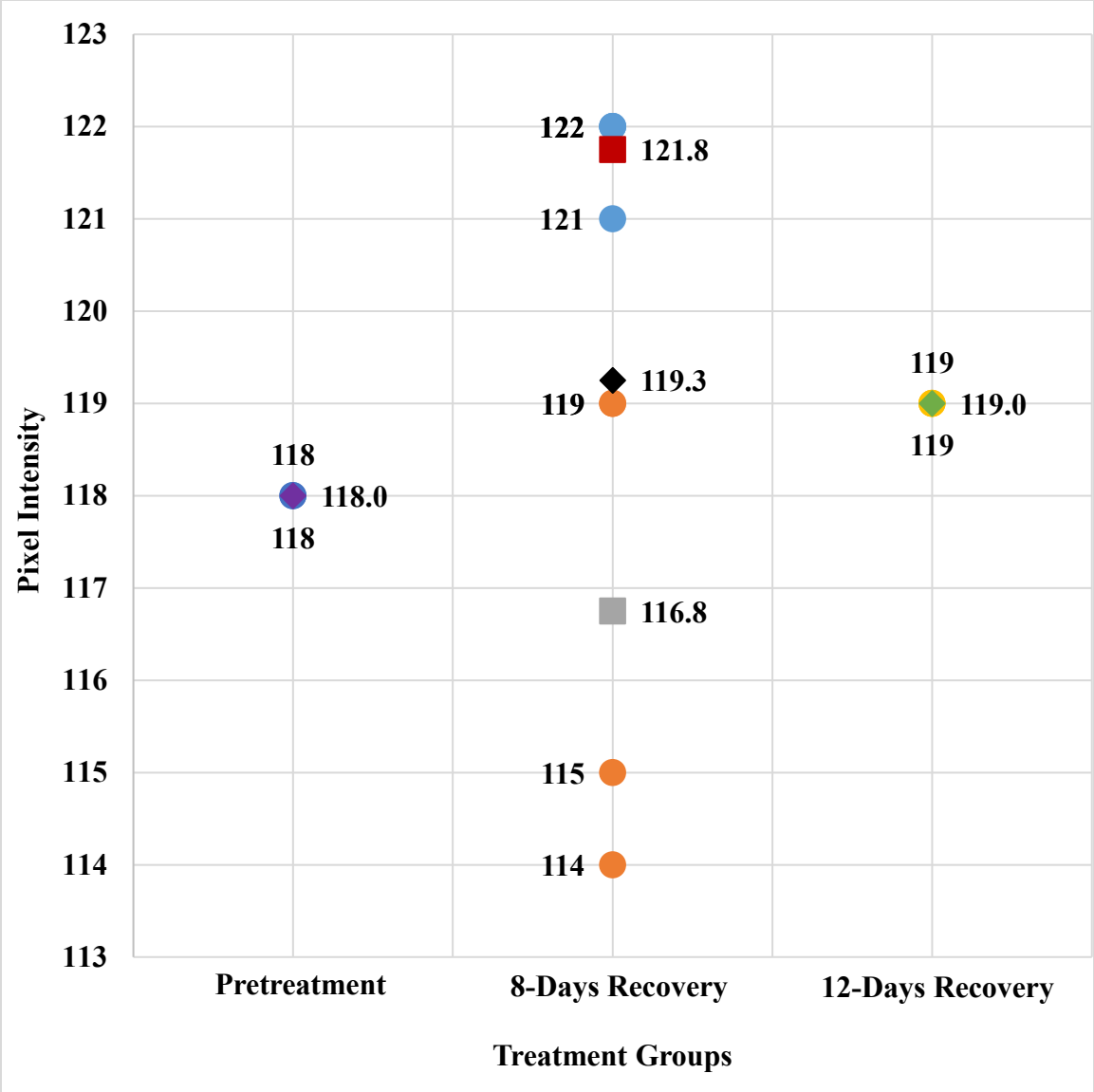

Figure 71 Values of the mode of the pixel intensities for the iliac ring slices throughout the exploratory experiments. For the eight-day recovery group, the triangle markers indicate the internal iliac artery, and the circle markers indicate the external artery. The square markers indicate each artery's average. Diamond-shaped markers indicate a group's mean value.

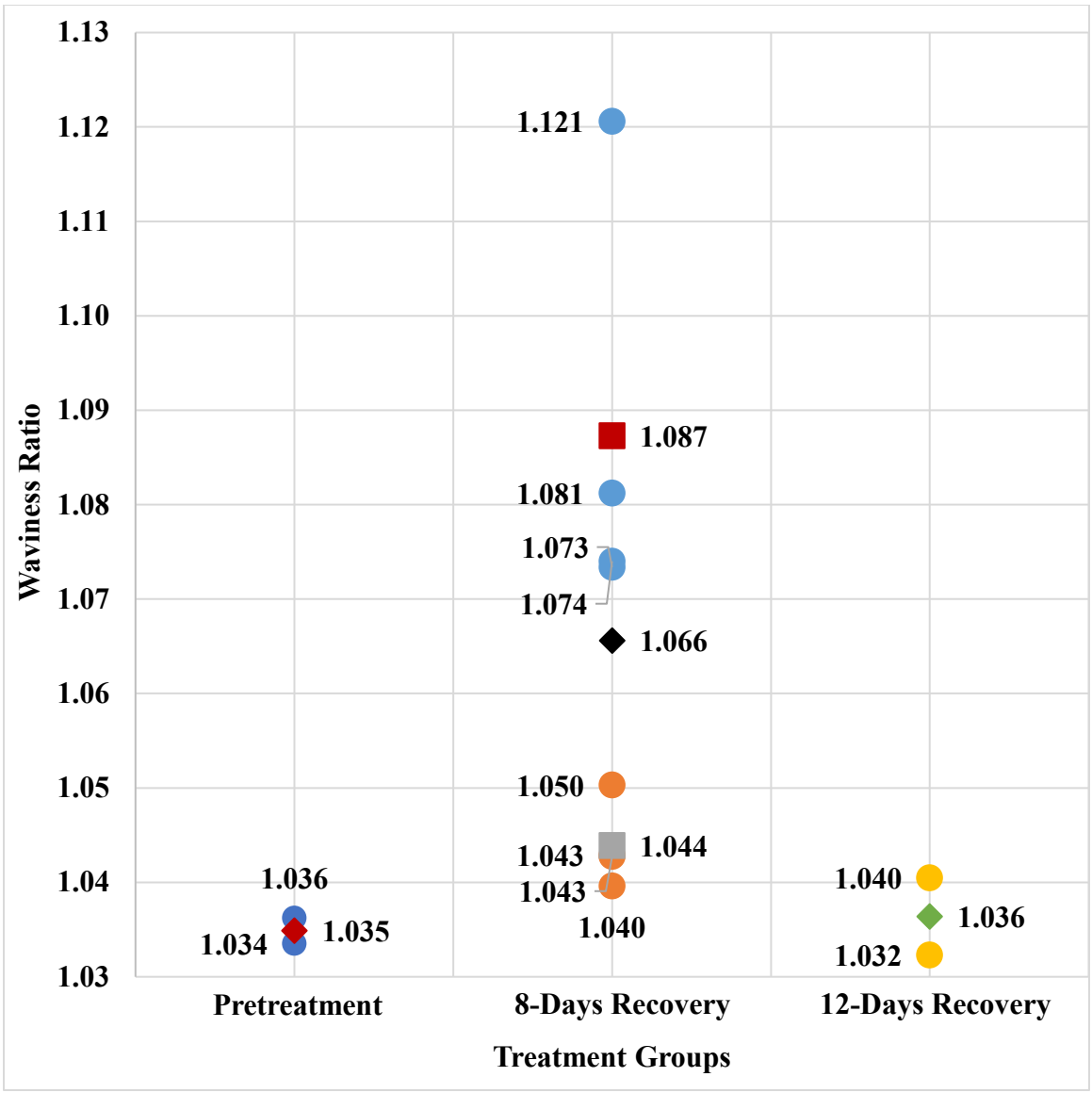

Figure 72 Values of the waviness ratios for the iliac arteries throughout the exploratory experiments. For the eight-day recovery group, the triangle markers indicate the internal iliac artery, and the circle markers indicate the external artery. The square markers indicate each artery's average. Diamond-shaped markers indicate a group's mean value.

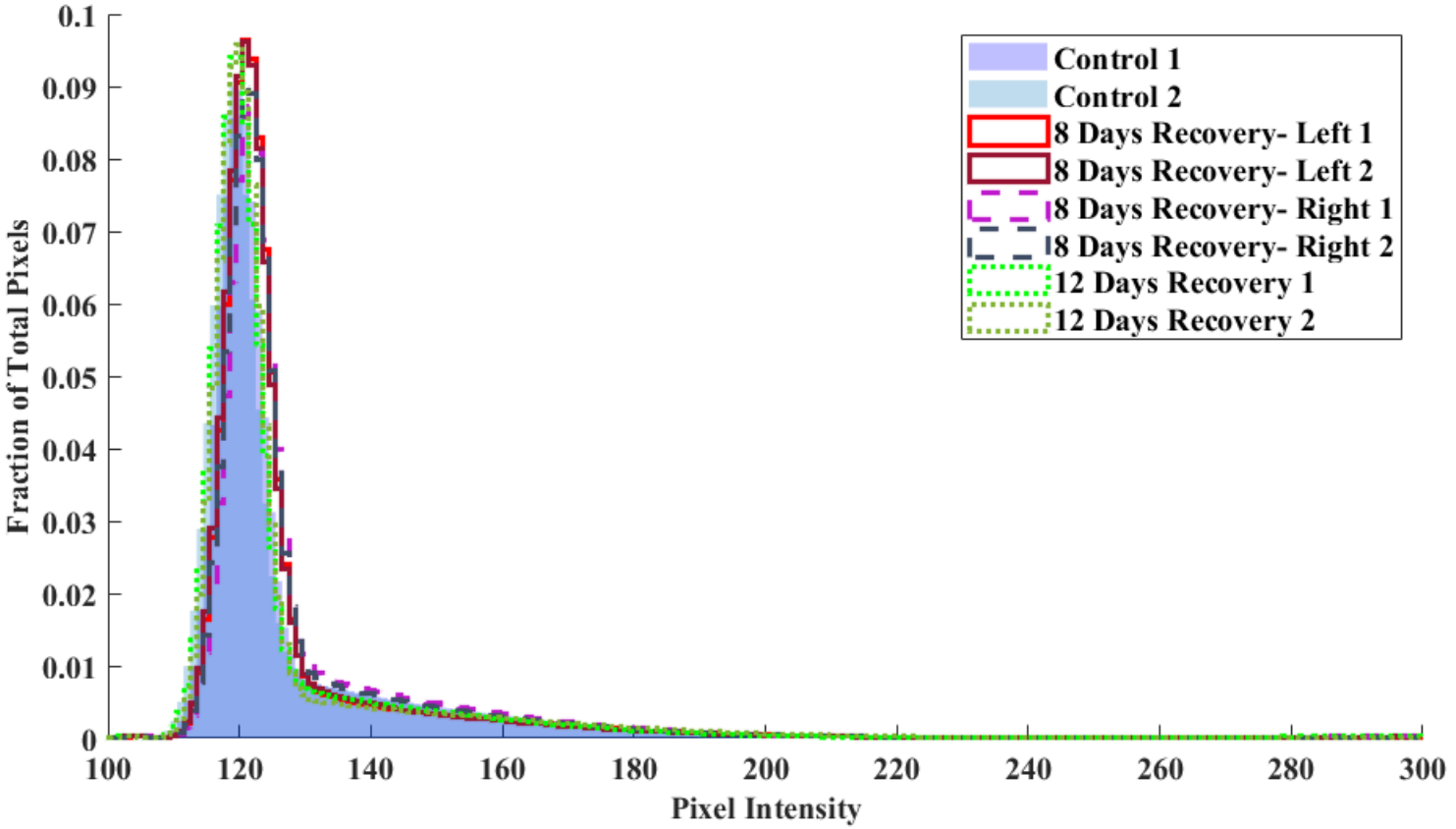

Figure 73 Histogram of pixel intensity from the CHP-stained histology images of the ring slices of the subclavian arteries throughout the exploratory experiments.

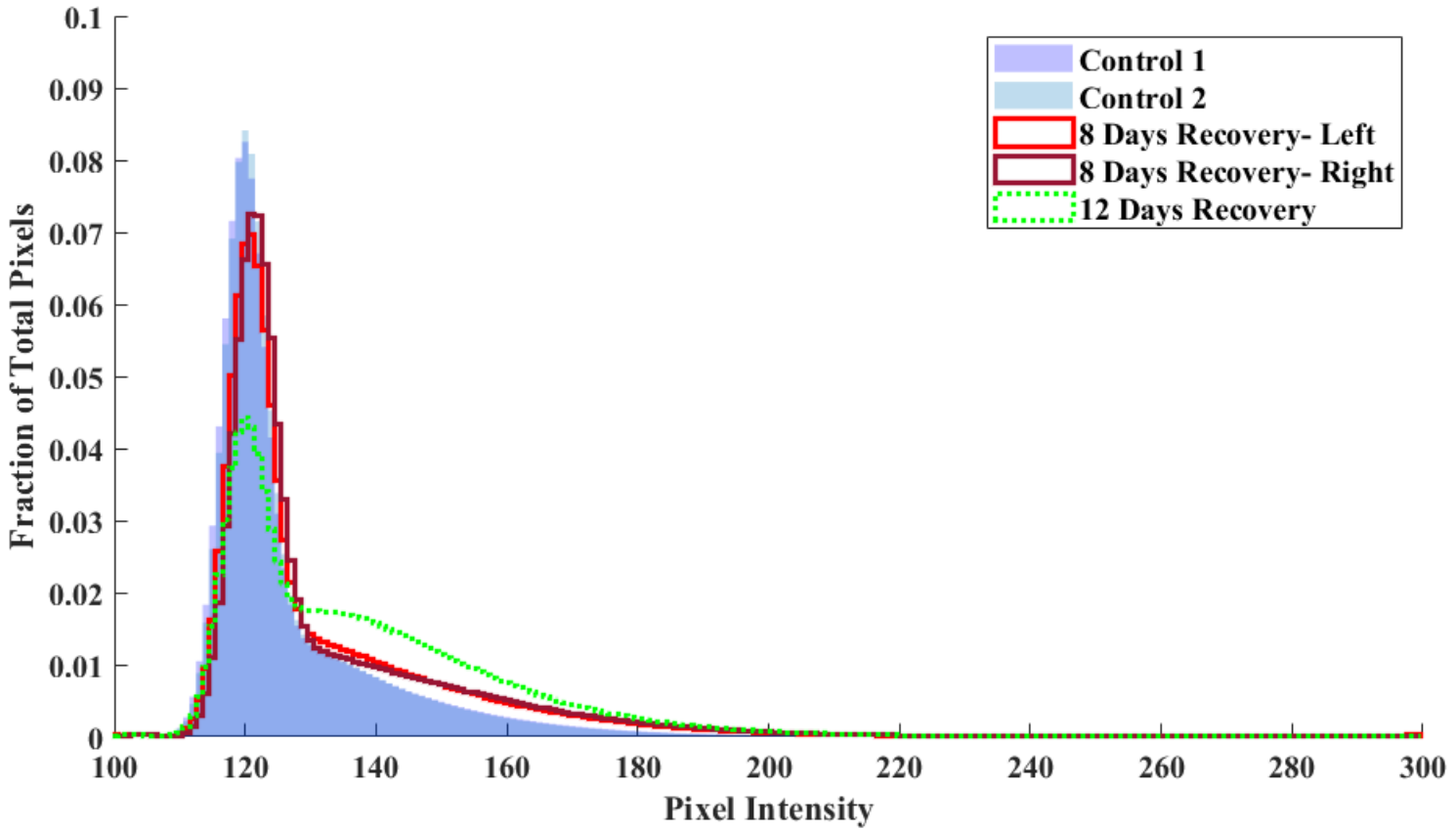

Figure 74 Histogram of pixel intensity from the CHP-stained histology images of the medial layer slices of the subclavian arteries throughout the exploratory experiments.

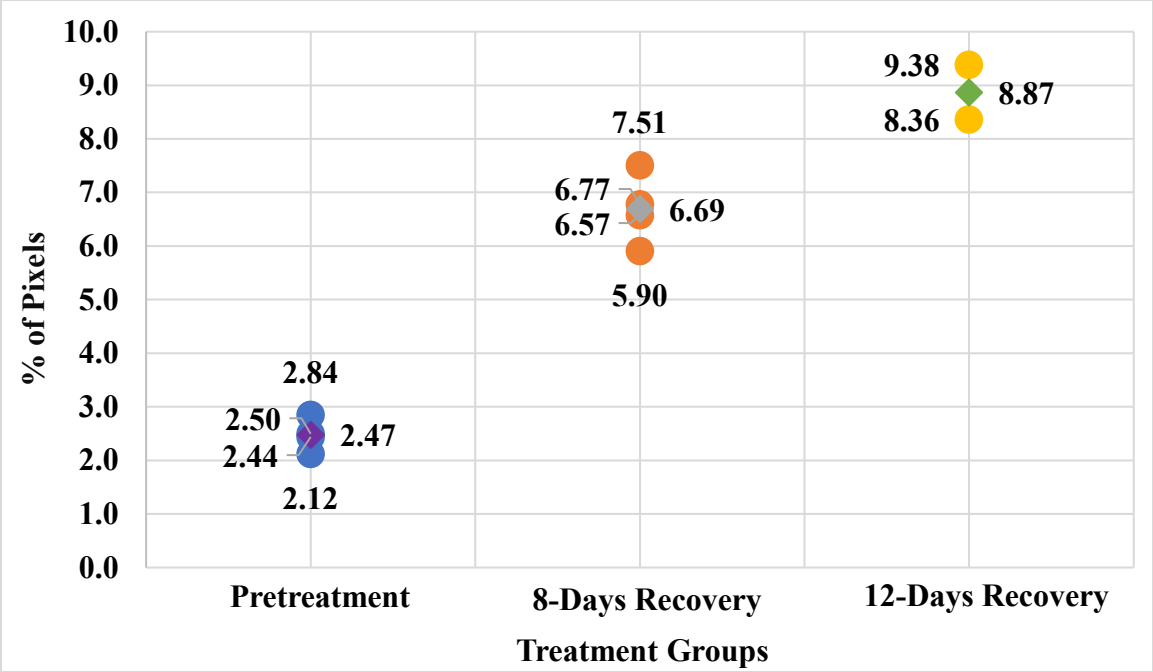

Figure 75 Values of the bright pixel percentages for the subclavian medial layer slices throughout the exploratory experiments. Diamond-shaped markers indicate a group's mean value.

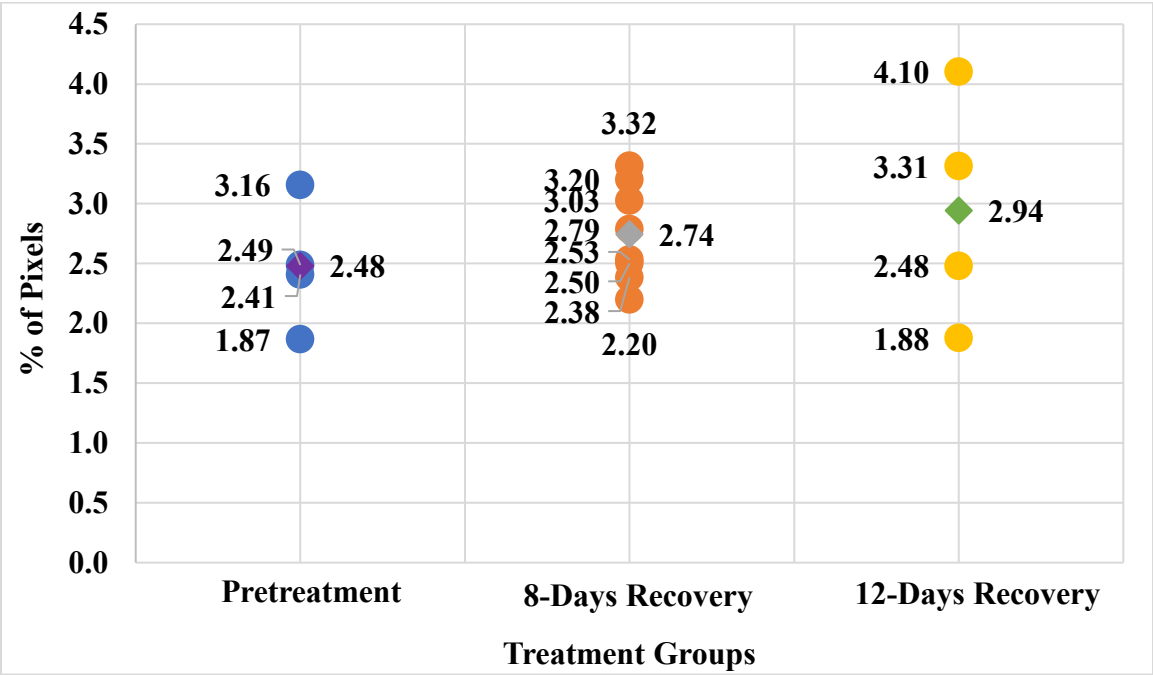

Figure 76 Values of the bright pixel percentage for the subclavian ring slices throughout the exploratory experiments. Diamond-shaped markers indicate a group's mean value.

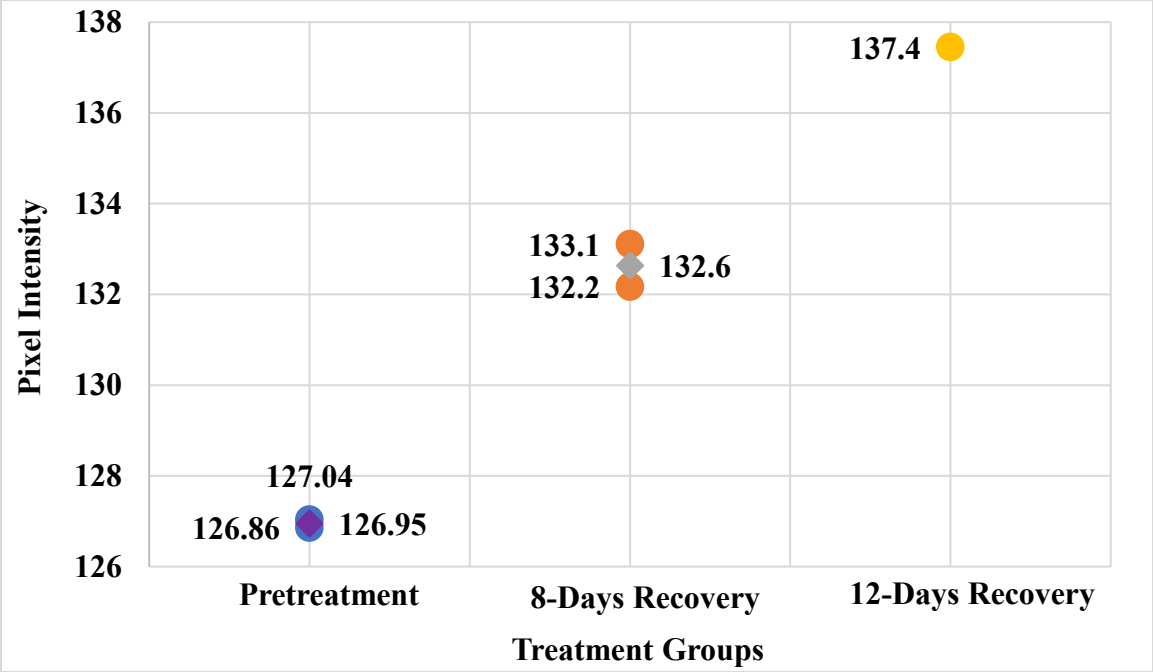

Figure 77 Values of the mean pixel intensities for the subclavian medial layer slices throughout the exploratory experiments. Diamond-shaped markers indicate a group's mean value.

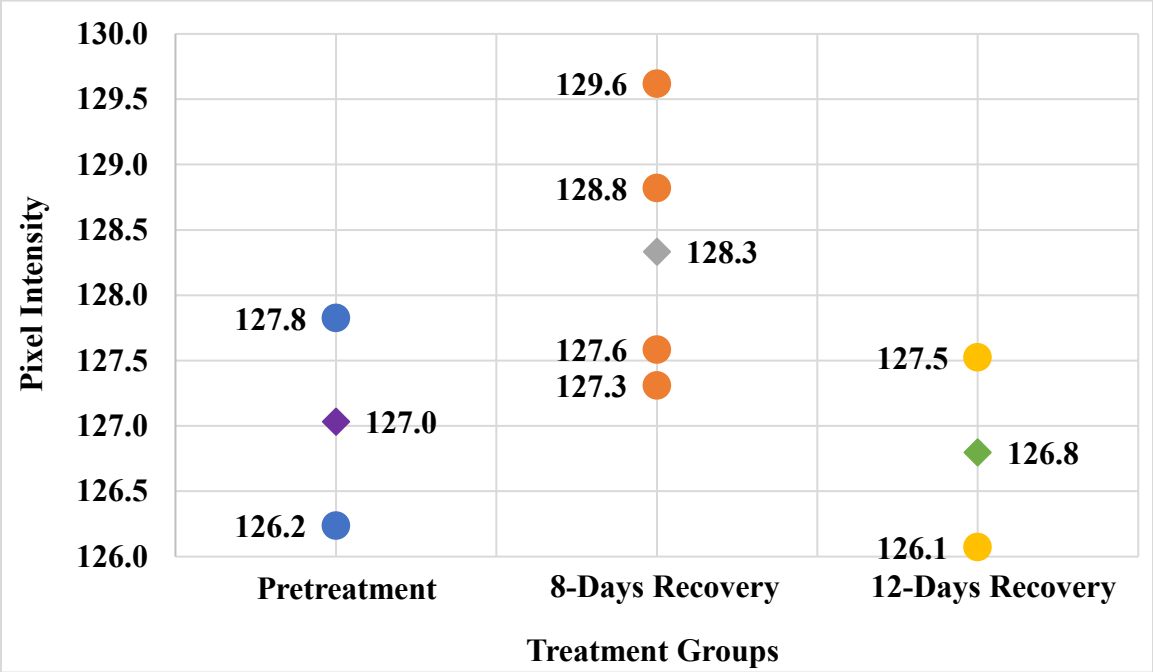

Figure 78 Values of the mean pixel intensities for the subclavian ring slices throughout the exploratory experiments. Diamond-shaped markers indicate a group's mean value.

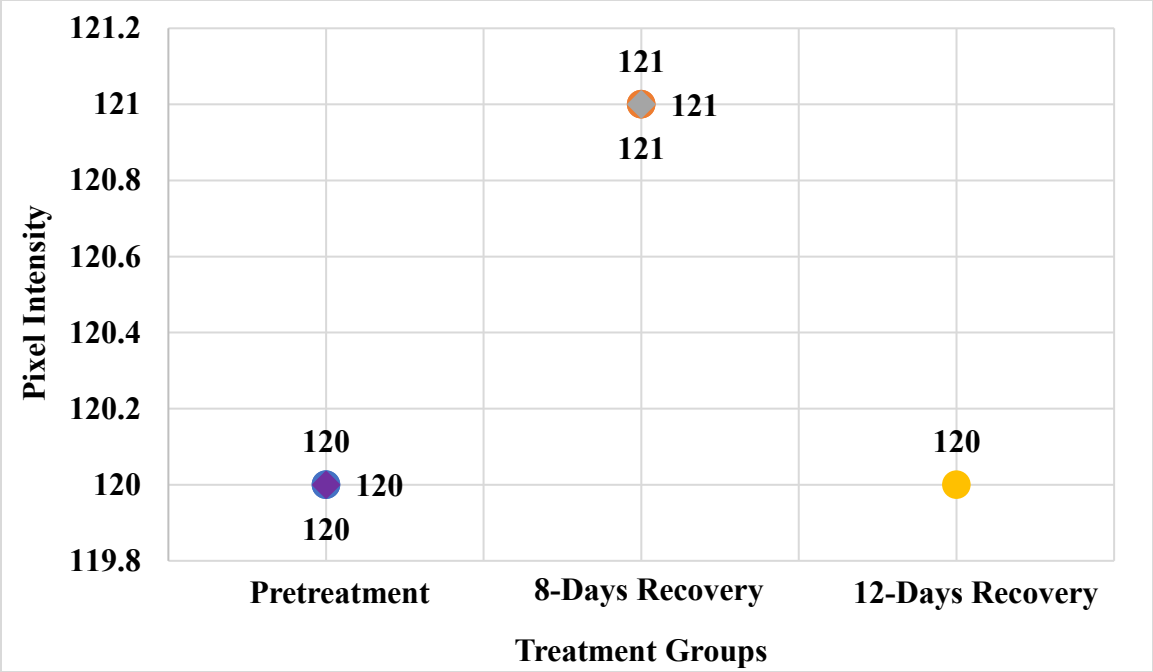

Figure 79 Values of the mode of the pixel intensities for the subclavian medial layer slices throughout the exploratory experiments. Diamond-shaped markers indicate a group's mean value.

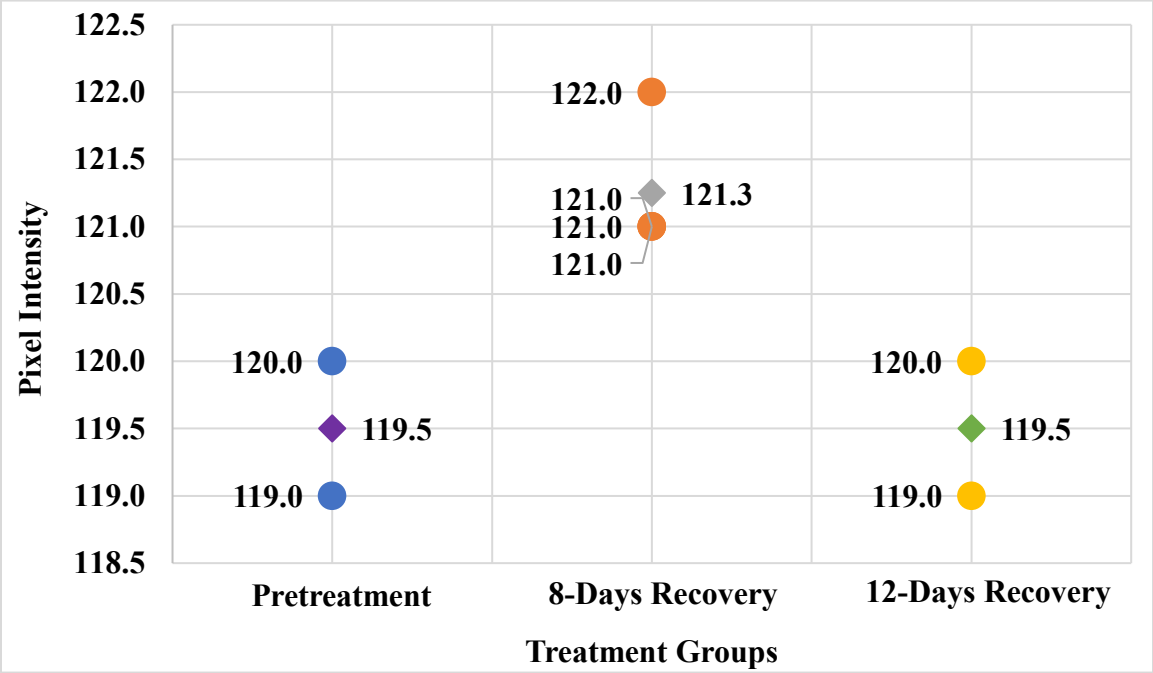

Figure 80 Values of the mode of the pixel intensities for the subclavian ring slices throughout the exploratory experiments. Diamond-shaped markers indicate a group's mean value.

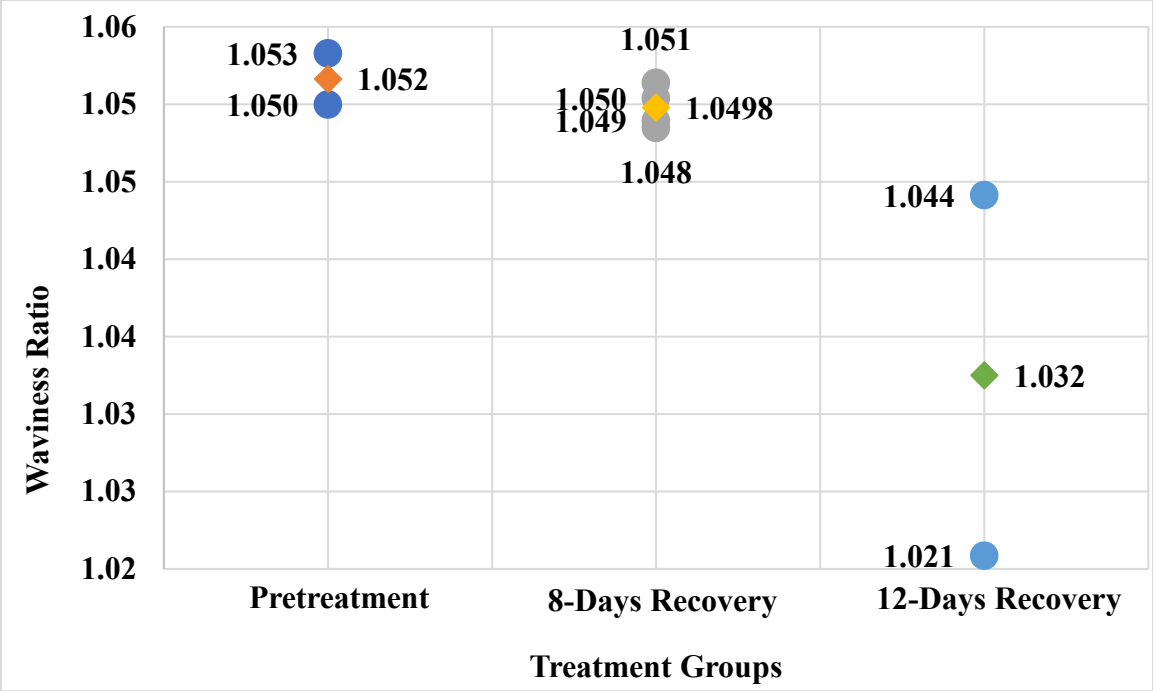

Figure 81 Values of the waviness ratios for the iliac arteries throughout the exploratory experiments. The diamond markers indicate a group's mean value.

CHAPTER 4

FUTURE STUDIES AND CONCLUSIONS

Future Studies

The results of the preceding investigations suggest several future studies outside of mitigating the limitations discussed in each chapter. The first would be to expand the types of arteries treated beyond what was done here to cranial and other peripheral arteries. Veins could also be included. This would provide a more complete description of angioplasty's effects throughout the body. The second would be to investigate how the active response of the artery is affected by angioplasty. The proceeding experiments both focused on passive mechanical properties and deactivated the SMCs in the arteries. The arteries' active response, caused by the SMCs, can also be evaluated before and after angioplasty. Combined with the passive mechanical response, this would better describe what occurs in vivo during angioplasty. Thirdly, these experiments could be repeated in human tissues. While procuring human samples is difficult, it would allow for clinically relevant results without extrapolating how they may differ from the animal model used. Fourth, in keeping with clinically relevant results, the experiments should be repeated in arteries in different disease states. Healthy arteries are not usually treated with angioplasty, so experiments on diseased tissue would reflect more real-world situations. Fifth, longer recovery times could be used for in vivo experiments to see exactly how

long the changes from angioplasty persist. This would help better answer questions about angioplasty's long-term efficacy and why retreatment is required as often as it is. Lastly, a more comprehensive material model could be utilized to capture the behavior and changes in arteries better.

Conclusions

In conclusion, this investigation has shown that angioplasty will cause significant softening to the axial and circumferential properties of carotid arteries. It will also cause damage to the microstructure of arteries throughout the body, causing an increase in CHP binding to the tissue and straightening the fibrous components of the artery wall. The artery can begin to recover from angioplasty but still shows the effects of it after twelve days. These results further the understanding of how angioplasty affects the arteries and can help improve the procedure and its outcomes. For example, a clinician will be able to better predict the amount of overstretch needed to achieve a desired diameter change following angioplasty. This will minimize the amount of stretch the artery experiences, which will minimize the damage and mechanical property changes. This could potentially reduce the time it takes for the artery to recover and reduce the rate of retreatment. Also, having an improved understanding of the microstructural damage and changes in the mechanical properties may allow for better prediction of treatment outcomes, such as side effects and the potential need for retreatment. All these improvements will provide a better framework for clinicians to evaluate the pros and cons of angioplasty for a patient and determine the treatment parameters when it is used.

APPENDIX

MATLAB CODE

```
%%%%%%%%%%%%%%e%%%%%%%%%%%%%%%%%%%%%%%%%%%%%%%%%%%%%%%%%%%%%%%%%%%%%%%%%%%%
%%%% Vessel Processing code written for Monson Lab, University of Utah.%%%%
%%%% Contributors include:                                                %%%%
%%%%       William Anderl, Matthew Converse, Ryan Tatton                 %%%%
%%%%                                                                     %%%%
%%%% This Version Created by Will Anderl                                 %%%%
%%%%       Contact At: william.anderl@gmail.com                          %%%%
%%%%%%%%%%%%%%%%%%%%%%%%%%%%%%%%%%%%%%%%%%%%%%%%%%%%%%%%%%%%%%%%%%%%%%%%%%%

clear
close all
clc

%%%%%%%%%%%%%%%%%%%%%%%%%%%%%%%%%%%%%%%%%%%%%%%%%%%%%%%%%%%%%%%%%%%%%%%%%%%
%populate vessel objects with data stored in vesselList excel sheet

%load('circVessels.mat');


%Call this function to start a new vessel list from an excel sheet

vesselList = populateVesselObjects();


%Call this function to update your vessel list. New vessel can be added to
%the excel sheet, and added to existing object lists. Inputs are the
%existing object list, and the row to start adding at.

% vesselList = updateVesselObjects(vesselList, 24);
%
%

%%%%%%%%%%%%%%%%%%%%%%%%%%%%%%%%%%%%%%%%%%%%%%%%%%%%%%%%%%%%%%%%%%%%%%%%%%%
%Stitch Vessels
% for i  = 11:11
%     [vesselList(i).stitchedImage,vesselList(i).blueStitched,...
%         vesselList(i).stitchIndex, vesselList(i).sliceIndex]...
%         = stitchvessel(vesselList(i).name);
%     %%%% SAVE YOUR OBJECT LIST HERE%%%%
```

```
%     save('renameVesselObjects','vesselList')
% end
filelist=uigetfile('*.tif','Select images to be processed.','MultiSelect','on');
for i=1:length(vesselList)
    filename=strcat(vesselList(i).name,'.tif');
    for j=1:length(filelist)
        if strcmp(filename,filelist{j})
            vesselList(i).stitchedImage=imread(filelist{j});
        end
    end
end


% %%%%%%%%%%%%%%%%%%%%%%%%%%%%%%%%%%%%%%%%%%%%%%%%%%%%%%%%%%%%%%%%%%%%%%%
% % mask Vessels
for i = 1:length(vesselList)
    % [vesselList(i).maskedImage, vesselList(i).mask]...
    % = CreateMask(vesselList(i).stitchedImage);
    [vesselList(i).maskedImage, vesselList(i).mask]...
        = createMaskAutoBasic(vesselList(i).stitchedImage);
end
%
% %%%%%
% %Assign Control Images - associates stiched controls with the correct
% %vessel object.
vesselList = assignControl(vesselList);

%%%%%%
%Set Vessel Comparison Threshold
threshold = 2;
vesselList = vesselThreshold(vesselList,threshold);

%%%%%%
% Quanitfy Vessel Brightness
% vesselList = quantifyBrightnessSimple(vesselList);
vesselList=noahQuant(vesselList);



%%%%%
% Display Results
% visualizeVesselRates(vesselList)
%%%SAVE VESSEL OBJECTS HERE%%%
save("renameVesselObjects","vesselList","-v7.3")


for i=1:length(vesselList)
    figure(i)
    imshow(uint16(vesselList(i).stitchedImage*16),[0,25000])
    title(vesselList(i).name)
end

intensitydata(1,1)="Sample Name";
intensitydata(1,2)="Control Name";
```

```
intensitydata(1,3)="Percent Bright Pixels";
for i=1:length(vesselList)
    intensitydata(i+1,1)=vesselList(i).name;
    intensitydata(i+1,2)=vesselList(i).controlName;
    intensitydata(i+1,3)=vesselList(i).percentBP;
end
```

Published with MATLAB® R2023a

```
%Auto Generate vessel objects from excel file
function vesselObjList = populateVesselObjects ()
vesselList = readtable("D:\CHP Devo- Confocal Images\vesselList.xlsx");

vesselList = table2array(vesselList);
[rows, ~] = size(vesselList);
vesselObjList(rows,1) = vessel();

for i  = 1: rows
    objectName = char(vesselList(i,1));
%     objectName = strcat('v',objectName);
    objectDirection = char(vesselList(i,2));
    objectSize=char(vesselList(i,3));
    objectRate=char(vesselList(i,4));
    objectControlName=char(vesselList(i,5));
    %vesselObjList(i) = assignin('base',objectName,vessel(objectName, objectDirection,
objectSize, objectRate, objectControlName));
    vesselObjList(i) = vesselUpdate(vesselObjList(i), objectName, objectDirection,
objectSize, objectRate, objectControlName);
end

%save VesselObjList
```

Published with MATLAB® R2023a

```
function vesselObjList = updateVesselObjects( existingVesselList, startRow )

vesselList = readtable('vesselList.xlsx');
vesselList = table2array(vesselList);
[rows, ~] = size(vesselList);
%vesselObjList(rows,1) = vessel();
existingVesselList(startRow:rows,1) = vessel();
vesselObjList = existingVesselList;

for i  = startRow: rows
    objectName = char(vesselList(i,1)); objectName = strcat('v',objectName);
    objectDirection = char(vesselList(i,2));
    objectSize=char(vesselList(i,3));
    objectRate=char(vesselList(i,4));
    objectControlName=char(vesselList(i,5));
```

```
    %vesselObjList(i) = assignin('base',objectName,vessel(objectName, objectDirection,
objectSize, objectRate, objectControlName));
    vesselObjList(i) = vesselUpdate(vesselObjList(i), objectName, objectDirection,
objectSize, objectRate, objectControlName);

end
```

Published with MATLAB® R2023a

```
function [ Imasked, Mask ] = createMaskAutoBasic( I )
% An adaptation of the original function to create a mask (see
% CreateMask.m). This will automatically create the basic mask, with no
% user input. Can be used if identical masking should be applied to all
% vessels.

% Convert to double
I = double(I);

% Determine which slice in array is brightest
intensity = zeros(1,size(I,3));
for k = 1:length(intensity)
    intensity(k) = sum(sum(I(:,:,k)));
end
max_int = max(intensity);
k_max = find(intensity==max_int,1,'first');

% Select threshold of background
Slice = I(:,:,k_max);
Slice_thresh = Slice;
[counts,centers]  = hist(Slice_thresh(:),100);
[~,loc] = findpeaks(-counts);
thresh = centers(loc(1));

%[thresh,dummy] = ginput(1); close all
% thresh = islocalmin(
% Set all background pixels equal to zero
Slice_thresh(Slice_thresh<thresh) = 1;
Slice_thresh(Slice_thresh>=thresh) = 0;
Mask1 = logical(Slice_thresh);

% Overlay slice with background
Slice_mask1 = Slice; Slice_mask1(Mask1) = 0;
SliceRGB = cat(3,Slice_mask1,Slice_mask1,Slice_mask1);
SliceRGB(Mask1) = 2^12-1;

% Allow user to outline additional bodies to add to mask
% figure(1)
% subplot(1,2,2)
% imshow(uint16(Slice*2^4));
% title('Original Image')
% subplot(1,2,1)
% imshow(uint16(SliceRGB*2^4));
```

```
% title('Draw polygon to add to mask; double click; repeat; close fig when done')
% set(gcf,'units','normalized','outerposition',[0 0 1 1])
% Mask2 = zeros(size(Slice));
% set(gcf,'currentchar','c')         % set a dummy character
% while get(gcf,'currentchar')=='c'  % which gets changed when key is pressed
%     BWi = roipoly;
%     if ~isnan(BWi)
%         Mask2 = Mask2 + double(BWi);
%     end
% end
% close all

% Combine both masks
Mask = double(Mask1); %+ Mask2;
Mask(Mask>0) = 1;
Mask = logical(Mask);

% Add to border of mask (because difficult to select polygon at edge)
thickness = 10; % vary number of pixels to fill around border
top = Mask(thickness,:) == 1; % gaps in mask at top
Mask(1:thickness-1,top) = 1;
bottom = Mask(end-thickness,:) == 1; % gaps in mask at bottom
Mask(end-thickness:end,bottom) = 1;
left = Mask(:,thickness) == 1; % gaps in mask on left edge
Mask(left,1:thickness) = 1;
right = Mask(:,end-thickness) == 1; % gaps in mask on right edge
Mask(right,end-thickness:end) = 1;

% % Display mask
% Slice_mask = Slice; Slice_mask(Mask) = 0;
% SliceRGB = cat(3,Slice_mask,Slice_mask,Slice_mask);
% SliceRGB(Mask) = 2^12-1;
% figure(2)
% subplot(2,1,2)
% imshow(uint16(Slice*2^4));
% title('Original Image')
% subplot(2,1,1)
% imshow(uint16(SliceRGB*2^4));
% title('Masked Image')

% Mask original matrix
Imasked = I;
for k = 1:size(I,3)
    slice_masked = Imasked(:,:,k);
    slice_masked(Mask) = 0;
    Imasked(:,:,k) = slice_masked;
end


end
```

Published with MATLAB® R2023a

```
function [ objectList ] = assignControl( objectList )
% this must be called after an object list is created, and stitched vessels
% are added to the appropriate objects.

for i = 1:length(objectList)
    currentControlName = objectList(i).controlName;
    for j = 1:length(objectList)
        if strcmp(objectList(j).direction,'control') &&
strcmp(objectList(j).name,currentControlName)
            objectList(i).controlImage = objectList(j).maskedImage;
            objectList(i).controlMask = objectList(j).mask;
            break
        end
    end
end




end
```

Published with MATLAB® R2023a

```
function [objectList ] = vesselThreshold( objectList,threshold )
for i= 1:length(objectList)
        objectList(i).threshold = threshold;
end



end
```

Published with MATLAB® R2023a

```
function vesselList = noahQuant(vesselList)
control_quantile = 0.975;
for i =1:length(vesselList)
    maskedControl = vesselList(i).controlImage.*~vesselList(i).controlMask;
    maskedControlNonZero = nonzeros(maskedControl);
    maskedControlIntensity = mean2(maskedControlNonZero);
    normalizedControl = maskedControlNonZero./maskedControlIntensity;

    h=histogram(normalizedControl,200,'Normalization','probability');
    threshold = quantile(h.Data, control_quantile);
    vesselList(i).brightPixImage = ...
              vesselList(i).maskedImage>...
              (maskedControlIntensity.*threshold);

        vesselList(i).percentBP =
```

```
100*sum(vesselList(i).brightPixImage(:))/sum(~vesselList(i).mask(:));
        figure(i)
        subplot(1,2,1)
        imshow(uint16(vesselList(i).maskedImage*16),[0 25000])
        subplot(1,2,2)
        imshow(vesselList(i).brightPixImage)
        figure(29)

%         disp(threshold)
%         normTest = kstest(h.Data);
%         display(normTest)
    thresholdFinal(i) = threshold;
end
%     if strcmp(vesselList(i).rate,'qs')
% visualizeVesselRatesWControl(vesselList)
disp(mean(thresholdFinal))
end
```

Published with MATLAB® R2023a

```
%leanVesselQuant Code. For use by a third party to evaluate and mask
%vessels with limited functionality.

classdef vessel
    properties
        name
        direction
        rate
        size
        stitchIndex
        sliceIndex
        stitchedImage
        maskedImage
        mask
        controlName
        controlImage
        blueStitched
        blueMasked
        blueMask
        threshold
        percentBP
        rawImageIntensity
        controlIntensity
        controlMask
        brightPixImage
        prKValue
        weight
        avgThickness
    end
    methods
        function namedVessel = vessel
        end
```

```
        function obj= vesselUpdate(obj, inputName,inputDirection,
inputSize,inputRate,inputControlName)
            obj.name = inputName;
            obj.direction = inputDirection;
            obj.size = inputSize;
            obj.rate= inputRate;
            obj.controlName = inputControlName;
        end

    end
end
```

Published with MATLAB® R2023a

```
% Title: MeasureCSA.m
% Purpose: measure the cross-sectional area of vessels using a single image
% of the cross-section

clc
close all
% clear
clearvars -except pathIn_data pathIn_video pathOut

% Read in image cross-section
if ~exist('pathIn_data','var');
    pathIn_data = uigetdir('C:\','Select folder with raw test data files');
end
[filename1,pathname1] = uigetfile([pathIn_data,'\*.*'],'Pick image of cross-section');
I = imread([pathname1,filename1]);

% % Load image scale
% [filename2,pathname2] = uigetfile([pathIn_data,'\*.*'],'Pick image of CS scale');
% I_scale = imread([pathname2,filename2]);
%
% % Calibrate image with scale bar
% imshow(I_scale)
% display('Calibrate image by selecting two points on scale bar')
% [x,y] = ginput(2); close all; clc
% perim_pix = ((x(2)-x(1))^2 + (y(2)-y(1))^2)^0.5;

% % Have user input actual length in mm
% imshow(I_scale); hold on; plot(x,y,'ro')
% val1 = inputdlg('Enter actual distnace between two selected points length (mm)');
% perim_mm = str2double(val1{1});
%
% % Calculate calibration
% mm_pix = perim_mm/perim_pix;
val = inputdlg('Enter calibration (mm/pix)');
mm_pix = str2double(val{1});

% Draw outer perimeter
```

```
display('Using several clicks, define outer perimeter')
[BWo,xo,yo] = roipoly(I); close all; clc
% Draw inner perimeter
display('Using several clicks, define inner perimeter')
[BWi,xi,yi] = roipoly(I); close all; clc

% Calculate area
AreaO_pix = sum(sum(BWo));
AreaI_pix = sum(sum(BWi));
CSA_pix = abs(AreaO_pix-AreaI_pix);
CSA = CSA_pix*(mm_pix)^2;

% Calcualte outer outer diameter
n = length(xo);
perim_pix = 0;
for i = 1:n
    x1 = xo(i); y1 = yo(i);
    if i == n
        x2 = xo(1); y2 = yo(1);
    else
        x2 = xo(i+1); y2 = yo(i+1);
    end
    len = ((x2-x1)^2+(y2-y1)^2)^0.5;
    perim_pix = perim_pix + len;
end
perim_mm = perim_pix*mm_pix;
OD = perim_mm/pi;

% Calculate wall thickness from measured CSA and outer diameter
ID = (OD^2-(4/pi)*CSA)^0.5;
h = (OD-ID)/2;

% % Manually measure wall thickness
% imshow(I)
% display('Using 2 clicks, measure wall thickness in 1 well-defined region')
% [x,y] = ginput(2); close all; clc
% len_pix = ((x(2)-x(1))^2+(y(2)-y(1))^2)^0.5;
% h2 = len_pix*mm_pix;
% ID2 = OD-2*h2;
% CSA2 = pi*(OD^2-ID2^2)/4;

% Plots
H = imshow(I); hold on
plot(xo,yo); hold on; plot(xi,yi)

% Compare wall thickness and cross-sectional area
display(['Wall thickness 1: ',num2str(h*1000),' um']);
% display(['Wall thickness 2: ',num2str(h2*1000),' um']);
display(['CSA 1: ',num2str(CSA),' mm^2']);
% display(['CSA 2: ',num2str(CSA2),' mm^2']);
display('OD pixel:');
    display(perim_pix/pi);
display('CSA pixel:');
display(CSA_pix);
```

```
% Option to save figure and data points
val = inputdlg('Do you want to save the figure? 1:Yes, 0:No');
val = str2double(val{1});
if val == 1
    if ~exist('pathOut','var')
        pathOut = uigetdir('C:\','Select output folder for image');
    end
    fullpath = fullfile(pathOut,'PFA CSA');
    saveas(H,fullpath,'png')
end
```

Published with MATLAB® R2023a

REFERENCES

Anderl, William J., Noah Pearson, Matthew I. Converse, S. Michael Yu, and Kenneth L. Monson. 2023. "Strain-Induced Collagen Denaturation Is Rate Dependent in Failure of Cerebral Arteries." *Acta Biomaterialia* 164: 282–92. https://doi.org/10.1016/j.actbio.2023.04.032.

Badimon, Juan Jose, Antonio Fernandez Ortiz, Beat Meyer, Alessandra Mailhac, John T. Fallon, Erling Falk, Lina Badimon, James H. Chesebro, and Valentin Fuster. 1998. "Different Response to Balloon Angioplasty of Carotid and Coronary Arteries: Effects on Acute Platelet Deposition and Intimal Thickening." *Atherosclerosis* 140, no. 2: 307–314. https://doi.org/10.1016/S0021-9150(98)00134-8.

Bonvini, Robert F., Aljoscha Rastan, Sebastian Sixt, Elias Noory, Thomas Schwarz, Ulrich Frank, Marco Roffi, et al. 2011. "Endovascular Treatment of Common Femoral Artery Disease." *Journal of the American College of Cardiology* 58, no. 8: 792–798. doi:10.1016/j.jacc.2011.01.070.

Chen, Huan, Yi Liu, Mikhail N. Slipchenko, Xuefeng Zhao, Ji-Xin Cheng, and Ghassan S. Kassab. 2011. "The Layered Structure of Coronary Adventitia Under Mechanical Load." *Biophysical Journal* 101, no. 11: 2555–62. https://doi.org/10.1016/j.bpj.2011.10.043.

Converse, Matthew I., and Kenneth L. Monson. 2021. "Biaxial Softening of Isolated Cerebral Arteries Following Axial Overstretch." *Journal of the Mechanical Behavior of Biomedical Materials* 118, no. 104447: 104447. https://doi.org/10.1016/j.jmbbm.2021.104447.

Converse, Matthew I., Kevin S. Nye, Mar Janna Dahl, Kurt H. Albertine, and Kenneth L. Monson. 2021. "Stretch-Induced Intimal Failure in Isolated Cerebral Arteries as a Function of Development." *Annals of Biomedical Engineering* 49, no. 12: 3540–49. https://doi.org/10.1007/s10439-021-02869-x.

Converse, Matthew I., Raymond G. Walther, Justin T. Ingram, Yang Li, S. Michael Yu, and Kenneth L. Monson. 2018. "Detection and Characterization of Molecular-Level Collagen Damage in Overstretched Cerebral Arteries." *Acta Biomaterialia* 67: 307–18. https://doi.org/10.1016/j.actbio.2017.11.052.

Cottin, Yves, Marc Kollum, Rosanna Chan, Balram Bhargava, Yoram Vodovotz, and Ron Waksman. 2000. "Vascular Repair After Balloon Overstretch Injury in Porcine Model Effects of Intracoronary Radiation." *Journal of the American College of Cardiology* 36, no. 4: 1389–95. https://doi.org/10.1016/s0735-1097(00)00851-2.

Ghazanfari, Samaneh., Anita Driessen-Mol, Gustav J. Strijkers, Frans M.W. Kanters, Frank. P.T. Baaijens, and Carlijn V.C. Bouten. 2012. "A Comparative Analysis of the Collagen Architecture in the Carotid Artery: Second Harmonic Generation Versus Diffusion Tensor Imaging." *Biochemical and Biophysical Research Communications* 426, no. 1: 54–58. https://doi.org/10.1016/j.bbrc.2012.08.031.

Giudici, Alessandro, Ian B. Wilkinson, and Ashraf W. Khir. 2021. "Review of the Techniques Used for Investigating the Role Elastin and Collagen Play in Arterial Wall Mechanics." *IEEE Reviews in Biomedical Engineering* 14: 256–69. https://doi.org/10.1109/RBME.2020.3005448.

Goode, Stephen D., Trevor J. Cleveland, Peter A. Gaines, and STAG trial collaborators. 2013. "Randomized Clinical Trial of Stents Versus Angioplasty for the Treatment of Iliac Artery Occlusions (STAG Trial): Stentsversusangioplasty for Treatment of Iliac Artery Occlusions." *The British Journal of Surgery* 100, no. 9: 1148–53. https://doi.org/10.1002/bjs.9197.

Holzapfel, Gerhard A., Thomas C. Gasser, and Ray W. Ogden. 2000. "A New Constitutive Framework for Arterial Wall Mechanics and a Comparative Study of Material Models." *Journal of Elasticity and the Physical Science of Solids* 61, no. 1: 1-48. https://doi.org/10.1023/A:1010835316564.

Humphrey, Jay D. 2003. "Review Paper: Continuum Biomechanics of Soft Biological Tissues." *Proceedings. Mathematical, Physical, and Engineering Sciences* 459, no. 2029: 3–46. https://doi.org/10.1098/rspa.2002.1060.

Kasapis, Christos, Peter K. Henke, Stanley J. Chetcuti, Gerald C. Koenig, John E. Rectenwald, Venkataramu N. Krishnamurthy, Paul Michael Grossman, and Hitinder S. Gurm. 2009. "Routine Stent Implantation vs. Percutaneous Transluminal Angioplasty in Femoropopliteal Artery Disease: A Meta-Analysis of Randomized Controlled Trials." *European Heart Journal* 30, no. 1: 44–55. https://doi.org/10.1093/eurheartj/ehn514.

Krasny, Witold, Claire Morin, Hélène Magoariec, and Stéphane Avril. 2017. "A Comprehensive Study of Layer-Specific Morphological Changes in the Microstructure of Carotid Arteries Under Uniaxial Load." *Acta Biomaterialia* 57: 342–51. https://doi.org/10.1016/j.actbio.2017.04.033.

Laird, John R., Barry T. Katzen, Dierk Scheinert, Johannes Lammer, Jeffrey Carpenter, Maurice Buchbinder, Rajesh Dave, et al. 2012. "Nitinol Stent Implantation vs.

Balloon Angioplasty for Lesions in the Superficial Femoral and Proximal Popliteal Arteries of Patients with Claudication: Three-Year Follow-up from the RESILIENT Randomized Trial." *Journal of Endovascular Therapy: An Official Journal of the International Society of Endovascular Specialists* 19, no. 1: 1–9. https://doi.org/10.1583/11-3627.1.

Meijering, Erik, Mathews Jacob, Juan-Carlos Floyd Sarria, Pascal Steiner, Harald Hirling, and Michael Unser. 2004. "Design and Validation of a Tool for Neurite Tracing and Analysis in Fluorescence Microscopy Images." *Cytometry. Part A: The Journal of the International Society for Analytical Cytology* 58, no. 2: 167–76. https://doi.org/10.1002/cyto.a.20022.

Mogharrabi, Farshad, Jonathan Kuhlenhoelter, Blake Anderson, Katalin Kauser, and Kenneth Monson. 2019. "Effect of Photoactivated Cross-Linking Compound on Mechanical Properties of Porcine Carotid Arteries Post-Angioplasty." In Volume 3: *Biomedical and Biotechnology Engineering. American Society of Mechanical Engineers*.

Mousa, Albeir Y., John E. Campbell, Patrick A. Stone, Mike Broce, Mark C. Bates, and Ali F. AbuRahma. 2012. "Short- and Long-Term Outcomes of Percutaneous Transluminal Angioplasty/Stenting of Renal Fibromuscular Dysplasia Over a Ten-Year Period." *Journal of Vascular Surgery* 55, no. 2: 421–27. https://doi.org/10.1016/j.jvs.2011.09.006.

Mustapha, Jihad A., Sara M. Finton, Larry J. Diaz-Sandoval, Fadi A. Saab, and Larry E. Miller. 2016. "Percutaneous Transluminal Angioplasty in Patients with Infrapopliteal Arterial Disease: Systematic Review and Meta-Analysis: Systematic Review and Meta-Analysis." *Circulation. Cardiovascular Interventions* 9, no. 5: 1-10. https://doi.org/10.1161/CIRCINTERVENTIONS.115.003468

Okamoto, Ei-ichi, Tracey Couse, Hector De Leon, Jakob Vinten-Johansen, Richard B. Goodman, Neal A. Scott, and Josiah N. Wilcox. 2001. "Perivascular Inflammation After Balloon Angioplasty of Porcine Coronary Arteries." *Circulation* 104, no. 18: 2228–35. https://doi.org/10.1161/hc4301.097195.

Rezakhaniha, Rana, Aristotelis Agianniotis, Jelle T.C. Schrauwen, Alessandra Griffa, Daniel Sage, Carlijn V.C. Bouten, Frans N. van de Vosse, Michael Unser, and Nikos Stergiopulos. 2012. "Experimental Investigation of Collagen Waviness and Orientation in the Arterial Adventitia Using Confocal Laser Scanning Microscopy." *Biomechanics and Modeling in Mechanobiology* 11, no. 3–4: 461–73. https://doi.org/10.1007/s10237-011-0325-z.

Roy, Sylvain, Christophe Boss, Rana Rezakhaniha, and Nikos Stergiopulos. 2010. "Experimental Characterization of the Distribution of Collagen Fiber

Recruitment." *Journal of Biorheology* 24, no. 2: 84–93. https://doi.org/10.1007/s12573-011-0027-2.

Sáez, Pablo, Alberto García, Estefanía Peña, T. Christian Gasser, and Miguel Ángel Martínez. 2016. "Microstructural Quantification of Collagen Fiber Orientations and Its Integration in Constitutive Modeling of the Porcine Carotid Artery." *Acta Biomaterialia* 33: 183–93. https://doi.org/10.1016/j.actbio.2016.01.030.

Schillinger, Martin, Schila Sabeti, Petra Dick, Jasmin Amighi, Wolfgang Mlekusch, Oliver Schlager, Christian Loewe, Manfred Cejna, Johannes Lammer, and Erich Minar. 2007. "Sustained Benefit at 2 Years of Primary Femoropopliteal Stenting Compared with Balloon Angioplasty with Optional Stenting." *Circulation* 115, no. 21: 2745–49. https://doi.org/10.1161/CIRCULATIONAHA.107.688341.

Snyder, Daniel J., Robert S. Zilinyi, Sonal Pruthi, Sareena George, Daniela Tirziu, Alexandra Lansky, Ari J. Mintz, Sanjum S. Sethi, and Sahil A. Parikh. 2023. "Percutaneous Transluminal Angioplasty for Infrapopliteal Chronic Limb-Threatening Ischemia: A Systematic Review and Meta-Analysis of Primary Patency and Binary Restenosis Rates." *Journal of Endovascular Therapy: An Official Journal of the International Society of Endovascular Specialists*, 1-15. https://doi.org/10.1177/15266028231212133.

Steele, Peter M., James H. Chesebro, Anthony W. Stanson, David R. Holmes Jr, Mrinal K. Dewanjee, Lina Badimon, and Valentin Fuster. 1985. "Balloon Angioplasty. Natural History of the Pathophysiological Response to Injury in a Pig Model." *Circulation Research* 57, no. 1: 105–12. https://doi.org/10.1161/01.res.57.1.105.

Tepe, Gunnar, John Laird, Peter Schneider, Marianne Brodmann, Prakash Krishnan, Antonio Micari, Christopher Metzger, et al. 2014. "Drug-Coated Balloon Versus Standard Percutaneous Transluminal Angioplasty for the Treatment of Superficial Femoral and Popliteal Peripheral Artery Disease." *Circulation* 131, no. 5: 495–502. https://doi.org/10.1161/CIRCULATIONAHA.114.011004

Tsao, Connie W., Aaron W. Aday, Zaid I. Almarzooq, Cheryl A. M. Anderson, Pankaj Arora, Christy L. Avery, Carissa M. Baker-Smith, et al. 2023. "Heart Disease and Stroke Statistics-2023 Update: A Report from the American Heart Association." *Circulation* 147, no. 8: e93–621. https://doi.org/10.1161/CIR.0000000000001123.

Vito, Raymond P., and Stacey A. Dixon. 2003. "Blood Vessel Constitutive Models-1995-2002." *Annual Review of Biomedical Engineering* 5, no. 1: 413–39. https://doi.org/10.1146/annurev.bioeng.5.011303.120719.

Vossen, Rianne J., Anco C. Vahl, Vanessa J. Leijdekkers, Alexander D. Montauban van Swijndregt, and Ron Balm. 2018. "Long-Term Clinical Outcomes of Percutaneous Transluminal Angioplasty with Optional Stenting in Patients with Superficial Femoral Artery Disease: A Retrospective, Observational Analysis."

European Journal of Vascular and Endovascular Surgery: The Official Journal of the European Society for Vascular Surgery 56, no. 5: 690–98. https://doi.org/10.1016/j.ejvs.2018.06.063.

Xu, Yongle, Xin Jia, Jiwei Zhang, Baixi Zhuang, Weiguo Fu, Danming Wu, Feng Wang, et al. 2018. "Drug-Coated Balloon Angioplasty Compared with Uncoated Balloons in the Treatment of 200 Chinese Patients with Severe Femoropopliteal Lesions: 24-Month Results of AcoArt I." *JACC. Cardiovascular Interventions* 11, no. 23: 2347–53. https://doi.org/10.1016/j.jcin.2018.07.041.

Yu, Xunjie, Yunjie Wang, and Yanhang Zhang. 2018. "Transmural Variation in Elastin Fiber Orientation Distribution in the Arterial Wall." *Journal of the Mechanical Behavior of Biomedical Materials* 77: 745–53. https://doi.org/10.1016/j.jmbbm.2017.08.002.